

---

Theses and Dissertations

---

Summer 2012

# A multiscale investigation of the role of variability in cross-sectional properties and side tributaries on flood routing

Jared Wendell Barr  
*University of Iowa*

Copyright 2012 Jared Wendell Barr

This thesis is available at Iowa Research Online: <https://ir.uiowa.edu/etd/3256>

---

## Recommended Citation

Barr, Jared Wendell. "A multiscale investigation of the role of variability in cross-sectional properties and side tributaries on flood routing." MS (Master of Science) thesis, University of Iowa, 2012.  
<https://doi.org/10.17077/etd.n1qn87ry>.

---

Follow this and additional works at: <https://ir.uiowa.edu/etd>

 Part of the [Civil and Environmental Engineering Commons](#)

A MULTISCALE INVESTIGATION OF THE ROLE OF VARIABILITY IN CROSS-  
SECTIONAL PROPERTIES AND SIDE TRIBUTARIES ON FLOOD ROUTING

by  
Jared Wendell Barr

A thesis submitted in partial fulfillment  
of the requirements for the Master of  
Science degree in Civil and Environmental Engineering  
in the Graduate College of  
The University of Iowa

July 2012

Thesis Supervisors: Professor Larry J. Weber  
Assistant Research Scientist Ricardo Mantilla

Graduate College  
The University of Iowa  
Iowa City, Iowa

CERTIFICATE OF APPROVAL

---

MASTER'S THESIS

---

This is to certify that the Master's thesis of

Jared Wendell Barr

has been approved by the Examining Committee  
for the thesis requirement for the Master of Science  
degree in Civil and Environmental Engineering at the July  
2012 graduation.

Thesis Committee:

\_\_\_\_\_  
Larry J. Weber, Thesis Supervisor

\_\_\_\_\_  
Ricardo Mantilla, Thesis Supervisor

\_\_\_\_\_  
Witold F. Krajewski

\_\_\_\_\_  
Nathan C. Young

To my Grandfather, Oliver Wendell Barr

Education is the power to think clearly, the power to act well in the world's work, and the power to appreciate life.

Brigham Young

## ACKNOWLEDGMENTS

First I would like to thank God for giving me all of the talents and opportunities that have led me to this point. I am indebted to my Parents for all of the support and encouragement given through my life. I have much gratitude and appreciation for those who have given me direction and support in this work, specifically for Dr. Larry Weber who provided me with much encouragement and inspiration to continue, and always made time for me when requested during his busy schedule; for Dr. Nathan Young who gave valuable information and training in the use of HEC-RAS and in hydraulic model development, without which none of this work could be completed. He also directed me towards many necessary resources and data; for Ricardo Mantilla for his enlightening conversations about hydrologic processes and multi-scale hydrology; and for Dr. Witold Krajewski for imparting much knowledge to me concerning hydroscience in general as well as statistical analysis. Finally I would like to acknowledge the support of the Iowa Flood Center and IIHR-Hydroscience and Engineering for funding my education at the University of Iowa and providing the necessary computational resources.

## TABLE OF CONTENTS

LIST OF TABLES .....	vii
LIST OF FIGURES.....	viii
CHAPTER I: INTRODUCTION.....	1
CHAPTER II: LITERATURE REVIEW.....	3
2.1 Hydraulic Flood Routing.....	3
2.1.1 Numerical Hydraulic Flood Routing.....	6
2.2 Hydrologic Flood Routing.....	11
2.3 Hydraulic Geometry.....	13
2.4 Horton Order and Stream Scaling Laws.....	16
2.4.1 Horton Ordering.....	16
2.4.2 Horton’s Law of Stream Numbers.....	18
2.4.3 Horton’s Law of Stream Lengths.....	19
2.4.4 Horton’s Law of Drainage Areas.....	21
2.4.5 Hack’s Law.....	21
2.4.6 Tokunaga Trees.....	23
2.4.7 Relation between Tokunaga’s Law and Horton’s Laws.....	26
CHAPTER III: THE EFFECT OF CROSS-SECTIONAL PROPERTIES ON FLOOD ROUTING .....	30
3.1 Model Framework.....	30
3.1.1 Inflow Hydrograph.....	31
3.1.2 Downstream Boundary Condition and Initial Condition.....	35
3.1.3 Channel Geometry.....	35
3.1.4 Hydraulic Resistance.....	37
3.1.5 Monte Carlo Experiment.....	38
3.1.6 Baseline Simulation.....	42
3.1.7 Evaluation Criteria.....	44
3.2 Results and Analysis.....	45
CHAPTER IV: THE EFFECT OF SIDE TRIBUTARIES ON FLOOD ROUTING MODELS .....	65
4.1 Model Framework.....	65
4.1.1 Stream and Network Model.....	66
4.1.2 Inflow Hydrographs and Downstream Boundary Condition.....	67
4.1.3 Simulations.....	67
4.2 Results and Analysis.....	68
4.3 Future Work.....	72
CHAPTER V: CASE STUDY ON THE IOWA RIVER.....	74
5.1 Model Framework.....	74
5.1.1 Inflow Hydrographs.....	74
5.1.2 Downstream Boundary Condition.....	76
5.1.3 Channel and Floodplain Geometry.....	77
5.1.4 Hydraulic Resistance and Model Calibration.....	78
5.1.5 CUENCAS Model.....	79
5.1.6 Evaluation Criteria.....	80
5.2 Results and Analysis.....	81

CHAPTER VI: SUMMARY, CONCLUSIONS, AND FUTURE WORK .....	86
6.1 Variability in Hydraulic Geometry .....	86
6.2 Simplification to Tributaries and Lateral Inflows.....	87
6.3 Future Work.....	88
REFERENCES.....	90

## LIST OF TABLES

Table 1 Coefficients and exponents used for hydraulic geometry relationships.....	16
Table 2 Time to peak discharge and peak discharge of the inflow hydrograph for each Horton order .....	33
Table 3 Mean geometric properties used in the simulations for each Horton order stream.....	37
Table 4 Sampling properties of input variables used in MC simulations .....	42
Table 5 Peak discharge, time to peak discharge, and time of duration for baseline hydrographs of a given Horton order.....	42
Table 6 95% bootstrap confidence intervals on simulated hydrograph characteristics.....	61
Table 7 Summary of comparison metrics for simulation on Mandelbrot-Vicsek tree.....	71
Table 8 Muskingum routing parameters used in routing lateral inflows .....	75
Table 9 Average Manning's n for calibrated models and its coefficient of variation (CV). .....	79

## LIST OF FIGURES

Figure 1	Graphical description of the Preissmann scheme .....	7
Figure 2	Mandelbrot-Vicsek tree with Horton-Strahler order 5 .....	25
Figure 3	Inflow hydrographs used in simulations. (a) Horton orders 1-3 (b) Horton orders 4-6 (c) Horton orders 7-9 .....	34
Figure 4	Compound cross-section shape used in simulations.....	36
Figure 5	Comparison of observed variability in channel bottom width with simulated variability in channel bottom width. (a) 331 cross-sections observed in the Iowa River between Iowa City, IA and Lone Tree, IA (b) 331 simulated cross-sections with equal mean to observed cross sections and $CV = 1/6$ .....	40
Figure 6	Comparison of 331 observed cross-sections in the Iowa River between Iowa City, IA and Lone Tree, IA with 331 simulated cross-sections of equal scale .....	40
Figure 7	Variability in simulated Manning's resistance coefficient along a channel length for overbank and main channel flow .....	41
Figure 8	Baseline simulation hydrographs. (a) Horton orders 1-3 (b) Horton orders 4-6 (c) Horton orders 7-9.....	43
Figure 9	Definition of hydrograph characterization parameters $Q_p$ , $t_p$ , and $t_b$ .....	45
Figure 10	Histograms describing simulation outputs for Horton order 1. (a) Peak discharge (b) Time to peak discharge (c) Time of duration .....	46
Figure 11	Histograms describing simulation outputs for Horton order 2. (a) Peak discharge (b) Time to peak discharge (c) Time of duration .....	47
Figure 12	Histograms describing simulation outputs for Horton order 3. (a) Peak discharge (b) Time to peak discharge (c) Time of duration .....	48
Figure 13	Histograms describing simulation outputs for Horton order 4. (a) Peak discharge (b) Time to peak discharge (c) Time of duration .....	49
Figure 14	Histograms describing simulation outputs for Horton order 5. (a) Peak discharge (b) Time to peak discharge (c) Time of duration.....	50
Figure 15	Histograms describing simulation outputs for Horton order 6. (a) Peak discharge (b) Time to peak discharge (c) Time of duration.....	51
Figure 16	Histograms describing simulation outputs for Horton order 7. (a) Peak discharge (b) Time to peak discharge (c) Time of duration.....	52
Figure 17	Histograms describing simulation outputs for Horton order 8. (a) Peak discharge (b) Time to peak discharge (c) Time of duration.....	53

Figure 18 Histograms describing simulation outputs for Horton order 9. (a) Peak discharge (b) Time to peak discharge (c) Time of duration.....	54
Figure 19 Spectrum of all routed hydrographs from the simulations. (a) Horton order 1 (b) Horton order 2 (c) Horton order 3.....	55
Figure 20 Spectrum of all routed hydrographs from the simulations. (a) Horton order 4 (b) Horton order 5 (c) Horton order 6.....	56
Figure 21 Spectrum of all routed hydrographs from the simulations. (a) Horton order 7 (b) Horton order 8 (c) Horton order 9.....	57
Figure 22 Coefficient of variation vs. Horton order. (a) CV for peak discharge (b) CV for time to peak discharge (c) CV for time of duration.....	58
Figure 23 Nash-Sutcliffe efficiency vs. Horton order.....	59
Figure 24 Relative differences vs. Horton order. (a) relative difference in peak discharge (b) relative difference in time to peak discharge (c) relative difference in time of duration.....	60
Figure 25 Side tributary structure for main stream of an order 9 Mandelbrot-Vicsek tree.....	66
Figure 26 Hydrographs from simulations on Mandelbrot-Vicsek tree network.....	69
Figure 27 Plot of Simulations S2, S3, and S4 vs baseline simulation (S1). Red line is the 1:1 line.....	70
Figure 28 Inflow hydrographs observed in 2008. (a) Observed hydrograph at USGS gauge on the Iowa River near Iowa City, IA (b) Inflow hydrograph at the Iowa River from Old Man's Creek (c) Inflow hydrograph at the Iowa River from the English River.....	76
Figure 29 Stage hydrograph observed in 2008 at USGS gauge on Iowa River near Lone Tree, IA. Used as downstream boundary condition for river models.....	77
Figure 30 Summary of model performance. Ellipses represent detailed hydraulic routing model, squares represent calibrated approximate hydraulic model, diamonds represent approximate hydraulic model, triangles represent CUENCAS hydrologic model.....	82
Figure 31 Outflow hydrographs at Lone Tree, IA.....	83
Figure 32 Plot of maximum and minimum water surface profiles computed by the three hydraulic routing models.....	85

## CHAPTER I: INTRODUCTION

Rivers and flood plains are of great interest to human societies. A significant majority of humans live near rivers or in floodplains and rely on them for water supply, food, power, transport, recreation, waste disposal, and other essential aspects of daily life (Bridge 2003; Chang 2002). Because so many human operations depend on the dynamics of streams and rivers, and because of the potential risk of damage due to flooding, there has long been a need to model and predict how water moves through a river channel over time (Choudhury et al. 2002; Di Baldassarre and Uhlenbrook 2012; Jin and Fread 1997). In particular the process of calculating the evolution of a flood hydrograph is known as flood routing (Henderson 1966). There are two classical methods within the engineering community for addressing the problem of flood routing, namely hydraulic flood routing and hydrologic flood routing of a hydrograph (Todini 1988; Hsu et al. 2003).

Hydraulic flood routing methods describe changes in the water surface elevation along the channel, and the evolution of the hydrograph in space and time by numerically solving the 1D Saint Venant equations. The Saint Venant equations are considered to be the most complete theoretical approach available to describing unsteady open channel flow (Keskin and Agiralioglu 1997; Sivapalan et al. 1997; Yen and Tsai 2001). The difficulty with applying this methodology is the need for extensive a priori data about the channel geometry and hydraulic characteristics of the stream reach of interest (Di Baldassarre and Uhlenbrook 2012; Dooge et al. 1982; Karmegam et al. 1991; Shrestha et al. 2005; Wormleaton and Karmegam 1984). The required data for hydraulic flood routing makes the method cost prohibitive in many circumstances and is the primary reason for its limited use in general practice (Aldama 1990; Dooge et al. 1982; Hicks 1996).

The alternative to hydraulic flood routing is hydrologic flood routing. Hydrologic flood routing is a simplified approach based only on the mass continuity equation and an

assumed storage-discharge relationship (Aldama 1990; Kim et al. 2001; Todini 1988). These simple models generally give satisfactory results, but the parameters of these relationships are not physically based or measurable, hence they require a series of flood hydrographs at the upstream and downstream boundaries of the stream channel for parameter calibration (Chang et al. 1983; France 1985). A problem arises with hydrologic flood routing because the events of interest are often of low probability of occurrence, which makes it rare for extreme events to be contained within the calibration data set. Furthermore it is often the case that calibration data is not available for the region of interest because drainage basins in many parts of the world are ungauged (Sivapalan et al. 2003). There have been efforts to estimate model parameters for ungauged basins based upon other basins with similar characteristics, but these results are uncertain at best (McCuen 1998). Despite the shortcomings of hydrologic flood routing, it still remains one of the most popular methods in engineering analysis (Blackburn and Hicks 2002; Chang et al. 1983; Hicks 1996, Sivapragasam et al. 2008).

Given the limitations of hydrologic flood routing models in terms of available calibration data sets, and the restriction of hydrologic flood routing models to only provide hydrograph outputs at gauge locations (Hicks 1996), a deterministic model is desirable. Hydraulic flood routing provides a suitable option to overcome the difficulties associated with hydrologic flood routing; however the channel cross-sectional geometry and hydraulic characteristics must be prescribed as well as the hydrography of the basin. The present study is an investigation of the required level of detail in channel properties needed to route a flood hydrograph through a river reach with satisfactory results. This study consists of four components: analysis of the effect of simplified cross-sectional geometry and hydraulic characteristics on hydraulic flood routing, the effect of a simplified channel network topology on hydraulic flood routing, an evaluation of a simple, physically based hydrologic flood routing model, and a case study of flood routing on the Iowa River with simplified channel geometry and topology.

## CHAPTER II: LITERATURE REVIEW

Flood routing is an aspect of a much larger field, river engineering. Current and past research has demonstrated that river engineering is not based solely on a simple understanding of the hydrodynamic forces in the channel, but also on the interactions with the watershed that supplies water and sediment to the dynamic river system (Chang 2002; Julien 2002). Understanding of river systems must include an understanding of geomorphology and hydrology in addition to the hydrodynamic forces governing the motion of water and sediment (Chang 2002, Julien 2002). There has been significant research devoted to an understanding of the interaction of these watershed processes and how the processes are affected by watershed scale.

### 2.1 Hydraulic Flood Routing

Hydraulic flood routing includes the full 1D unsteady continuity equation, and all or part of the momentum equation (Sturm 2010). While there has been much development and research of simplified forms of the momentum equation that arise from neglecting inertial and pressure terms (e.g., Cappelaere 1997; Dooge and Napiłrkowski 1987; Moussa and Bocquillon 1996; Hager et al. 1986; Sabur and Steffler 1996; Sivapalan et al. 1997; Tsai 2005; Venutelli 2011; Yen and Tsai 2001), here the term hydraulic flood routing will refer only to models which employ all terms of the momentum equation, namely those which are formed by the full 1D Saint Venant equations (Brunner 2010) as follows:

The 1D unsteady continuity equation which is a statement of the conservation of mass

$$\frac{\partial A}{\partial t} + \frac{\partial Q}{\partial x} - q_l = 0 \quad (2.1)$$

The 1D unsteady momentum equation, which states that the time rate of change in momentum is equal to the external forces applied to the system

$$\frac{\partial Q}{\partial t} + \frac{\partial QV}{\partial x} + gA \left( \frac{\partial z}{\partial x} + S_f \right) = 0 \quad (2.2)$$

Equations 2.1 and 2.2 form the 1D Saint Venant equations similar to those derived in many classical and modern works on open channel hydraulics (e.g., Brunner 2010a, p. 28-34; Chang 2002, p. 59-63; Henderson 1966, p. 3-4, 285-287; Julien 2002, p. 122-129; Sturm 2010, p. 301-306). In equations 2.1 and 2.2,  $t$  is the time ordinate,  $x$  is the space ordinate in the stream wise direction,  $A$  is the cross-sectional area of flow,  $Q$  is the volumetric flow rate,  $q_l$  is the lateral inflow per unit length along the floodplain,  $V$  is the cross-sectional average flow velocity,  $z$  is the elevation of the water surface from a fixed datum, and  $S_f$  is the friction slope, defined for U.S. Customary units as:

$$S_f = \frac{Q|Q|n^2}{2.208R^{4/3}A^2} \quad (2.3)$$

where  $R$  is the hydraulic radius and  $n$  is the Manning friction coefficient.

It is well recognized that flow in a natural river system has some dominant two-dimensional characteristics, especially when the flow enters the floodplain (Brunner 2010a; Tayefi et al. 2007). Several attempts have been made to address the problem of channel and floodplain flow, one of which is to separate the flow in the channel and floodplain and neglect momentum exchange between them (Brunner 2010a). This is the method chosen in the development of the modeling software developed by the U. S. Army Corps of Engineers, HEC-RAS (Brunner 2010a, 2010b). From this approximation, the 1D Saint Venant equations become:

The unsteady continuity equation for the channel and floodplain flow with an added storage term,  $S$ , for non-conveying portions of the cross-section respectively

$$\frac{\partial A_c}{\partial t} + \frac{\partial(\varphi Q)}{\partial x_c} - q_f = 0 \quad (2.4)$$

$$\frac{\partial A_f}{\partial t} + \frac{\partial[(1-\varphi)Q]}{\partial x_f} + \frac{\partial S}{\partial t} - q_c - q_l \quad (2.5)$$

The unsteady momentum equation for the channel and floodplain flow respectively

$$\frac{\partial \varphi Q}{\partial t} + \frac{\partial(\varphi^2 Q^2 / A_c)}{\partial x_c} + g A_c \left( S_{fc} + \frac{\partial Z}{\partial x_c} \right) = 0 \quad (2.6)$$

$$\frac{\partial(1-\varphi)Q}{\partial t} + \frac{\partial((1-\varphi)^2 Q^2 / A_f)}{\partial x_f} + g A_f \left( S_{ff} + \frac{\partial Z}{\partial x_f} \right) = 0 \quad (2.7)$$

where the subscripts  $c$  and  $f$  refer to the channel and floodplain respectively, and  $\varphi$  is a ratio of the flow conveyance in the channel to the total conveyance in the cross-section. The terms  $q_c$  and  $q_f$  are the lateral flow exchanges between the channel and floodplain per unit length.

Equations 2.4, 2.5, 2.6, and 2.7 form a hyperbolic system of partial differential equations (PDEs) which must be solved numerically in all but the most simple of cases (Aral et al. 1998; Garcia and Kahawita 1986; Hicks and Steffler 1994). There have been numerous numerical solution techniques proposed in the literature for solving the 1D Saint Venant equations. While they will not be extensively reviewed here, an extensive review of common methods can be found in Sturm (2010).

### 2.1.1 Numerical Hydraulic Flood Routing

There are many available computer models available for solving the Saint Venant equations in a river channel or network (Stelling and Verwey 2006); however in this study the model used, HEC-RAS, uses an implicit finite difference method, the Preissmann scheme, to numerically integrate the Saint Venant equations (Brunner 2010a; Castellarin et al. 2009).

The Preissmann scheme has been widely used in hydraulic flood routing and is extensively reviewed in literature (e.g., Liu et al. 1992; Lyn and Goodwin 1987; Venutelli 2002). The method is known to be very stable and to perform well under most conditions (Lyn and Goodwin 1987; Singh et al. 2010; Szymkiewicz 2010). A further discussion of the stability criteria for the method will be included after presentation of the method.

There are many ways to discretize the Saint Venant equations using the Preissmann scheme (e.g., Chang 2002; Julien 2002; Sturm 2010), but the discretization presented here is that used in the HEC-RAS model as shown in Brunner (2010a).

The Preissmann scheme is a four-point implicit scheme developed on a rectangular solution grid in the space-time domain as shown in Figure 1 (Brunner 2010a; Sturm 2010; Szymkiewicz 2010). The space derivatives and the function values are defined to implicitly include the future time step, resulting in a system of equations that must be solved simultaneously for the entire river reach (Brunner 2010a; Sturm 2010; Szymkiewicz 2010).

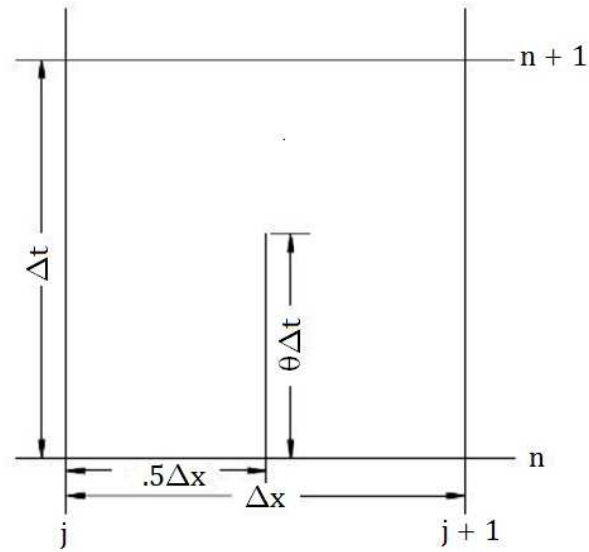


Figure 1 Graphical description of the Preissmann scheme

For ease in developing the method, the following notation is defined:

$$f_j = f_j^n \quad (2.8)$$

$$\Delta f_j = f_j^{n+1} - f_j^n \quad (2.9)$$

Using the notation of equations 2.8 and 2.9, the general finite difference forms used in the Preissmann scheme are defined as:

1. Time derivative

$$\frac{\partial f}{\partial t} \approx \frac{\Delta f}{\Delta t} = \frac{0.5(\Delta f_{j+1} + \Delta f_j)}{\Delta t} \quad (2.10)$$

## 2. Space derivative

$$\frac{df}{dx} \approx \frac{\Delta f}{\Delta x} = \frac{(f_{j+1}-f_j)+\theta(\Delta f_{j+1}-\Delta f_j)}{\Delta x} \quad (2.11)$$

## 3. Function value

$$f \approx \bar{f} = 0.5(f_{j+1} + f_j) + 0.5\theta(\Delta f_{j+1} + \Delta f_j) \quad (2.12)$$

Using the definitions in equations 2.10, 2.11, and 2.12, equations 2.4, 2.5, 2.6, and 2.7 can be approximated as finite difference equations.

Beginning by writing the continuity equations, 2.4 and 2.5, as differences, and adding them together

$$\Delta Q + \frac{\Delta A_f}{\Delta t} \Delta x_f + \frac{\Delta A_c}{\Delta t} \Delta x_c + \frac{\Delta S}{\Delta t} \Delta x_f - \bar{Q}_l = 0 \quad (2.13)$$

where  $\bar{Q}_l$  is the average lateral inflow.

Writing the momentum equations 2.6 and 2.7 as finite difference equations and adding them together yields

$$\frac{\Delta(\varphi Q \Delta x_c + (1-\varphi) Q \Delta x_f)}{\Delta t} + \Delta(\beta V Q) + g \bar{A} (\Delta Z + \bar{S}_f \Delta x_e) = 0 \quad (2.14)$$

where  $\Delta x_e$  is defined as an equivalent flow path,  $V$  is the cross-sectional average flow velocity, and  $\beta$  is a velocity distribution factor

$$\Delta x_e = \frac{(A_{cj} + A_{cj+1}) \Delta x_{cj} + (A_{fj} + A_{fj+1}) \Delta x_{fj}}{A_j + A_{j+1}} \quad (2.15)$$

$$V = \frac{Q}{A_c + A_f} \quad (2.16)$$

$$\beta = \frac{(V_c \varphi Q + V_f (1 - \varphi) Q)}{QV} \quad (2.17)$$

Equations 2.13 and 2.14 yield a non-linear system of algebraic equations. While there are many robust computational techniques to solve such a system of equations (Bradie 2006; Brunner 2010a; Chang 2002; Sturm 2010), Preissmann proposed a more efficient method of computation by linearizing the equations as outlined in detail by Brunner (2010a) and presented here.

$$C1_j \Delta Q_j + C2_j \Delta Z_j + C3_j \Delta Q_{j+1} + C4_j \Delta Z_{j+1} = CB_j \quad (2.18)$$

$$M1_j \Delta Q_j + M2_j \Delta Z_j + M3_j \Delta Q_{j+1} + M4_j \Delta Z_{j+1} = MB_j \quad (2.19)$$

where the coefficients are calculated as:

$$C1_j = \frac{-\theta}{\Delta x_{ej}} \quad (2.20)$$

$$C2_j = \frac{0.5}{\Delta t \Delta x_{ej}} \left[ \left( \frac{dA_c}{dz} \right)_j \Delta x_{cj} + \left( \frac{dA_f}{dz} + \frac{dS}{dz} \right)_j \Delta x_{fj} \right] \quad (2.21)$$

$$C3_j = \frac{\theta}{\Delta x_{ej}} \quad (2.22)$$

$$C4_j = \frac{0.5}{\Delta t \Delta x_{ej}} \left[ \left( \frac{dA_c}{dz} \right)_{j+1} \Delta x_{cj} + \left( \frac{dA_f}{dz} + \frac{dS}{dz} \right)_{j+1} \Delta x_{fj} \right] \quad (2.23)$$

$$CB_j = -\frac{Q_{j+1} - Q_j}{\Delta x_{ej}} + \frac{Q_l}{\Delta x_{ej}} \quad (2.24)$$

$$M1_j = \frac{\Delta x_{cj}\varphi_j + \Delta x_{fj}(1-\varphi_j)}{2\Delta t\Delta x_{ej}} - \frac{\beta_j V_j \theta}{\Delta x_{ej}} + \theta g \bar{A} \frac{S_{fj}}{Q_j} \quad (2.25)$$

$$M2_j = g\theta \left( \left( \frac{(Z_{j+1}-Z_j)}{2\Delta x_{ej}} + \frac{\bar{S}_f}{2} \right) \left( \frac{dA}{dz} \right)_j - \frac{\bar{A}S_{fj}}{K_j} \left( \frac{dK}{dZ} \right)_j - \frac{\bar{A}}{\Delta x_{ej}} \right) \quad (2.26)$$

$$M3_j = \frac{\Delta x_{cj}\varphi_{j+1} + \Delta x_{fj}(1-\varphi_{j+1})}{2\Delta t\Delta x_{ej}} - \frac{\beta_{j+1} V_{j+1} \theta}{\Delta x_{ej}} + \frac{\theta g \bar{A} S_{fj+1}}{Q_{j+1}} \quad (2.27)$$

$$M4_j = g\theta \left( \left( \frac{(Z_{j+1}-Z_j)}{2\Delta x_{ej}} + \frac{\bar{S}_f}{2} \right) \left( \frac{dA}{dz} \right)_{j+1} - \frac{\bar{A}S_{fj+1}}{K_{j+1}} \left( \frac{dK}{dZ} \right)_{j+1} + \frac{\bar{A}}{\Delta x_{ej}} \right) \quad (2.28)$$

$$MB_j = \frac{\beta_{j+1} V_{j+1} Q_{j+1} - \beta_j V_j Q_j + g \bar{A} (Z_{j+1} - Z_j)}{\Delta x_{ej}} + g \bar{A} (\bar{S}_f) \quad (2.29)$$

In addition to equations 2.18 and 2.19, the system requires two boundary conditions to close the system. The required boundary conditions are a flow hydrograph at the upstream of the river reach and a stage hydrograph, or stage discharge relationship at the downstream cross-section of the river reach.

As mentioned, the implicitly defined Preissmann scheme is known to be stable under most conditions. There have been many studies, both analytical and numerical, demonstrating the stability of the method (e.g. Lyn and Goodwin 1987; Samuels and Skeels 1990; Szymkiewicz 1996; Venutelli 2002), and the conditions under which stability is unconditional. Most of the studies use the von Neumann stability analysis method which expresses the finite difference equations in terms of the Fourier components (Bradie 2006). By this method stability has been shown unconditionally for  $\theta \geq 0.5$  (Brunner 2010a; Lyn and Goodwin 1987; Samuels and Skeels 1990; Sturm 2010).

## 2.2 Hydrologic Flood Routing

Hydrologic flood routing is based upon the unsteady 1D continuity equation, which is a statement of mass conservation, and a simplified storage-discharge relationship (Aldama 1990; Kim et al. 2001; Todini 1988). There have been many such flood routing models proposed with varying levels of complexity e.g. the Muskingum method, the Muskingum-Cunge method, the modified Att-Kin method, and the kinematic wave approximation (Chang et al. 1983; Dooge and Napiórkowski 1987; McCuen 1998; Moussa and Bocquillon 1996; Sivapalan et al. 1997; Todini 1988; Yen and Tsai 2001). Of these, one promising method is a link based model developed from the mass continuity equation (Gupta and Waymire 1998; Jothityangkoon and Sivapalan 2003; Mantilla and Gupta 2005; Mantilla et al. 2006; Menabde and Sivapalan 2001; Reggiani et al. 2001).

The link based model separates a river reach into finite segments and constructs for each link the continuity equation with the upstream boundary condition equal to the discharge from the upstream links of the stream network. The method results in a system of coupled ordinary differential equations (ODEs) which in general are nonlinear, but can be made linear under certain simplifying velocity discharge relationships. The governing equations of this model are derived from the mass continuity equation as:

Beginning with the unsteady 1D continuity equation 2.1, and integrating over the length of the link

$$\int_0^L \left( \frac{\partial A}{\partial t} + \frac{\partial Q}{\partial x} - q_l \right) dx = \int_0^L \frac{\partial A}{\partial t} dx + Q|_0^L - q_l|_0^L \quad (2.30)$$

Recognizing that the length of the link,  $L$ , is not dependent on time and that the lateral inflow is 0 at the beginning of the link, equation 2.30 becomes

$$\frac{\partial L\bar{A}}{\partial t} = \frac{dS}{dt} = I - Q + R \quad (2.31)$$

where  $\bar{A}$  is the average cross-sectional area over the length of the link as defined by the Mean Value theorem for integration,  $S$  is the storage within the link,  $I$  is the total inflow from the upper links,  $Q$  is the total outflow from the link, and  $R$  is the total runoff entering into the link.

From the continuity equation, a relationship between flow and velocity can be derived as follows (Henderson 1966):

$$q = VA \quad (2.32)$$

Where  $q$  is the flow passing through a cross-section,  $V$  is the cross-sectional average velocity normal to the cross-section area, and  $A$  is the area of the cross-section.

Because the average cross-sectional area over the link is always greater than or equal to zero, and the outflow,  $Q$ , is always greater than or equal to zero, the Intermediate Value theorem for calculus guarantees the existence of a velocity,  $V_c$ , such that:

$$\bar{A} = \frac{Q}{V_c} \quad (2.33)$$

where in general, all the parameters are functions of time.

Several authors have suggested that  $V_c$  is a function of the outflow,  $Q$  (Jothityangkoon and Sivapalan 2003; Mantilla and Gupta 2005; Mantilla et al. 2006; Mantilla 2007; Menabde and Sivapalan 2001; Reggiani et al. 2001) such that:

$$V_c = v_0 Q^{\lambda_1} A_d^{\lambda_2} \quad (2.34)$$

where  $v_0$ , is a reference velocity,  $A_d$ , is the drainage area for the basin at the link outlet, and  $\lambda_1$ , and  $\lambda_2$ , are parameters derived from a combination of geomorphic and hydraulic relationships (Mantilla 2007).

By combining equations 2.31, 2.33, and 2.34, a nonlinear ODE for  $Q$  is derived which can be solved by one of many robust computational schemes

$$\frac{dQ}{dt} = \frac{V_c}{L(1-\lambda_1)} (I - Q + R) \quad (2.35)$$

The model equation of 2.35 is implemented in a powerful geographic information system (GIS) platform, CUENCAS (Mantilla and Gupta 2005; Mantilla 2009). CUENCAS is capable of complete watershed analysis, and will be used in comparing hydrologic flood routing with hydraulic flood routing.

### 2.3 Hydraulic Geometry

There is great interest among geologists, geomorphologists, and hydraulic engineers to provide a quantitative description of river channel geometry and hydraulic characteristics (Leopold and Maddock 1953; Park 1976; Phillips and Harlin 1984) Since the seminal work of Leopold and Maddock (1953), the classical approach to the quantitative description of channel geometry has been to use observed power law relationships, known as hydraulic geometry relations, that relate cross-sectional hydraulic characteristics to discharge (Dingman 2007; Singh 2003; Singh et al. 2003; Stewardson 2005). The variables expressed through these power laws are most commonly top width, hydraulic depth, mean velocity, mean slope, and mean friction (Knighton 1975; Singh et al. 2003).

There are two proposed forms of hydraulic geometry, downstream hydraulic geometry, and at-a-station hydraulic geometry (Leopold and Maddock 1953). Downstream hydraulic geometry is a method to describe how cross-sectional properties and channel form change in the downstream direction for a given frequency in discharge.

The alternative, at-a-station hydraulic geometry, is the quantitative description of how cross-sectional properties and channel form vary at a given cross-section with different frequency discharges. A thorough description of the development of these two concepts is provided in Leopold and Maddock (1953).

While the hydraulic geometry relationships were initially developed from observed datasets, many researchers have made attempts to deduce the power law form from theoretical arguments (e. g. Dingman 2007; Singh 2003; Singh et al. 2003; Singh and Zhang 2008). The most common approach to deriving hydraulic geometry relationships is from the continuity equation, a resistance equation, the sediment transport equation, and a morphologic relation (Dingman 2007; Eaton and Church 2007; Huang and Nanson 2000; Singh 2003; Yang et al. 1981). The morphologic relationship is derived from various hypotheses, usually extremal in nature such as minimum or maximum entropy. An extensive review of these hypotheses is provided by Singh (2003).

The relationships for hydraulic geometry are:

$$W = aQ_m^b \quad (2.36)$$

where  $W$ , is the top width,  $a$  and  $b$  are constants, and  $Q_m$  is bankfull discharge.

Bankfull discharge,  $Q_m$ , has been measured by many researchers, and related to flow frequency. Most often the bankfull discharge is reported to occur with a return period between 1.0 and 2.0 years (Castro and Jackson 2001; Johnson and Heil 1996; Wilkerson 2008; Williams 1978). Due to this result,  $Q_m$  was estimated using the 2001 USGS regression equations for Iowa with a return period of 2.0 years (Eash 2001).

$$D = cQ_m^f \quad (2.37)$$

where  $D$  is the hydraulic depth defined as cross-sectional area divided by the top width (Harman et al. 2008; Henderson 1966), and  $c$  and  $f$  are constants.

$$V = kQ_m^m \quad (2.38)$$

where  $V$  is the cross-sectional average velocity, and  $k$  and  $m$  are constants.

The constants  $a$ ,  $c$ ,  $k$ ,  $b$ ,  $f$ , and  $m$  have been measured by numerous researchers in various regions of the world (e. g. Dodov and Foufoula-Georgiou 2004; Leopold and Maddock 1953; Phillips and Harlin 1984; Stewardson 2005). While there has been some variation in observed values reported, the coefficients are bound by the theoretical constraints:

$$ack = 1.0; \quad b + f + m = 1.0 \quad (2.39)$$

There have been a few researchers that have extended the concept of hydraulic geometry to use drainage area as the independent variable rather than discharge (Singh 2003). Mejia and Reed (2011b) suggested a relationship between channel bed slope and drainage area as follows

$$S_o = \varepsilon A_d^\vartheta \quad (2.40)$$

where  $S_o$ , is the channel bed slope,  $\varepsilon$  and  $\vartheta$ , are constants.

Given the wide variation in reported in the literature, it is necessary to define the values used in the present study. A summary of the exponents and coefficients used in equations 2.36, 2.37, and 2.40, are found in Table 1.

<b>Variable</b>	<b>coefficient</b>	<b>exponent</b>	<b>source</b>
W	16	0.11	Stewardson (2005)
D	0.51	0.28	Stewardson (2005)
S <sub>o</sub>	0.015	-0.31	Mejia and Reed (2011b)

Table 1 Coefficients and exponents used for hydraulic geometry relationships

### 2.4 Horton Order and Stream Scaling Laws

There is a great deal of empirical evidence suggesting that river networks are governed by scaling laws (Dodds and Rothman 1999; Maritan et al. 1996; Reis 2006). Theoretical and experimental research has shown scaling laws exist for both topological and geometric properties (Abrahams 1984; Dodds and Rothman 1999; Maritan et. al 1996; Scheidegger 1968a, 1968b; Strahler 1957). These scaling laws are most often formulated based upon exponents and ratios of fundamental watershed quantities and hold true in a statistical sense for natural river networks (Beer and Borgas 1993; Dodds and Rothman 1999; Peckham and Gupta 1999). However, study of these well-known empirical observations of scaling laws has not yielded a fundamental understanding of their origin in nature (Dodds and Rothman 1999).

#### 2.4.1 Horton Ordering

The quantitative study of river networks and the recognition of scaling laws in network properties began with the seminal work of Horton in 1945 (Abrahams 1984; Horton 1945; Peckham 1995; Scheidegger 1968a; Strahler 1957). Horton first introduced the concept of stream ordering to subdivide a river network into major and minor tributaries (Abrahams 1984; Peckham 1995). Horton's method of stream ordering was slightly modified by Strahler (1957) to provide an objective, purely topological method to

enumerate stream order (Dodds and Rothman 1999; Peckham 1995; Peckham and Gupta 1999; Scheidegger 1968a; Strahler 1957). This modified Horton (Horton-Strahler) ordering is the basic tool used in river network analysis (Dodds and Rothman 1999; Peckham and Gupta 1999; Strahler 1957).

There are two common methods for describing the Horton-Strahler ordering scheme, one a natural, intuitive pruning technique, and the other a recursive assignment rule (Dodds and Rothman 1999; Peckham 1995; Peckham and Gupta 1999). Both approaches are equivalent and view a river network as a topological tree graph, rooted at the network outlet and with exterior links given the lowest order, 1.

The first technique to describe Horton-Strahler ordering is the pruning technique first described by Melton (Dodds and Rothman 1999; Melton 1959; Peckham 1995; Peckham and Gupta 1999). The technique allows for an insightful and natural definition of Horton-Strahler streams. The method begins by considering a river network with exterior streams considered as source streams. The idea of Melton was to prune all of these exterior links and their downstream nodes and classify them as order 1 streams. After the pruning process, a coarser river network remains, again with external links that have no incoming tributaries and are comprised of what was a contiguous chain of interior links. Again the exterior links and their downstream nodes are pruned and these are classified as order 2 streams. The procedure is repeated with the exterior links classified order  $(k-1)$  after the  $k$ th iteration of pruning. After a finite number of pruning iterations the tree is reduced to a single stream which is the highest order stream in the network and the trunk of the tree rooted at the outlet. As pointed out by Peckham (1995), a natural definition for Horton-Strahler streams are channels that remain invariant under this process of pruning way exterior links without being severed.

Horton-Strahler ordering can also be defined using a recursive rule as follows. All exterior links are labeled as order 1 streams. For each interior link, the link is assigned the highest order of the incoming tributaries at a node, or if two links of equal order,  $\omega$ , enter

at a node, the downstream link is assigned order  $\omega+1$ . In other words the stream order only increases when two streams of equal order come together, otherwise the highest order is maintained by the outflowing stream. In mathematical terms, at each node the assigned order of the downstream link is given by

$$\omega = \max(\omega_1, \omega_2) + \delta(\omega_1, \omega_2) \quad (2.41)$$

where  $\delta()$  is the Kronecker delta,  $\omega$  is the outflowing stream order, and  $\omega_1, \omega_2$  are the stream orders of inflowing tributaries.

#### 2.4.2 Horton's Law of Stream Numbers

One of the first steps in river network analysis is counting stream segments of each order and analyzing how their numbers change with increasing order (Strahler 1957). Horton first recognized that a ratio of the number of streams of consecutive orders is independent of stream order (Dodds and Rothman 1999; Peckham and Gupta 1999; Scheidegger 1968a; Strahler 1957). This ratio, defined by equation 2.42, is referred to as the bifurcation ratio. The bifurcation ratio has a theoretical lower limit of 2.0, which comes from the fact that at least two streams are required a stream order to increase (Beer and Borgas 1993). Various researchers have reported the bifurcation ratio to be between 2.0 - 4.0 (e.g. Scheidegger 1968a; Strahler 1957).

$$R_B = \frac{N_i}{N_{i+1}} \quad (2.42)$$

where  $R_B$  is the bifurcation ratio,  $N_i$  is the number of streams with order  $i$ , and  $N_{i+1}$  is the number of streams with order  $i+1$ .

From the definition of the bifurcation ratio, Horton's law of stream numbers naturally follows as equation 2.43. Horton's law of stream numbers has given rise to the

concept of structurally Hortonian river networks (Scheidegger 1968a). A network is structurally Hortonian if all complete basins and subbasins in a network follow the same bifurcation ratio as the network itself. There have been several researchers that have attempted to rationalize the observed adherence to Horton's law of stream numbers using hypothesis of structurally Hortonian networks. While it is clear that all structurally Hortonian networks follow Horton's law of stream numbers, there are also structurally not Hortonian networks that obey this law (Scheidegger 1968a). Scheidegger (1968a) arguing that not all river networks in nature are structurally Hortonian, conducted a simulation of random topological trees with no assumption of structure. The results of the simulation were that in dealing with statistical expectation values, Horton's law of stream numbers holds for structurally Hortonian networks as well as with the random topological networks which have an equal probability of structurally Hortonian and non-Hortonian constructs. Other researchers have confirmed that observed networks in nature quickly converge to a constant bifurcation ratio as the greatest order of the stream increases toward infinity (Peckham 1995).

$$N_{\omega} = R_B^{\Omega - \omega} \quad (2.43)$$

where  $\Omega$  is the maximum order of the basin, i.e. the order of the link terminating at the basin outlet.

#### 2.4.3 Horton's Law of Stream Lengths

Horton's law of stream numbers is a purely topological result, but a similar result can be developed for geometric characteristics of a river network. A ratio, known as Horton's length ratio can be defined as equation 2.44, and from that definition a statistical law of stream lengths can be derived (equation 2.45). Observations in natural stream

networks have shown that Horton's length ratio varies between 1.5 and 3.0 (Dodds and Rothman 1999; Scheidegger 1968b).

$$R_L = \frac{\overline{L_{i+1}}}{\overline{L_i}} \quad (2.44)$$

$$\overline{L_\omega} = \overline{L_1} R_L^{\omega-1} \quad (2.45)$$

where  $R_L$  is the Horton's length ratio,  $\overline{L_{i+1}}$  is the average length of streams of order  $i+1$ ,  $\overline{L_i}$  is the average length of streams of order  $i$ ,  $\overline{L_\omega}$  is the average length of streams of order  $\omega$ , and  $\overline{L_1}$  is the average length of streams with order 1.

There have been various researchers that have attempted to develop a rational explanation of Horton's law of stream lengths (e.g. Dodds and Rothman 1999; Peckham and Gupta 1999; Scheidegger 1968b). One common hypothesis is that the constancy of the Horton length ratio is an outcome of the fact that river networks are self-similar with regard to stream order, but this assumption implies that river networks are structurally Hortonian (Scheidegger 1968b). This is not the case in natural river networks however because, as demonstrated by Scheidegger (1968b), such an assumption leads to the relationship that the bifurcation ratio is equivalent to the length ratio, which is not observed in nature. Scheidegger (1968a, 1968b) suggested that difficulties between these relationships may be rooted in the fact that of the statistical ensemble of possible river networks there are certainly networks that are structurally non-Hortonian. While Horton's law of stream lengths does not hold exact for all natural river networks, it has been shown to hold in a statistical average (Peckham 1995, Scheidegger 1968b). Furthermore, this asymptotic convergence of Horton's laws has been shown to occur rapidly for networks greater in order than 3 (Peckham 1995, Scheidegger 1968b).

#### 2.4.4 Horton's Law of Drainage Areas

One final statistical law that is useful in analysis of natural river networks is Horton's law of drainage areas. Beginning again by defining the Horton's area ratio, equation 2.46, Horton's drainage area law is derived as equation 2.47. In natural river networks Horton's area ratio has been observed to range between 3.0 and 6.0 (Abrahams 1984; Dodds and Rothman 1999).

$$R_A = \frac{\overline{A_{i+1}}}{\overline{A_i}} \quad (2.46)$$

$$\overline{A_\omega} = \overline{A_1} R_A^{\omega-1} \quad (2.47)$$

where  $R_A$  is the Horton area ratio,  $\overline{A_{i+1}}$  is the average drainage area for streams of order  $i+1$ ,  $\overline{A_i}$  is the average drainage area of Horton streams with order  $i$ ,  $\overline{A_\omega}$  is the average drainage area of streams with order  $\omega$ , and  $\overline{A_1}$  is the average drainage area of Horton order 1 streams.

Similar to the Horton laws for stream numbers and lengths, Horton's law of drainage areas has been shown to hold well for natural river networks (Dodds and Rothman 1999; Peckham 1995; Strahler 1957).

#### 2.4.5 Hack's Law

One of the most well-known and widely discussed scaling laws observed in natural river networks is Hack's law (Dodds and Rothman 1999; Maritan et. al. 1996; Rigon et. al. 1996). Hack demonstrated the applicability of a power function in relating the drainage area of a basin to the length of the principal river of the basin (Maritan et. al. 1996; Rigon et. al. 1996). The exponent observed in nature varies from region to region, but is typically reported to be slightly below 0.6 (Rigon et. al. 1996). As such, Hack's law is typically stated as

$$L \propto A^h \quad h > 0.5 \quad (2.48)$$

where  $L$  is the length of the longest stream in the river network, known as the diameter of the tree in graph theory (Peckham 1995),  $A$  is the drainage area of the basin, and  $h$  is referred to as Hack's exponent. In this study, the Hack's exponent is equated to 0.53 and a coefficient of proportionality is used to produce equivalence of 1355 meters. The drainage area is used in square kilometers.

One of the most intriguing aspects of Hack's law is that the exponent is not equal to 0.5 as would be expected from dimensional analysis (Dodds and Rothman 1999). This departure from the Euclidean value of 0.5 led to early speculations on the fractal nature of river networks (Maritan et. al 1996). An exponent of 0.5 would be expected also if there was geometric similarity preserved as drainage basins increase in area downstream, and the fact that  $h > 0.5$  indicates anisotropy in the basin shape (Maritan et. al. 1996; Rigon et. al. 1996). The classical explanation is that Hack's exponent is due to a tendency of basins to elongate, or grow faster in length than in width, but this is still a point of much debate among researchers (Maritan et. al. 1996; Peckham 1995; Rigon et. al. 1996).

Using both theoretical arguments and analysis of real river networks from digital elevation models (DEMs), Rigon et. al. (1996) showed that Hack's exponent could be related to fractal sinuosity in river channels and to basin elongation, with the major contribution being fractal sinuosity. The research of Rigon et. al. (1996) confirmed that river networks tend to elongate in nature and that basin shapes are self-affine. It was also reported that Hack's law, like the Horton laws, only hold true in a statistical sense (Dodds and Rothman 1999; Peckham 1995; Rigon et. al. 1996).

Using the arguments that river channels are self-affine curves, river networks are topologically self-similar, and that drainage density (stream length per area) is uniform, both Peckham (1995), and Dodds and Rothman. (1999), related Hack's exponent to the Horton ratios as

$$h = \frac{\ln(R_L)}{\ln(R_B)} \quad (2.49)$$

#### 2.4.6 Tokunaga Trees

In the study of river networks there are infinite classes of trees which can be used for models. These network models can be either random or deterministic in nature (Abrahams 1984; Mantilla 2007; Peckham 1995; Peckham and Gupta 1999; Scheidegger 1968a, 1968b). Of these various topologic tree models, one useful subset of deterministic self-similar trees are known as Tokunaga trees. Various researchers have been able to use Tokunaga trees to obtain insightful, analytic results which correspond well with those observed in nature (Dodds and Rothman 1999; Menabde and Sivapalan 2001; Peckham 1995). They have also been used to understand the connections between Hack's law and Horton's laws as described in section 2.4.5 (Dodds and Rothman 1999; Peckham 1995).

Tokunaga trees are self-similar in the topologic sense, also referred to as structurally self-similar (Dodds and Rothman 1999; Peckham 1995). To understand what is meant by topologic self-similarity, consider the class of deterministic trees where every stream of order  $\omega$  has  $b \geq 2$  upstream tributaries of order  $(\omega-1)$  and  $T_{\omega,k}$  side tributaries of order  $k$ , where  $\omega$  varies from 2 up to the maximum order of the network,  $\Omega$ , and  $k$  varies from 1 up to  $(\omega-1)$ . Then the numbers  $T_{\omega,k}$  can be arranged into a square lower triangular matrix as (Peckham 1995)

$$\begin{pmatrix} T_{2,1} & 0 & \dots & 0 \\ T_{3,1} & T_{3,2} & \dots & 0 \\ \vdots & \vdots & \ddots & \vdots \\ T_{\Omega,1} & T_{\Omega,2} & \dots & T_{\Omega,\Omega-1} \end{pmatrix} \quad (2.50)$$

This set of numbers will define a self-similar tree if the matrix in equation 2.50 is a Toeplitz matrix, or in other words the values are constant along the diagonals such that

$$T_{\omega, \omega-k} = T_k \quad (2.51)$$

Self-similar trees require, in general,  $(\Omega-1)$  parameters to completely define the generating matrix defined in equation 2.50. Tokunaga trees have an additional constraint which reduces the number of required parameters to two. The additional constraint that defines Tokunaga trees is as follows

$$\frac{T_{k+1}}{T_k} = R_T \quad (2.52)$$

where  $R_T$  is a fixed constant for a given network. From 2.52 Tokunaga's numbers  $T_k$  can all be defined by two fundamental parameters as

$$T_k = T_1 R_T^{k-1} \quad (2.53)$$

where  $T_1$  is the average number of major side tributaries per stream segment, i.e. there will be on average  $T_1$  side tributaries of order  $(k-1)$  entering a stream of order  $k$  for each segment (Dodds and Rothman 1999).

One famous self-similar Tokunaga tree is the Mandelbrot-Vicsek tree (Mandelbrot and Vicsek 1989). This is a fractal tree constructed by recursive replacement, and can be described using Tokunaga's law (equation 2.53) as (Peckham 1995)

$$T_1 = 0, \quad T_k = 2^{k-2}, \quad k > 1 \quad (2.54)$$

Figure 2 is a Mandelbrot-Vicsek tree at the 4<sup>th</sup> step of recursion, and corresponds to a network of Horton-Strahler order 5. A similar tree will be used further on in the thesis with a Horton-Strahler order 9.

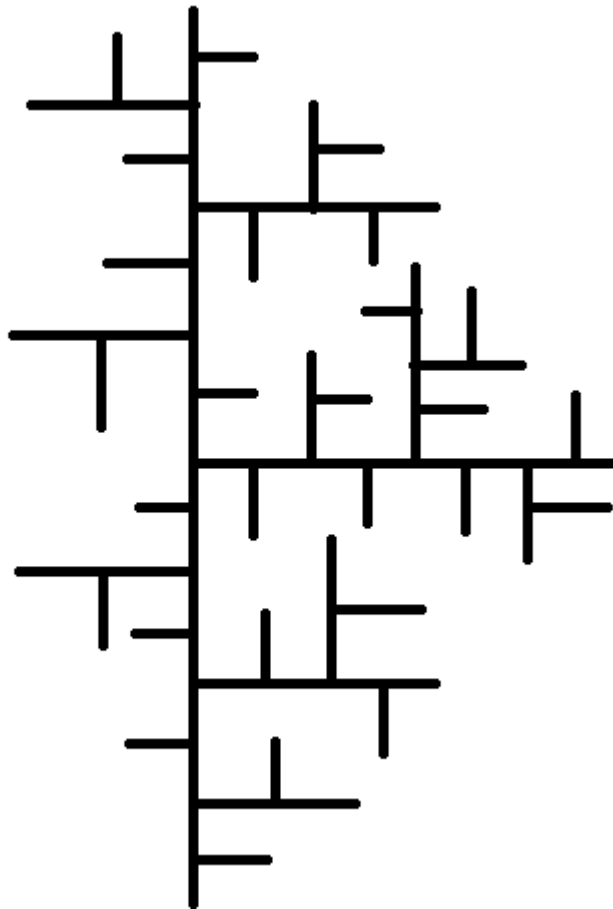


Figure 2 Mandelbrot-Vicsek tree with Horton-Strahler order 5

### 2.4.7 Relation between Tokunaga's Law and Horton's Laws

There have been several authors who have attempted to understand what the relationship is between Tokunaga's law and Horton's laws, most recently Peckham (1995), and Dodds and Rothman (1999) have attempted to understand the connections and how they arise from self-similarity in the topological structure of the network. One important aspect of this research is that it has shown that Horton's laws are not an artifact of the Horton-Strahler ordering scheme (Kirchner 1993; Peckham and Gupta 1999). The study of the relationship between these laws in river networks has given a unified understanding of scaling laws and what properties of river networks lead to them.

Peckham and Gupta (1999) stated that log linearity of Horton plots is a mathematical consequence of the recursive formulas that all self-similar tree graphs obey. Using these relationships, several researchers have shown that Tokunaga's law leads to Horton's laws and other scaling laws under the following three assumptions: 1. river networks are topologically self-similar, 2. individual streams are self-affine curves, and 3. drainage density is uniform across a basin (e. g. Dodds and Rothman 1999; Peckham 1995). These three assumptions are to be discussed in the following paragraphs and then an outline of the derived connection between the various scaling laws.

The first assumption is that river networks are topologically self-similar. This property of self-similarity has been observed in many river networks over a large range of scales (Dodds and Rothman 1999). Self-similarity in the context discussed here is the property by which the matrix of equation 2.50 is a Toeplitz matrix. This essentially means that the relative difference between the number of successive Horton-Strahler order streams is the same for all orders. It is important to note that this property in river networks has a physical range of applicability, namely an upper limit which is the overall scale of the landscape, and a lower limit which is the characteristic separation of channels (Dodds and Rothman 1999). This can be understood that at the smallest scales processes

are dominated by the hillslope dynamics and at the largest scales processes are dominated by the geologic structure of the region, and at the intermediate scales, self-similarity arises in the network topology.

The second assumption is that individual stream shapes are self-affine (Dodds and Rothman 1999). This assumption is consistent with the work and observation of others (Maritan et. al. 1996; Rigon et. al. 1996) who found that both main channels and watershed boundaries are self-affine curves. The main consequence of this assumption is that streams grow in length at a faster rate than the basin does, and the basin grows in length at a faster rate than it does in width. This property has been observed in many natural watersheds throughout the world and is one of the main contributing factors to Hack's exponent being greater than 0.5 (Dodds and Rothman 1999; Peckham 1995; Rigon et. al. 1996).

The third, and final assumption made is that the drainage density is uniform throughout a watershed or basin (Dodds and Rothman 1999). Drainage density is a measure of average area drained per unit length of stream (Strahler 1957). A uniform drainage density can also be interpreted as the average distance between channels remains constant throughout the watershed (Dodds and Rothman 1999). This assumption has been found to be consistent with observations in nature (Dodds and Rothman 1999).

One of the first recursion relationships that arise naturally from Tokunaga's law (equation 2.53) is an expression for number of streams of a given order. This has been recognized by many to lead directly to Horton's law of stream numbers (equation 2.43) (Dodds and Rothman 1999; Peckham 1995). The expression for binary trees shown in equation 2.55 is presented both by Peckham (1995), and Dodds and Rothman (1999), where the definition for binary trees is given as those trees in which each stream of Horton-Strahler order  $\omega+1$  is headed by two streams of order  $\omega$ . It should be noted that order  $\omega$  streams can appear as side tributaries as well for any stream with order greater

than  $\omega$ . Given this condition of binary trees, Tokunaga trees follow the following relationship where the total number of streams,  $N_\omega$ , is given as

$$N_\omega = 2N_{\omega+1} + \sum_{k=1}^{\Omega-\omega} T_k N_{\omega+k} \quad (2.55)$$

Combining equation 2.55 with 2.53 and 2.43, Horton's bifurcation ratio is expressed in terms of the Tokunaga parameters as (Peckham 1995; Dodds and Rothman 1999)

$$R_B = \frac{1}{2} \left[ (2 + R_T + T_1) + \sqrt{(2 + R_T + T_1)^2 - 8R_T} \right] \quad (2.56)$$

Following from the assumption that the tributaries are evenly spaced and drainage density is uniform, Peckham (1995) developed the following expressions for the remaining Horton's ratios which hold true asymptotically in all Tokunaga trees

$$R_L = R_T \quad (2.57)$$

$$R_A = R_B \quad (2.58)$$

The redundancy found in equation 2.58 leads to the conclusion that there are only two independent Horton's ratios,  $R_B$ , and  $R_L$ , which compares with the two independent Tokunaga parameters (Dodds and Rothman 1999). Furthermore, the relationships can be inverted as shown by Dodds and Rothman (1999) such that the Tokunaga parameters are obtained by the two independent Horton ratios.

This invertible transformation between the parameters in Tokunaga's law and the Horton's ratios, in addition to the fact that there are only two independent Horton's ratios, leads to the conclusion that the Horton's laws are equivalent to Tokunaga's law (Dodds

and Rothman 1999). Dodds and Rothman further demonstrated that from the independent Horton's ratios and the fractal dimension of an individual stream channel, all other commonly used scaling laws can be derived. This result demonstrates the power and utility of the Horton's laws and the recognition of self-similarity in river networks.

## CHAPTER III: THE EFFECT OF CROSS-SECTIONAL PROPERTIES ON FLOOD ROUTING

Geometric and hydraulic properties of a cross-section play an important role in hydraulic flood routing, due to their influence on storage capacity and conveyance in the channel and floodplain (Ghavasieh et al. 2006; Mejia and Reed 2011a, 2011b). Because of this effect on the flow dynamics of a channel, and the considerable uncertainty in observing these parameters, many researchers have studied the impacts on flow attributed to the cross-section (e. g. Anderson et al. 2006; Johnson 1996; Myers 1991; Sholtes and Doyle 2011; Wohl 1998; Wolff and Burges 1994; Woltemade and Potter 1994). However, the primary focus of other studies has been either how flood frequency is modified by geometric properties, or how a particular geometric shape can affect the flood hydrograph (Mejia and Reed 2011a, 2011b; Orlandini and Rosso 1998). Little research has been found that considers variability in geometric scale of the cross-section and a comparison over a range of watershed scales, therefore the purpose of this chapter is to present an analysis of the effect of variability in cross-sectional properties on flood routing, with an emphasis on geometric scale and hydraulic resistance. The analysis is repeated for several basin sizes.

### 3.1 Model Framework

HEC-RAS was chosen to conduct the proposed simulations because it is widely and readily available, and it numerically solves the 1D Saint Venant equations (Brunner 2010a, 2010b). This provides a more general flood routing method, potentially eliminating error due to simplification of the flow dynamics (Henderson 1966; Mejia and Reed 2011a; Sturm 2010; Wormleaton and Karmegam 1984), which allows for a more direct evaluation of the effect from cross-sectional properties.

The model stream to be simulated is a straight channel with no lateral inflows along its length. The cross-section geometry is a simplified compound trapezoid to be

described in section 3.1.2. The length of the stream channel and the width parameters in the cross-section geometry are scaled with respect to the Horton order of the simulated stream. For each model the cross-sections are spaced at intervals of approximately 15 times the mean channel width (Castellarin et al 2009).

Monte Carlo (MC) simulation was chosen as the method of experimentation. Because of the highly nonlinear system with no known analytical solution, standard methods of uncertainty analysis could not be performed, so MC provided the most direct solution (Chang et al. 1994). Using the MC method, one thousand simulations were performed for each Horton order stream from order 1-9.

### 3.1.1 Inflow Hydrograph

The upstream boundary condition for the simulations is a flood hydrograph. For the simulations it was decided to choose a single peak hydrograph with a steep rising limb and gradual falling limb, as is often observed in nature (Hager et al. 1986; Henderson 1966). The hydrographs used were kept constant for all simulations for their respective Horton order. The peak discharge,  $Q_p$ , was scaled along with the time to peak discharge,  $t_p$ , according to the Horton order of the stream.

Much research has been put into synthesis of hydrographs for flood flows (Bhunya et al. 2003, 2008, 2011; McCuen 1998; Mediero et al. 2010; Singh 2009). While most of the methods developed are for unit hydrographs, they still permit appropriate scaling and provide the desired shape characteristics for this study. Of the available methods, the method of fitting a probability density function (pdf) to the hydrograph is used with increasing success (Bhunya et al. 2008, 2011; Pramanik et al. 2010) and was used in this study.

Following the procedure of Bhunya et al. (2003, 2008) a two parameter Gamma distribution is used to derive an inflow hydrograph for each Horton order 1-9. The form of the hydrograph is derived as (Bhunya et al. 2003, 2008; McCuen 1998):

$$Q(t) = Q_p \frac{t^n}{t_p^n} e^{-n\left(1-\frac{t}{t_p}\right)} \quad (3.1)$$

where  $Q_p$ , is the peak discharge,  $t_p$ , is the time to peak discharge,  $t$  is the time ordinate, and  $n$  is a shape parameter derived by Bhunya et al. (2008) as:

$$n \cong 1 + \pi\beta^2 + \beta\sqrt{1 + (\pi\beta)^2} \quad (3.2)$$

and

$$\beta = 0.584 \left(\frac{R_B}{R_A}\right)^{0.55} R_L^{0.05} \quad (3.3)$$

where  $R_B = 4.25$ , is the Horton bifurcation ratio;  $R_A = 4.5$ , is the Horton area ratio;  $R_L = 2.2$  is the Horton length ratio.

The time to peak discharge was calculated for each Horton order stream based on the length of the stream and the relationship from Bhunya et al. (2008)

$$t_p(\omega) = 1.584 \left(\frac{R_B}{R_A}\right)^{0.55} R_L^{-0.38} v^{-1} L_\omega \quad (3.4)$$

where  $v$  is the mean flow velocity in the stream reach and is assumed to be a constant 0.75 m/s for this study, which is consistent with the observations of other researchers (e. g. Blöschl and Sivapalan 1995; Carlston 1969; Leopold 1953; Phillips and Harlin 1984).  $L_\omega$ , is the length of the channel given according to Hack's Law as shown in equation 2.48.

The peak discharge for each Horton order stream was estimated using the 2001 USGS regression equation for the 100 yr return period flow (modified for S. I units) as (Eash 2001)

$$Q_p(\omega) = 50.97(0.386Ad_\omega)^{0.415} \quad (3.5)$$

where  $Ad_\omega$  is the drainage area for the Horton order stream calculated according to equation 2.47.

Combining equations 3.1 through 3.5 and adding an assumed baseflow similar to Wolff and Burges (1994), the final form of the inflow hydrograph is:

$$Q(t, \omega) = Q_p(\omega) \left( 0.3 + \frac{t}{t_p(\omega)} e^{-n \left( 1 - \frac{t}{t_p(\omega)} \right)} \right) \quad (3.6)$$

The hydrograph of equation 3.6 provides flow magnitudes that are expected to be out of bank for a given Horton order stream, and resemble conditions that are likely in a design flood scenario. Using equations 3.4 and 3.5, with addition of the assumed baseflow, Table 2 lists the peak discharge and time to peak discharge for each of the corresponding Horton orders 1-9. Figure 3 is a plot of the inflow hydrographs used in the simulations.

Horton order	tp (hr)	Qp (cms)
1	0.17	17
2	0.37	32
3	0.83	60
4	1.8	112
5	4	208
6	9	389
7	20	727
8	45	1356
9	99	2531

Table 2 Time to peak discharge and peak discharge of the inflow hydrograph for each Horton order

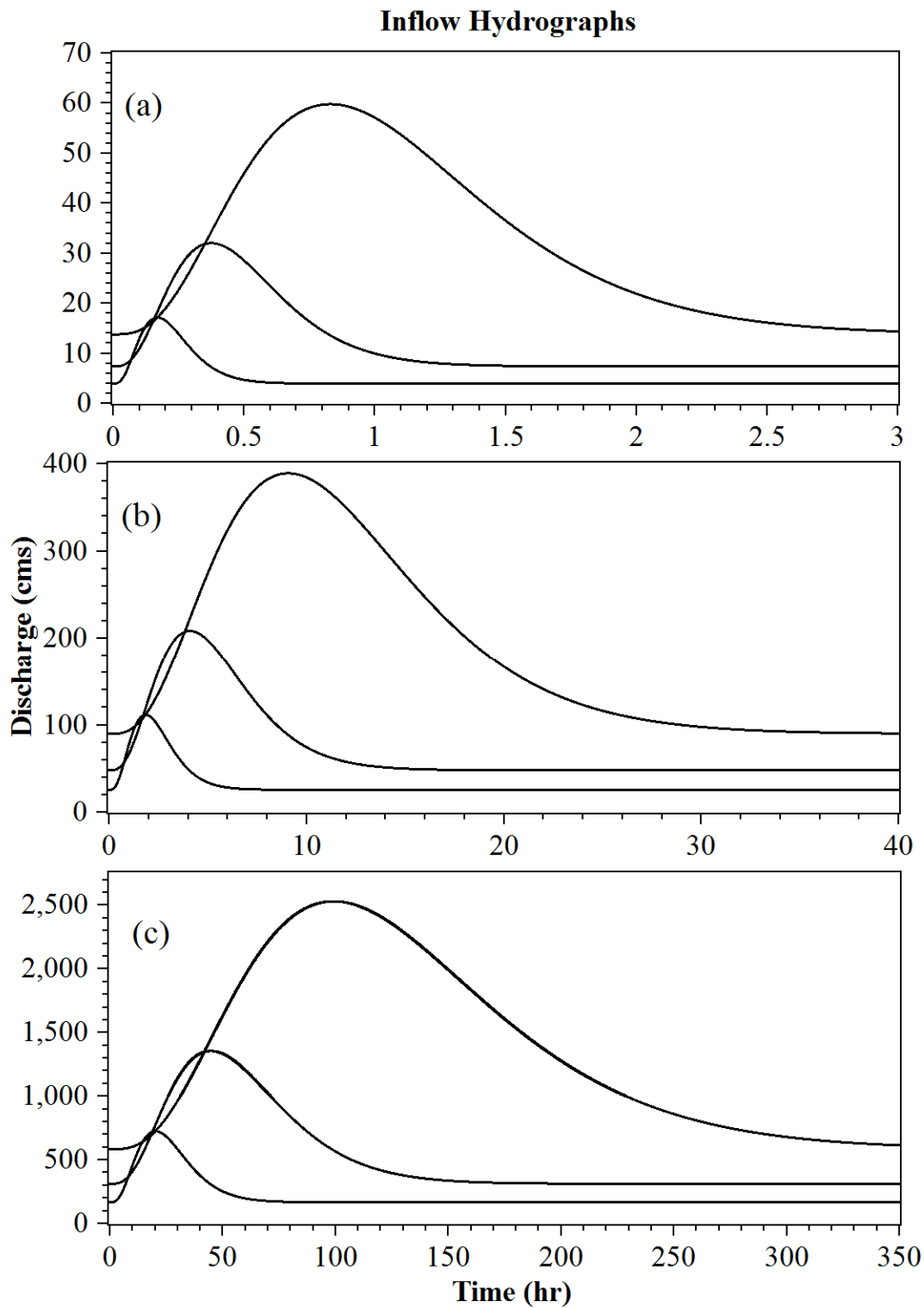


Figure 3 Inflow hydrographs used in simulations. (a) Horton orders 1-3 (b) Horton orders 4-6 (c) Horton orders 7-9

### 3.1.2 Downstream Boundary Condition and Initial Condition

Since the Saint Venant equations form a hyperbolic system of equations, a boundary condition is required at both ends of the channel (Dooge 1982; Henderson 1966, Sturm 2010). In the absence of a known control structure in the channel, a commonly used downstream boundary condition for flood routing is normal depth at the downstream cross-section (Brunner 2010a, Sturm 2010). While this is rarely the case in natural channels, it provides a way to systematically apply a boundary condition to the simulations that is consistent with engineering practice. For this reason the downstream boundary condition is assumed normal depth for all simulations.

The Saint Venant equations also require an initial condition of the water surface at the start of the simulation. The standard practice, unless other information is available, is to assume the channel flow is at steady state for sufficient time that the water surface in the channel has reached its steady state level prior to the simulation (Brunner 2010a). For all simulations performed an initial condition of steady state flow is assumed using the baseflow as the initial flow condition.

### 3.1.3 Channel Geometry

Channel geometry is a combination of all relevant geometric properties to the simulations, specifically the cross-sectional form and scale, the river channel length, and the bed slope of the channel. For the simulations, each of these properties was scaled according to the Horton order and the relationships presented in Chapter 2 and the scaling parameters listed in Table 1

The river channel length was developed based upon the Horton law for stream lengths, equation 2.44 for each stream of a given Horton order. Because the emphasis of this study was to understand the influence of variability in cross-sectional properties, the river channel length was maintained constant across simulations.

The bed slope of the channel was based on the drainage area scaling equation 2.40 and the Horton law for areas, equation 2.47. The channel bed slope was assumed constant over the length of the channel and was maintained constant across simulations to prevent its effect from influencing the results.

The cross-section form chosen is a compound trapezoid shown in Figure 4. This geometry was chosen because it is simple, allowing a specific description of the geometric parameters involved (i. e. width and depth), and because the cross-section width varies with depth, unlike rectangular sections, it provides a more realistic approximation to natural river channels (Mejia and Reed 2011a; Orlandini and Rosso 1998).

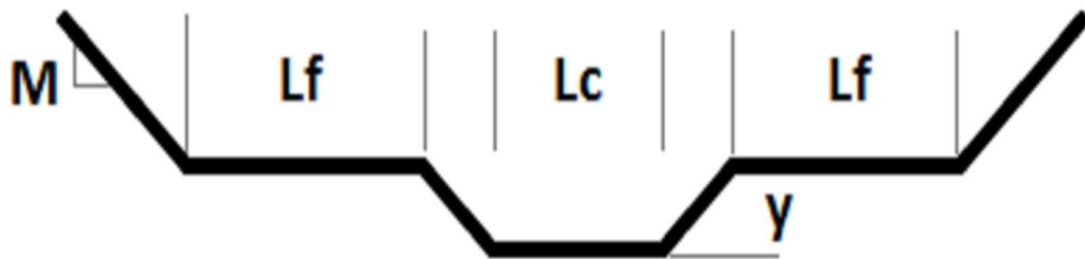


Figure 4 Compound cross-section shape used in simulations

Figure 4 shows the typical cross-section for all simulations. The cotangent of the channel and floodplain side slope,  $M$ , is maintained constant across simulations and Horton order streams as 1:1 H:V. The value was chosen arbitrarily as 1:1 because in natural streams the side slope can vary significantly; therefore there was no clear basis for choosing the value. The bankfull depth,  $y$ , was chosen as the mean hydraulic depth calculated from the hydraulic geometry scaling equation 2.37 and was kept at a constant value for all simulations of a given Horton order.  $L_f$  and  $L_c$  are the floodplain and channel bottom width respectively. Both  $L_f$  and  $L_c$  were considered as random variables

(RVs) for the simulations as will be discussed further in section 3.1.5.  $L_c$  has a mean value for a given Horton order as calculated from the hydraulic geometry relationship equation 2.36 and  $L_f$  has a mean value equal to 4.0 times  $L_c$  which is consistent with Wolff and Burges (1994).

The mean values for the channel geometry used in the simulations are listed in Table 3

<b>Mean Channel Geometry</b>					
Horton order	Channel length (m)	Bed slope (m/m)	y (m)	$L_c$ (m)	$L_f$ (m)
1	300	0.02	0.6	15.8	63.2
2	660	0.01	0.9	17.4	69.6
3	1452	0.008	0.9	18.9	75.6
4	3194	0.005	1.2	20.7	82.8
5	7028	0.003	1.5	22.9	91.6
6	15461	0.002	1.8	25	100
7	34014	0.001	2.1	27.1	108.4
8	74831	0.0007	2.4	29.6	118.4
9	164628	0.0005	3	32.3	129.2

Table 3 Mean geometric properties used in the simulations for each Horton order stream

### 3.1.4 Hydraulic Resistance

In addition to the channel geometry, hydraulic resistance is a significant variable to flood routing (Sturm 2010; Yen 2002). Because of this significance, many researchers have devoted much time towards its estimation (e. g. Henderson 1966; Sturm 2010; Yen 1992, 2002). However; even with modern research there is still much uncertainty in hydraulic resistance estimates (Johnson 1991; Wohl 1998), therefore it is appropriate that

an analysis of the influence of variability in hydraulic resistance on flood routing is performed.

There have been many empirical relationships suggested for open channel flow resistance, including the Darcy-Weisbach equation, Manning's formula, and the Chézy equation (Henderson 1966; Sturm 2010; Yen 1992, 2002). The most popular resistance equation is undoubtedly the Manning's formula, and because there is no theoretical preference for other equations (Yen 1992, 2002), it was used in this study.

For each cross-section, a Manning's resistance coefficient,  $n$ , was chosen for the main channel, and a separate coefficient for the overbank flow. Due to uncertainty in the parameter as observed in nature, and with intent on investigating the role its variability has in flood routing, the Manning's coefficients were treated as RVs with mean values of 0.048 and 0.08 for the main channel and the overbanks respectively. These values correspond well with an average of possible conditions reported by various researchers (e. g. Henderson 1966; McCuen 1998; Sturm 2010). There have been several researchers that suggest the Manning's resistance coefficient scales similarly to the hydraulic geometry (e. g. Knighton 1975; Singh et al. 2003), but for this study the Manning's resistance coefficient is treated as a scale invariant parameter.

### 3.1.5 Monte Carlo Experiment

MC experimentation is the procedure of repeating a process several times while varying some or all of the required inputs according to some prescribed manner (Chang et al. 1994). MC experimentation provides an effective tool to systematically investigate the effect of uncertainty in parameters for nonlinear models (Chang et al. 1994; Scharffenberg and Kavvas 2011; Warwick and Cale 1986). For this reason, and the large domain of input parameters for each simulation, MC simulation was chosen for this investigation.

For the experiment, 1,000 simulations were performed for each Horton order stream 1-9. For each simulation, both the geometric and the resistance characteristics at each cross-section were independently sampled from their respective distributions, resulting in a wide range of input conditions for the simulations. The resulting 1,000 routed hydrographs were then compared with a baseline simulation described in section 3.1.6 using the evaluation criteria discussed in section 3.1.7.

For the cross-sectional geometry, the width variables were treated as normally distributed RVs with mean value for each Horton order as listed in Table 3. A constant, scale invariant, coefficient of variation (CV) was chosen for each geometric parameter as  $1/6$ . This value is consistent with the observed CV from measured bathymetric data in the Iowa River between Iowa City, IA and Lone Tree, IA. Figure 5 shows a comparison between observed variability in the Iowa River of channel bottom width and simulated variability in channel bottom width. The bottom width for the observed cross-sections was defined by approximating a trapezoid to the cross-section which had the same area and top width between banks, and had a side slope cotangent of 1:1. As can be inferred from Figure 5, the variability between two cross-sections is greater in the simulated results due to an absence of correlation between two adjacent cross-sections. The overall variability for the observed cross-sections in terms of CV is on the order of  $1/6$ . Figure 6 shows a comparison of the range of observed cross-sections in the Iowa River and the range of simulated cross-sections. Figure 6 demonstrates that natural rivers have much variability in the form of their cross-sectional geometry, but the simulated cross-sections have a mean conveyance area comparable to the observed cross-sections.

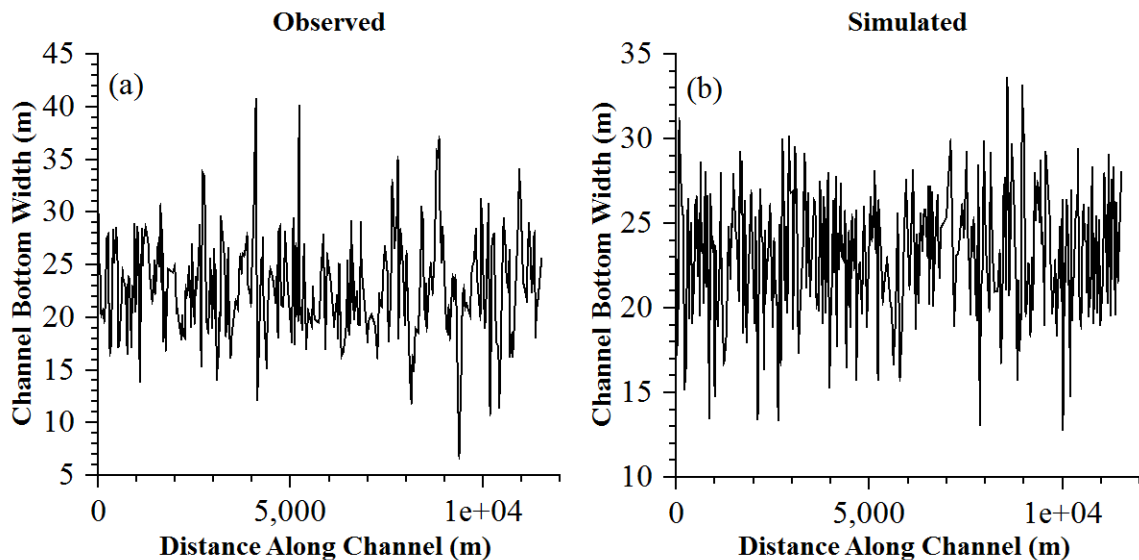


Figure 5 Comparison of observed variability in channel bottom width with simulated variability in channel bottom width. (a) 331 cross-sections observed in the Iowa River between Iowa City, IA and Lone Tree, IA (b) 331 simulated cross-sections with equal mean to observed cross sections and  $CV = 1/6$

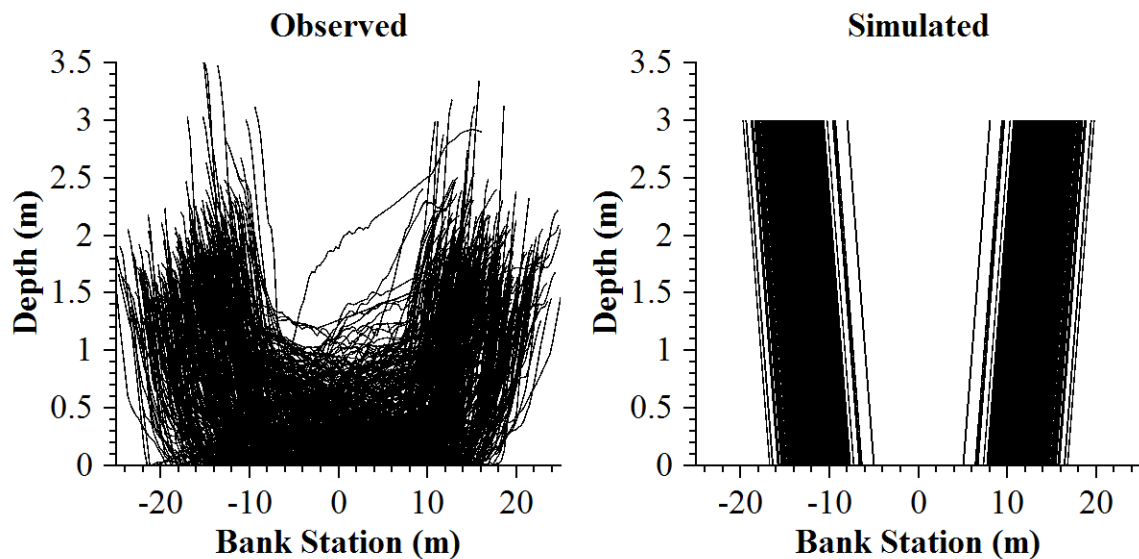


Figure 6 Comparison of 331 observed cross-sections in the Iowa River between Iowa City, IA and Lone Tree, IA with 331 simulated cross-sections of equal scale

The Manning's resistance coefficient,  $n$ , was assumed to be a RV with a uniform distribution with upper and lower bounds of 0.07 and 0.026 respectively for the main channel, and 0.12 and 0.04 for the overbank flow. While several researchers have reported various pdfs to describe variability in  $n$  in different geographic regions (e. g. Johnson 1991; Scharffenberg and Kavvas 2011), Johnson (1991) reported a uniform distribution based purely on a survey of estimates for a stream reach provided by a sample of professional engineers. Based upon the results of Johnson (1991), and without giving consideration to specific geographic regions, the uniform distribution is the most appropriate for the resistance coefficient. Figure 7 gives a graphical representation of the variability in the simulated resistance coefficients.

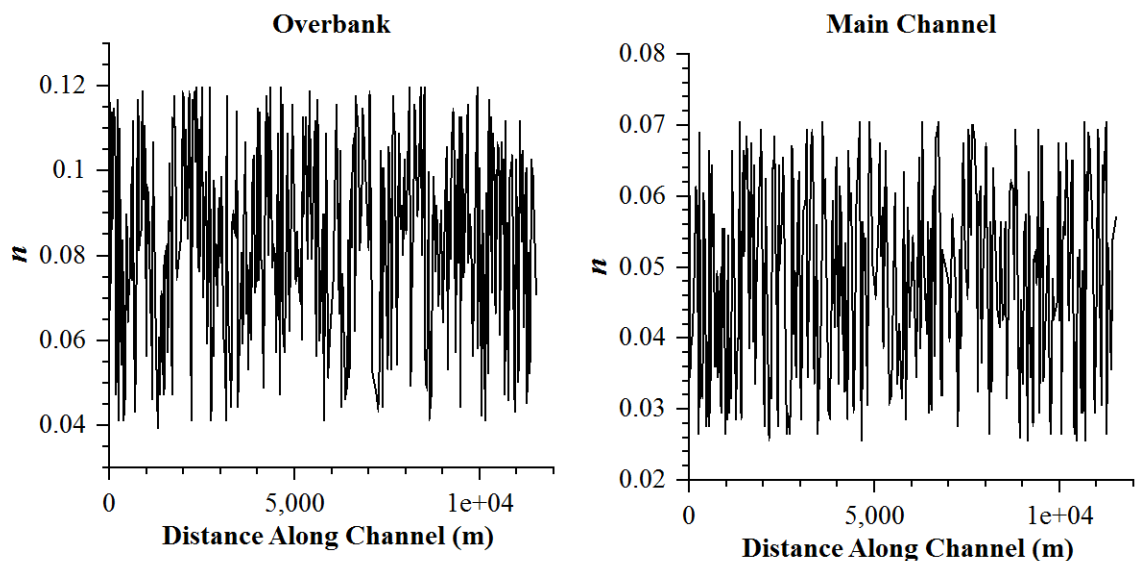


Figure 7 Variability in simulated Manning's resistance coefficient along a channel length for overbank and main channel flow

The sampling properties for the input variables (cross-section widths and resistance coefficients) used in the MC simulations are summarized in Table 4.

Input Variable	Distribution	Mean	CV
Lc (m)	normal	see Table 3	1/6
Lf (m)	normal	see Table 3	1/6
Overbank resistance	uniform	0.08	0.289
Main channel resistance	uniform	0.048	0.265

Table 4 Sampling properties of input variables used in MC simulations

### 3.1.6 Baseline Simulation

The baseline simulation for each Horton order stream is a prismatic channel with cross-sectional properties composed of the mean values listed in Table 3 and Table 4. This was chosen as the baseline case because it is unambiguous. The properties of the routed hydrographs: peak discharge,  $Q_p$ , time to peak discharge,  $t_p$ , and time of duration,  $t_b$ , are summarized in Table 5. The definition of these properties will be given in section 3.1.7. Figure 8 is a plot of the routed hydrographs for the baseline simulations.

Horton order	$Q_p$ (cms)	$t_p$ (hr)	$t_b$ (hr)
1	14	0.40	0.46
2	25	0.83	1.03
3	59	1.45	1.85
4	108	3	4
5	208	6	10
6	388	13	20
7	725	26	45
8	1353	56	98
9	2527	124	219

Table 5 Peak discharge, time to peak discharge, and time of duration for baseline hydrographs of a given Horton order

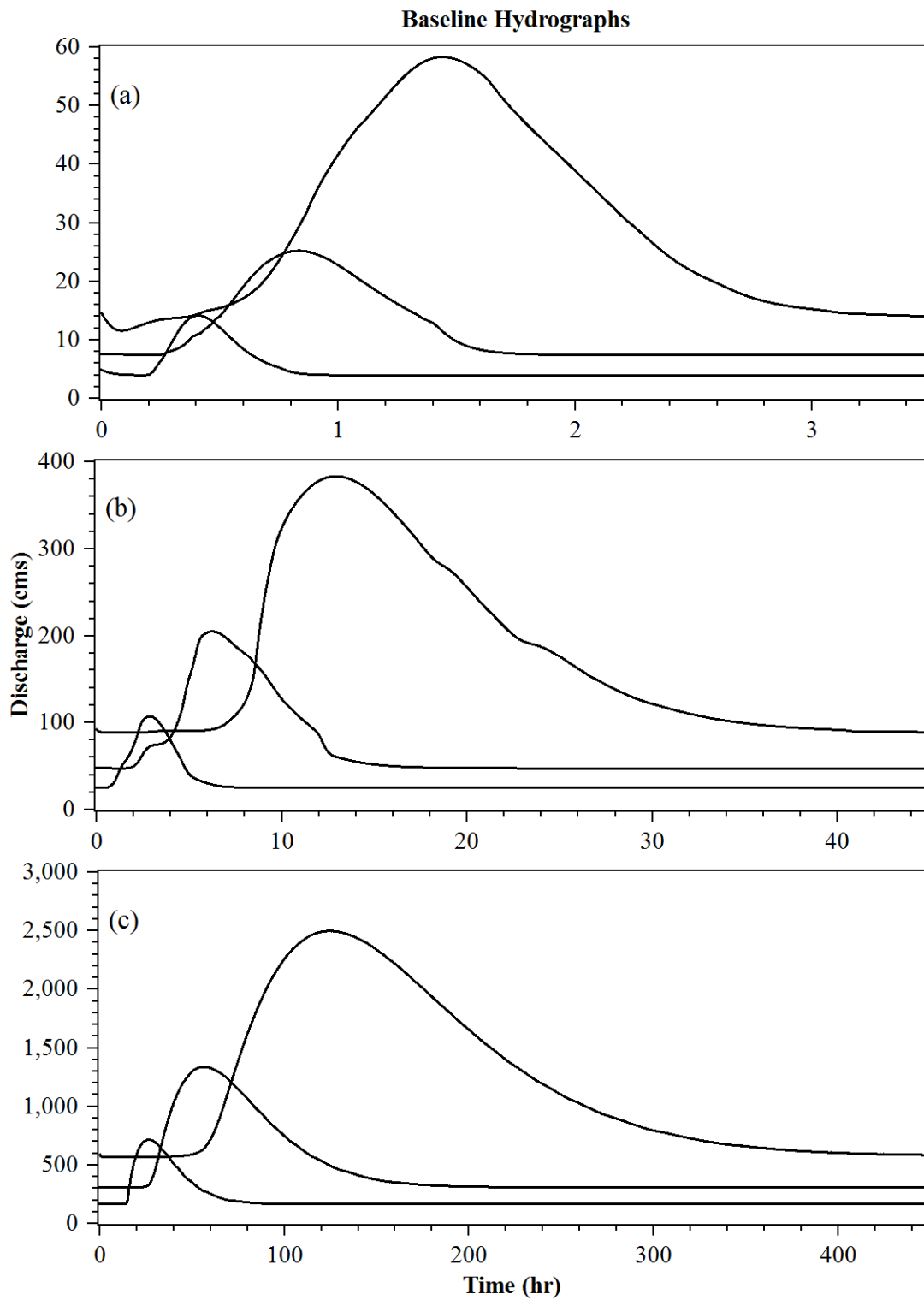


Figure 8 Baseline simulation hydrographs. (a) Horton orders 1-3 (b) Horton orders 4-6 (c) Horton orders 7-9

### 3.1.7 Evaluation Criteria

Because the output of each simulation was a time series rather than a single value, it was necessary to define a consistent method to compare one hydrograph to another. There has been much discussion of the problem of comparing two or more hydrographs with each other, or evaluating models, and there are many suggested evaluation parameters (e. g. McCuen et al. 2006; McCuen and Snyder 1975; Moriasi et al. 2007; Nash and Sutcliffe 1970). Four measures are defined here that were used to evaluate and compare the simulations; 3 measures of valued quantities in river flow forecasting and one as a measure of overall agreement between hydrographs.

To establish the first three measures, the hydrograph was first characterized, as in Figure 9 by;  $Q_p$ , which is the peak discharge, or maximum flow occurring in the hydrograph;  $t_p$ , which is the time to peak discharge, or the time at which the hydrograph reaches its maximum value; and  $t_b$ , which is the time of duration, or the length of time that the outflow hydrograph has a discharge greater than 35% of the peak discharge of the inflow hydrograph.

Using the characterization defined in the previous text and in Figure 9, a relative difference was used to compare and evaluate the simulated hydrographs. The relative difference, calculated by equation 3.7, was used to provide multiple criteria for the analysis, and because the ratio is a percentage, it permits comparisons across Horton orders.

$$RD_P = \frac{P_S - P_B}{P_B} \quad (3.7)$$

where RD is the relative difference, P is the parameter of interest, S is the simulated value of P and B is the baseline value of P.

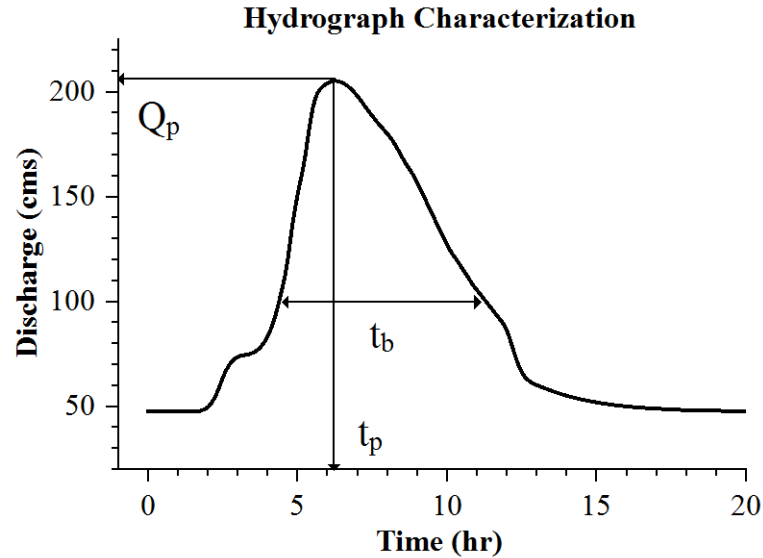


Figure 9 Definition of hydrograph characterization parameters  $Q_p$ ,  $t_p$ , and  $t_b$

The fourth measure chosen is the Nash-Sutcliffe efficiency (NSE) (McCuen et al. 2006; Moriasi et al. 2007; Nash and Sutcliffe 1970). NSE was chosen because it gives an indicator of overall agreement between two hydrographs. NSE, given by equation 3.8, can range from  $-\infty$  to 1.0 with 1.0 being perfect agreement between the hydrographs.

$$NSE = 1 - \frac{\sum_{i=1}^n (Q_i^{baseline} - Q_i^{simulated})^2}{\sum_{i=1}^n (Q_i^{baseline} - \overline{Q^{baseline}})^2} \quad (3.8)$$

### 3.2 Results and Analysis

The MC simulations provided 1,000 hydrographs for each Horton order stream 1-9. The hydrographs were then summarized by their characteristics  $Q_p$ ,  $t_p$ , and  $t_b$ . Figure 10-18 provide the histograms of  $Q_p$ ,  $t_p$ , and  $t_b$  for their respective Horton orders. Figure 19-21 present the spectrum of outflow hydrographs from the simulations.

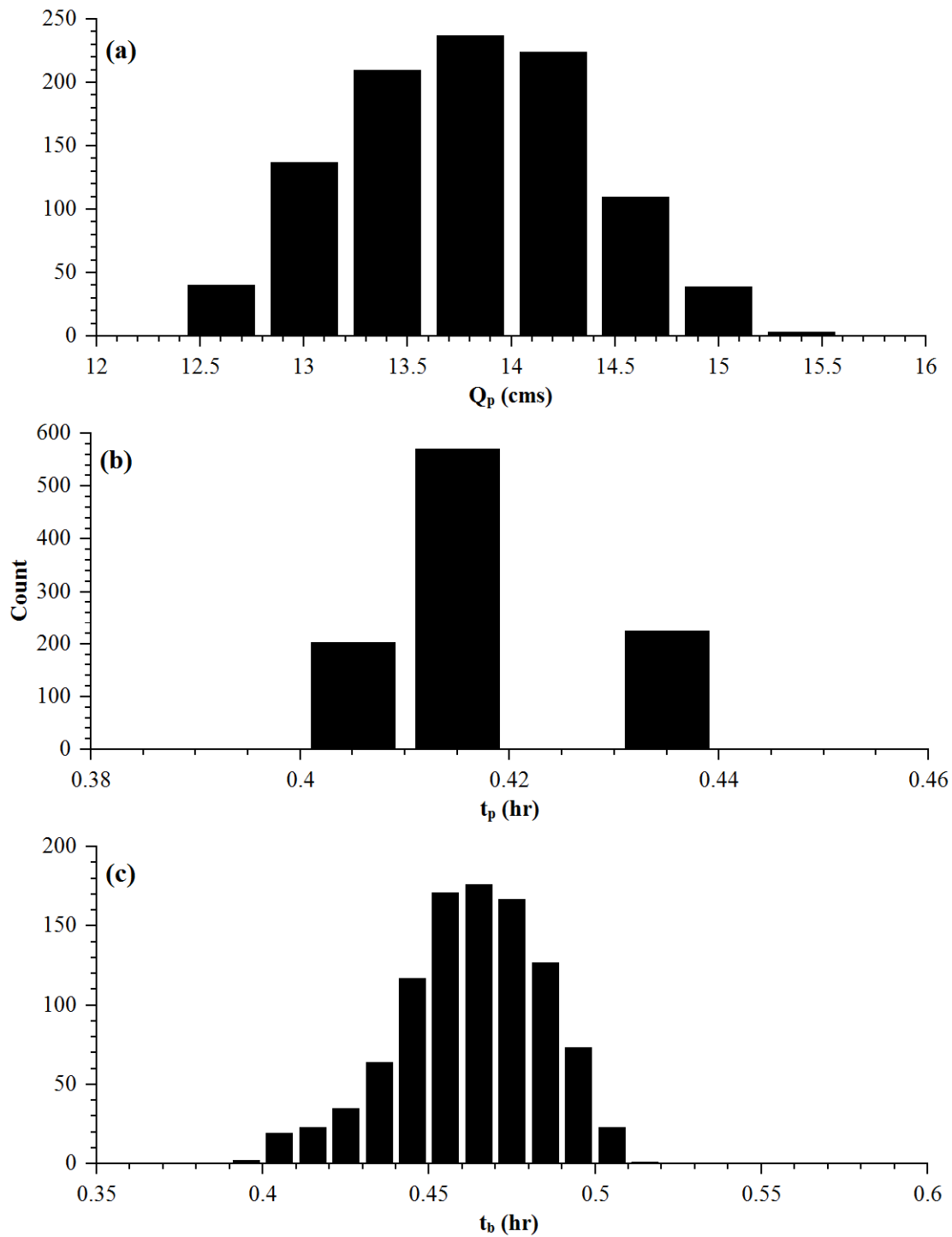


Figure 10 Histograms describing simulation outputs for Horton order 1. (a) Peak discharge (b) Time to peak discharge (c) Time of duration

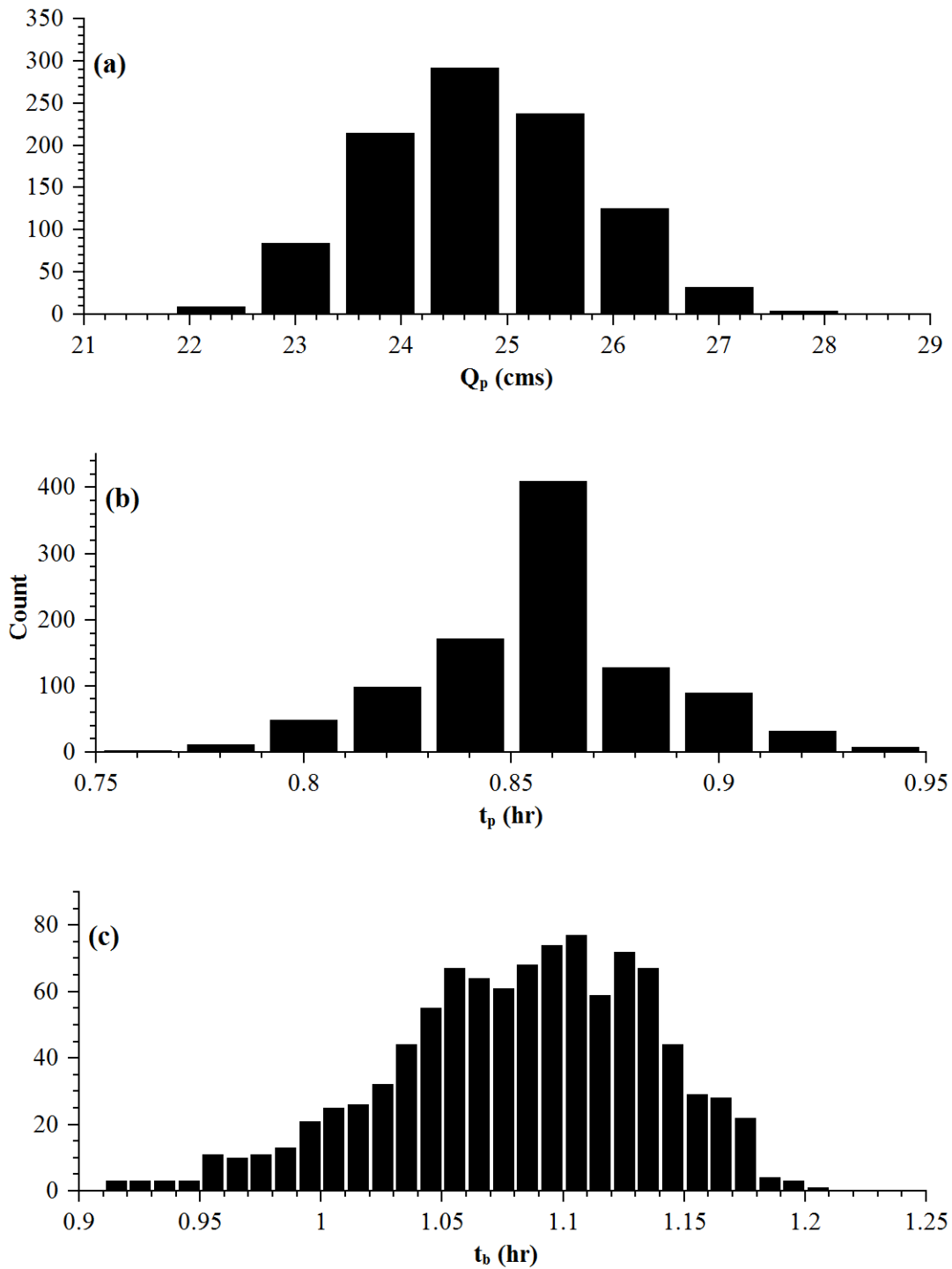


Figure 11 Histograms describing simulation outputs for Horton order 2. (a) Peak discharge (b) Time to peak discharge (c) Time of duration

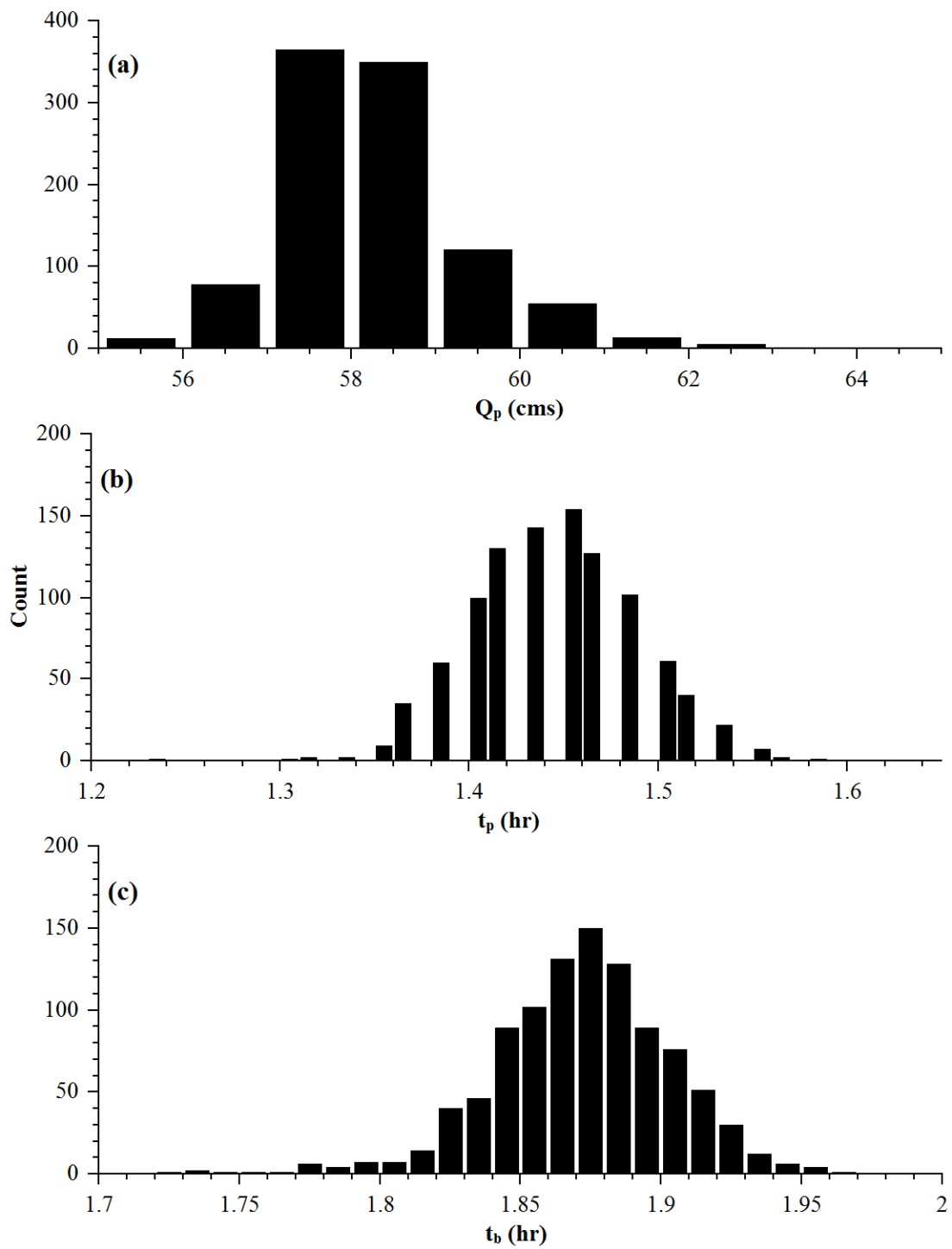


Figure 12 Histograms describing simulation outputs for Horton order 3. (a) Peak discharge (b) Time to peak discharge (c) Time of duration

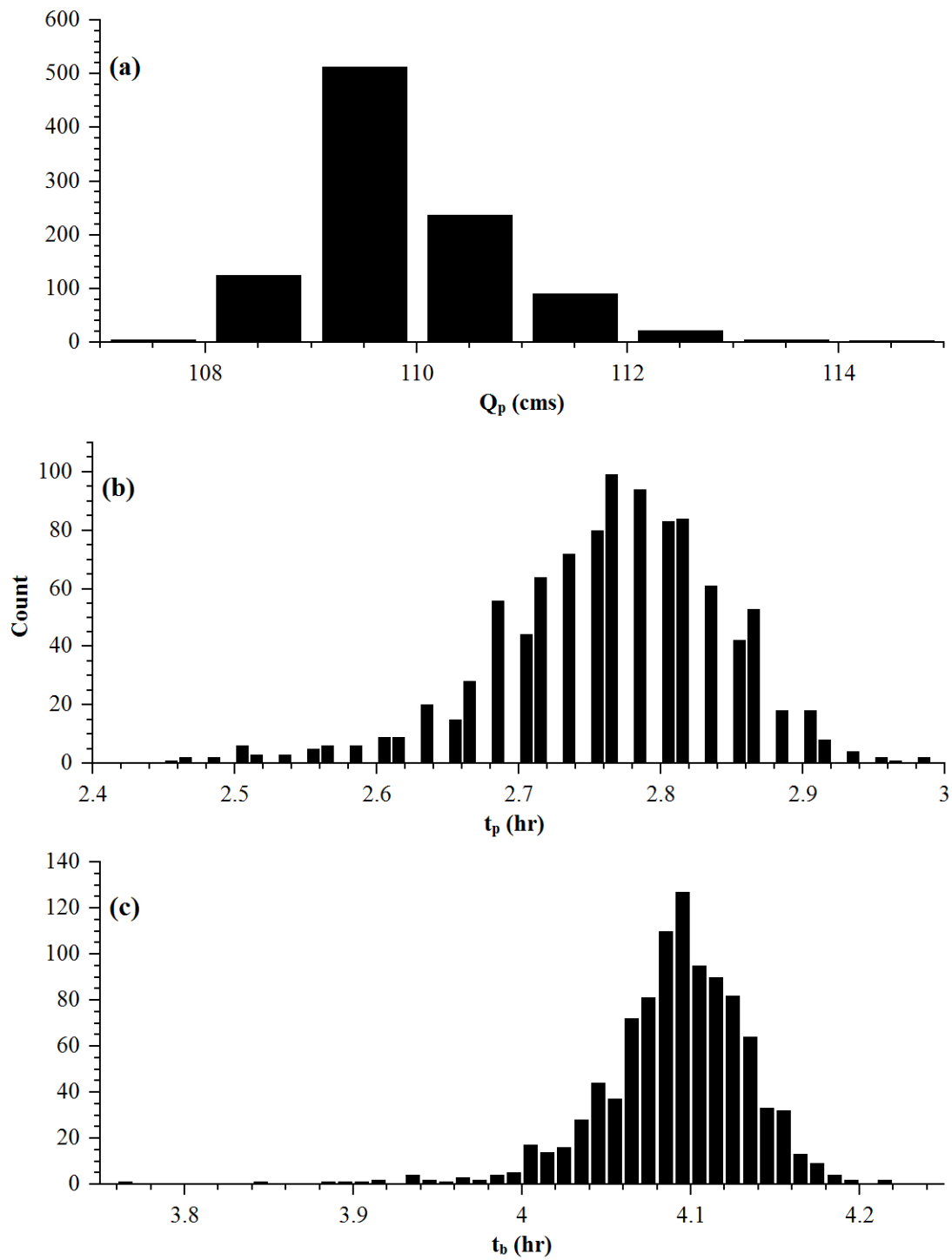


Figure 13 Histograms describing simulation outputs for Horton order 4. (a) Peak discharge (b) Time to peak discharge (c) Time of duration

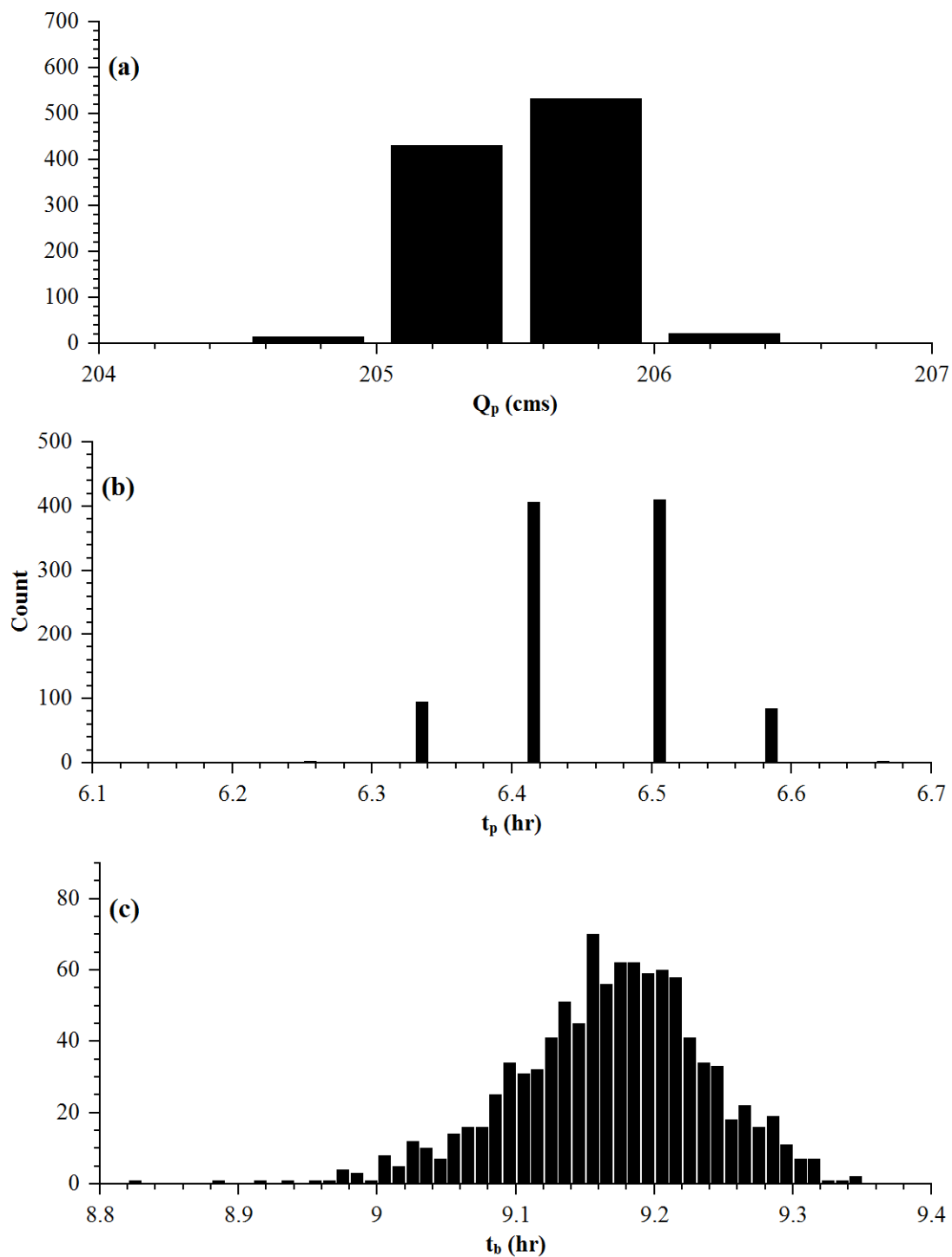


Figure 14 Histograms describing simulation outputs for Horton order 5. (a) Peak discharge (b) Time to peak discharge (c) Time of duration

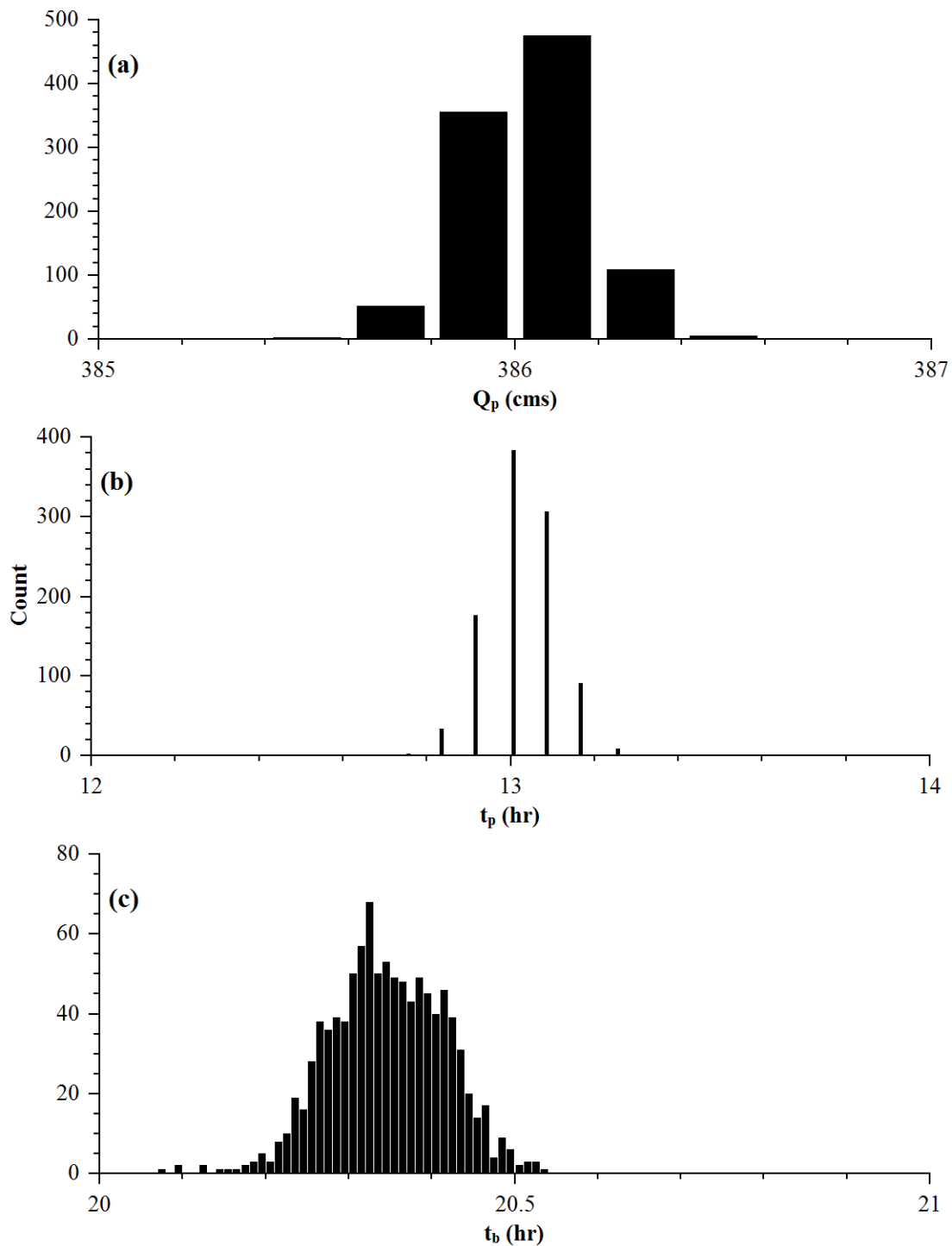


Figure 15 Histograms describing simulation outputs for Horton order 6. (a) Peak discharge (b) Time to peak discharge (c) Time of duration

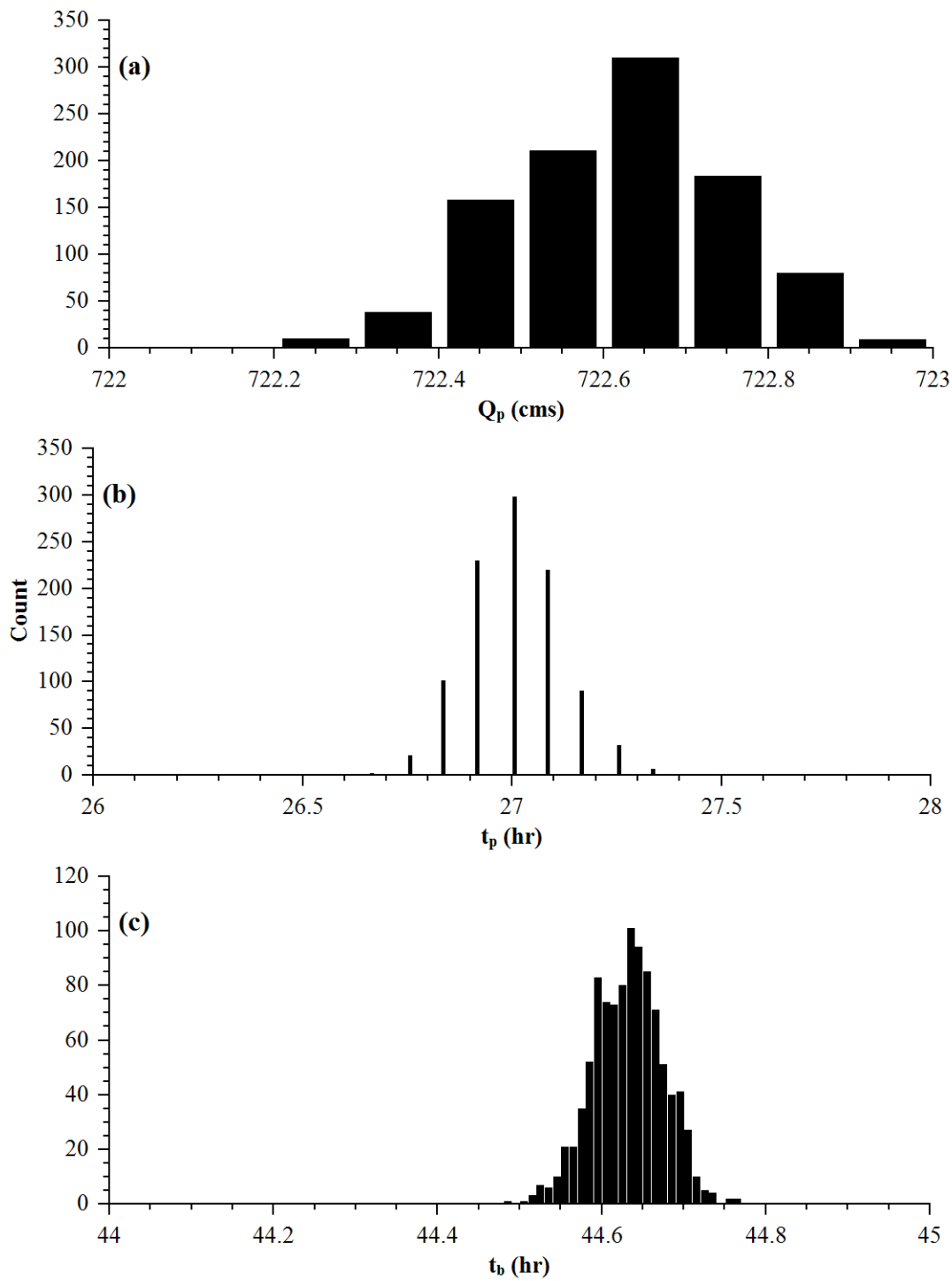


Figure 16 Histograms describing simulation outputs for Horton order 7. (a) Peak discharge (b) Time to peak discharge (c) Time of duration

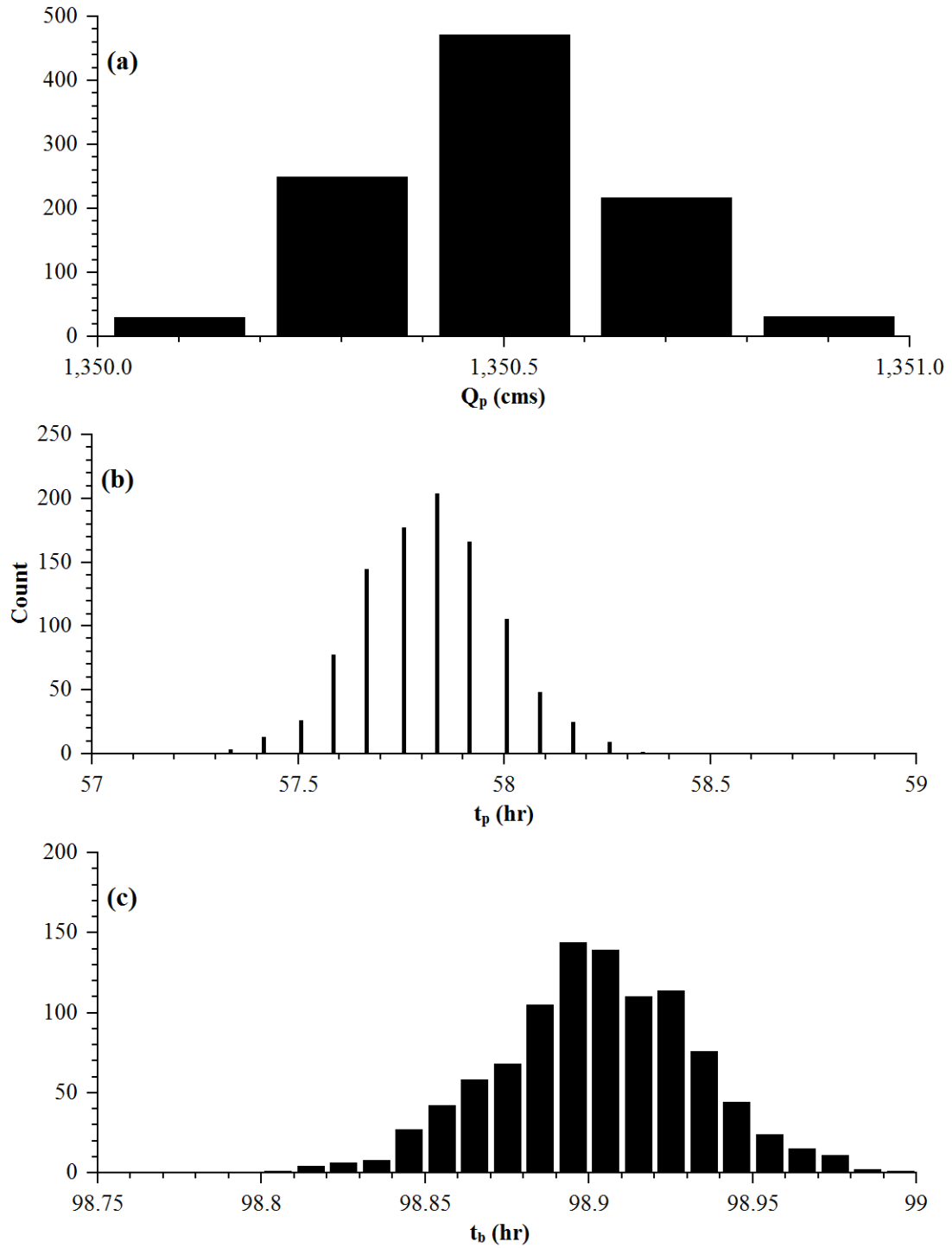


Figure 17 Histograms describing simulation outputs for Horton order 8. (a) Peak discharge (b) Time to peak discharge (c) Time of duration

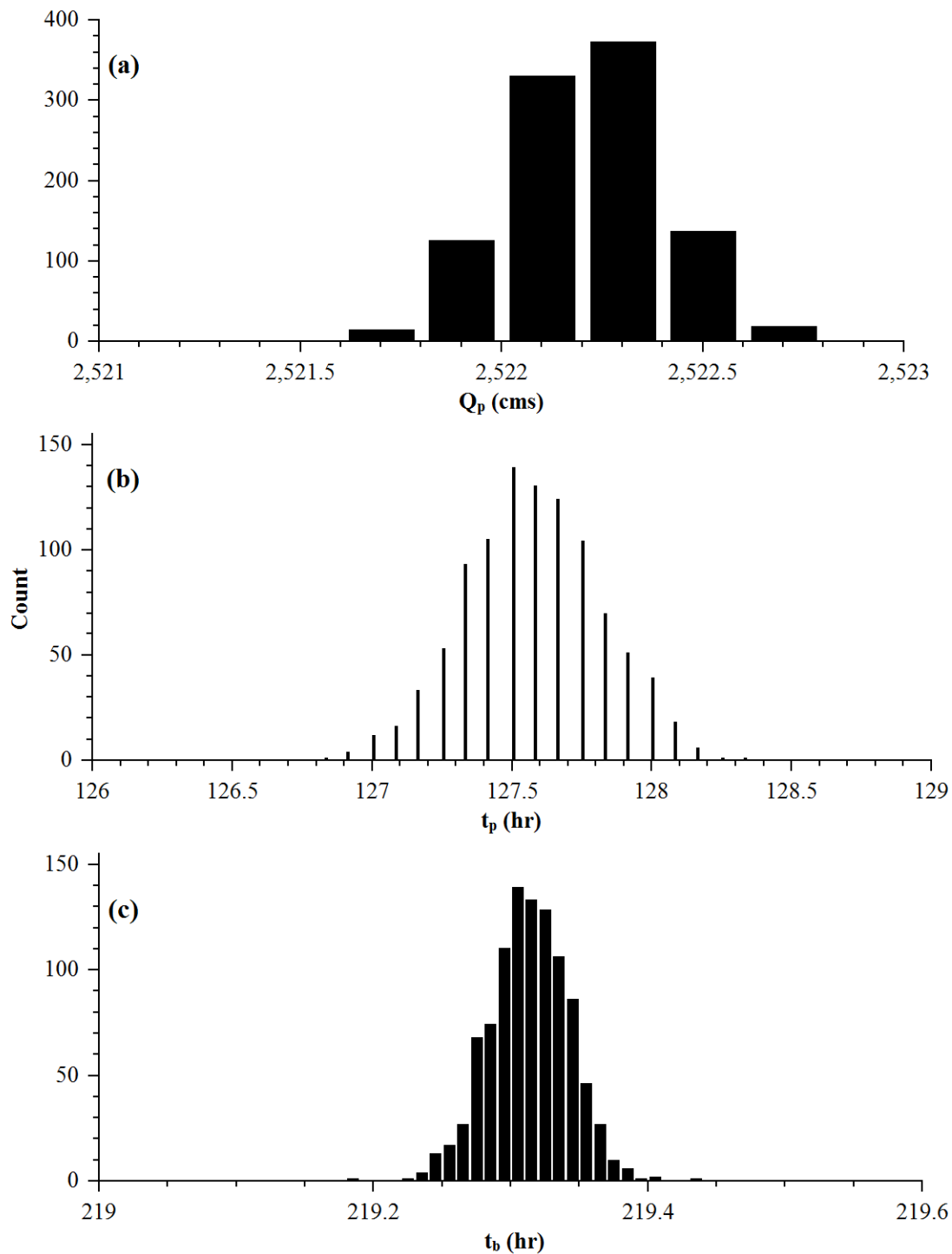


Figure 18 Histograms describing simulation outputs for Horton order 9. (a) Peak discharge (b) Time to peak discharge (c) Time of duration

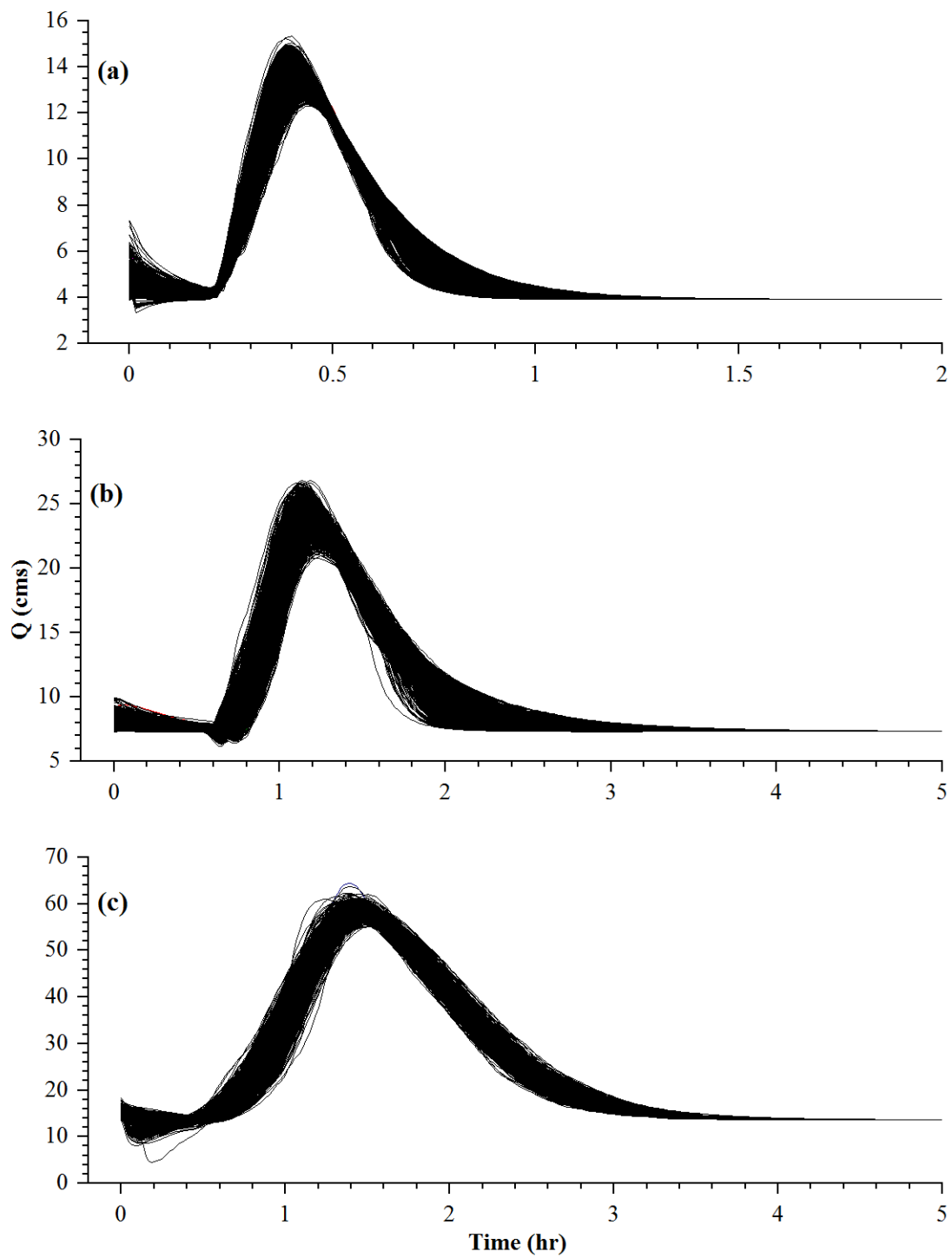


Figure 19 Spectrum of all routed hydrographs from the simulations. (a) Horton order 1 (b) Horton order 2 (c) Horton order 3

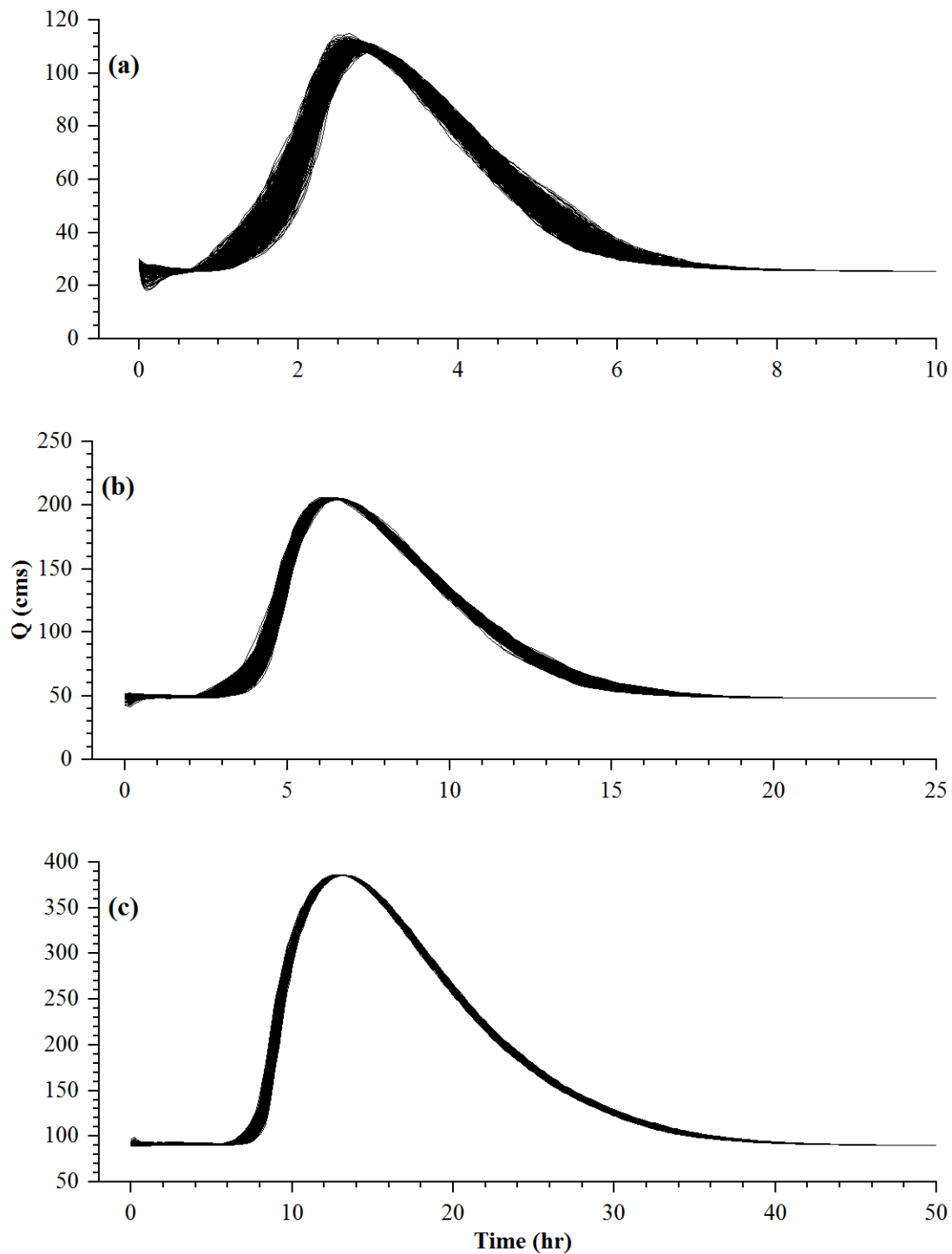


Figure 20 Spectrum of all routed hydrographs from the simulations. (a) Horton order 4 (b) Horton order 5 (c) Horton order 6

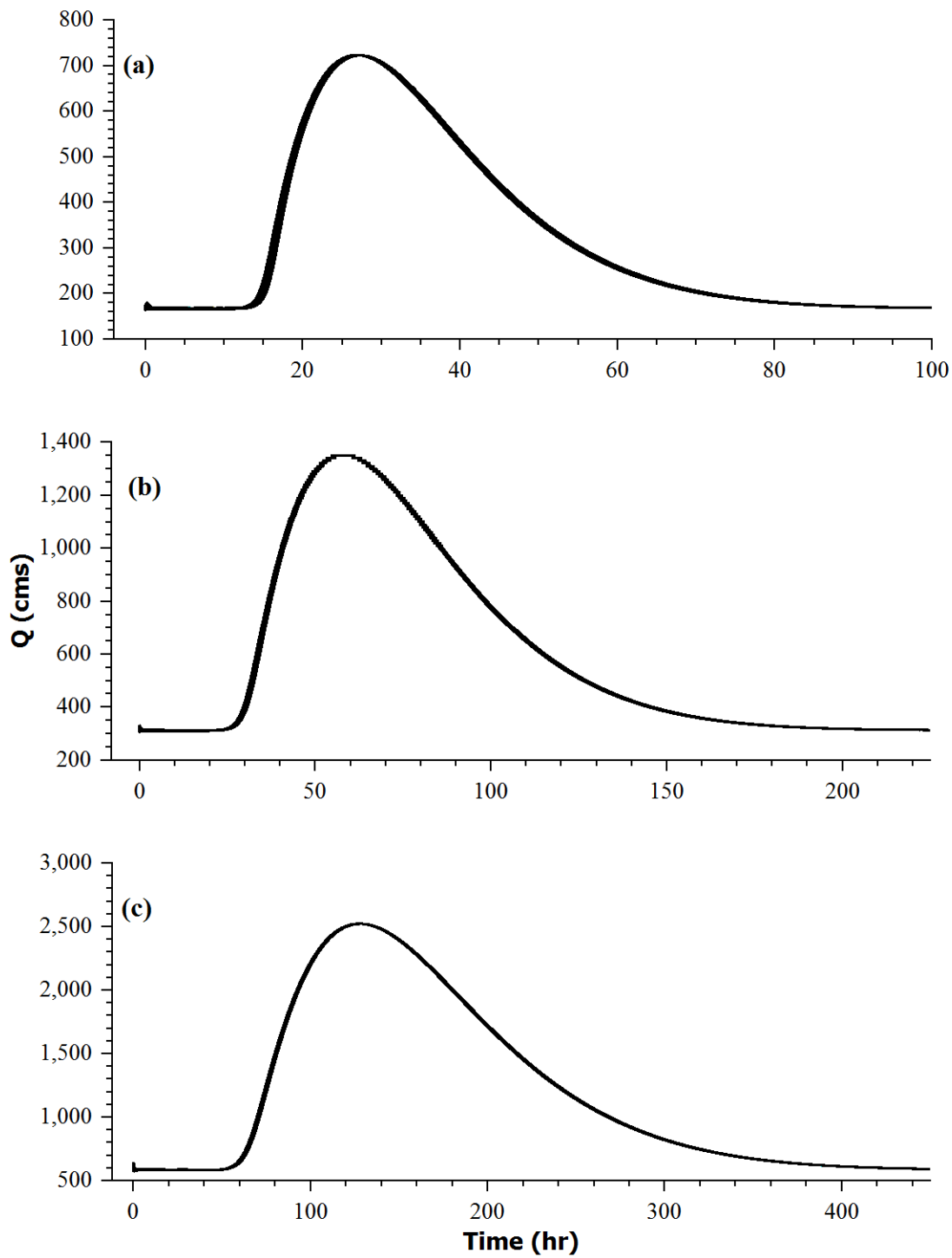


Figure 21 Spectrum of all routed hydrographs from the simulations. (a) Horton order 7 (b) Horton order 8 (c) Horton order 9

As can be observed from Figures 10-21, there is a relatively small spread in the 1,000 simulated hydrographs for each Horton order, and the range of values decreases with increasing order. Further analysis of the coefficient of variation (CV) for the metrics,  $Q_p$ ,  $t_p$ , and  $t_b$ , demonstrates the narrow range of values computed from the simulations, and also the trend for variability to reduce with increased Horton order.

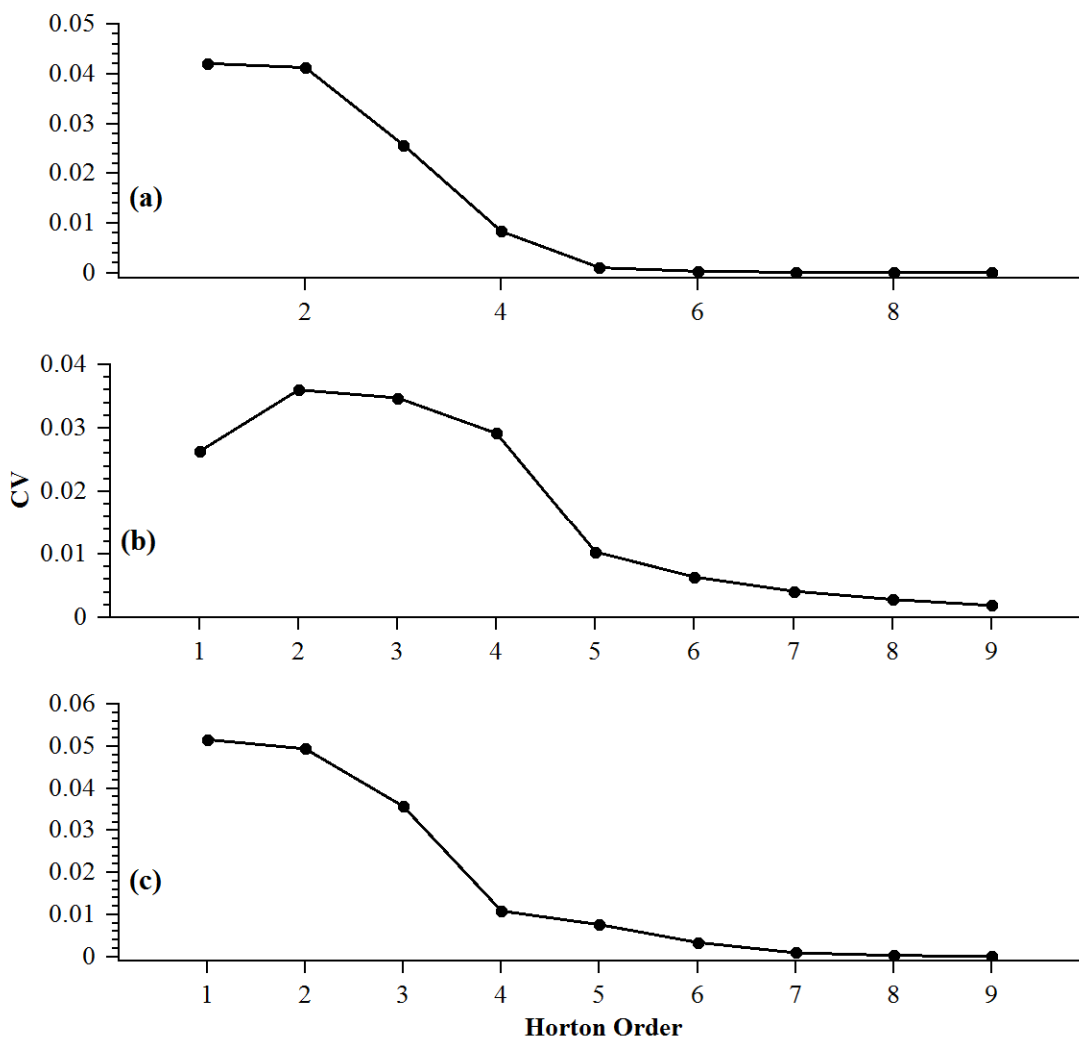


Figure 22 Coefficient of variation vs. Horton order. (a) CV for peak discharge (b) CV for time to peak discharge (c) CV for time of duration

In addition to comparing the simulations with each other, it was desired to see how each simulation compared with a baseline simulation. As discussed in section 3.1.6, the baseline simulation is a model with the input parameters comprised of the mean values of the input domain. The criteria for comparing the simulations are the relative difference (equation 3.7), and the Nash-Sutcliffe efficiency (equation 3.8).

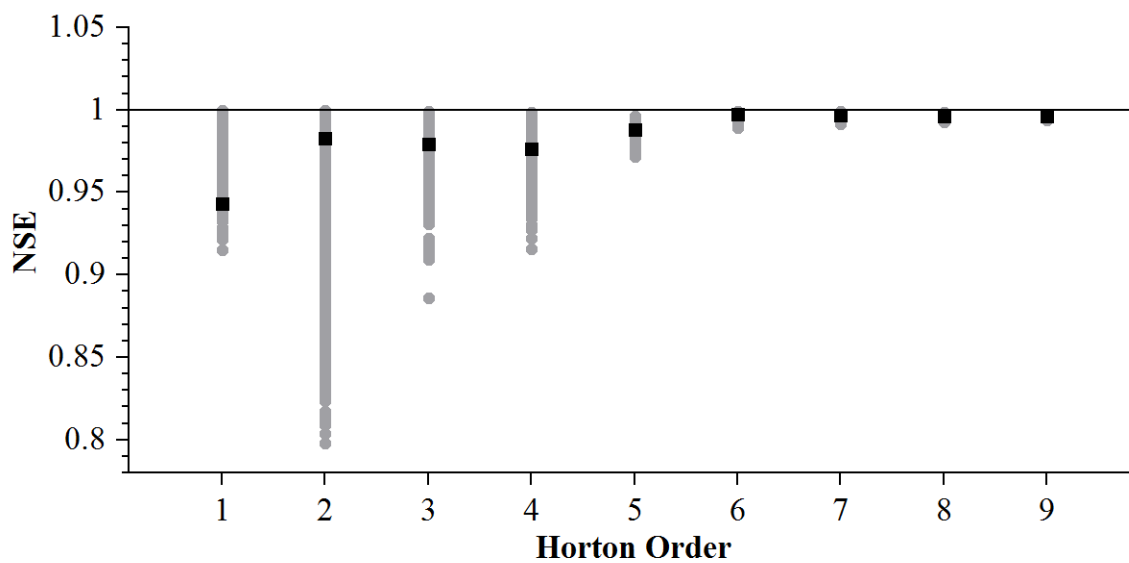


Figure 23 Nash-Sutcliffe efficiency vs. Horton order

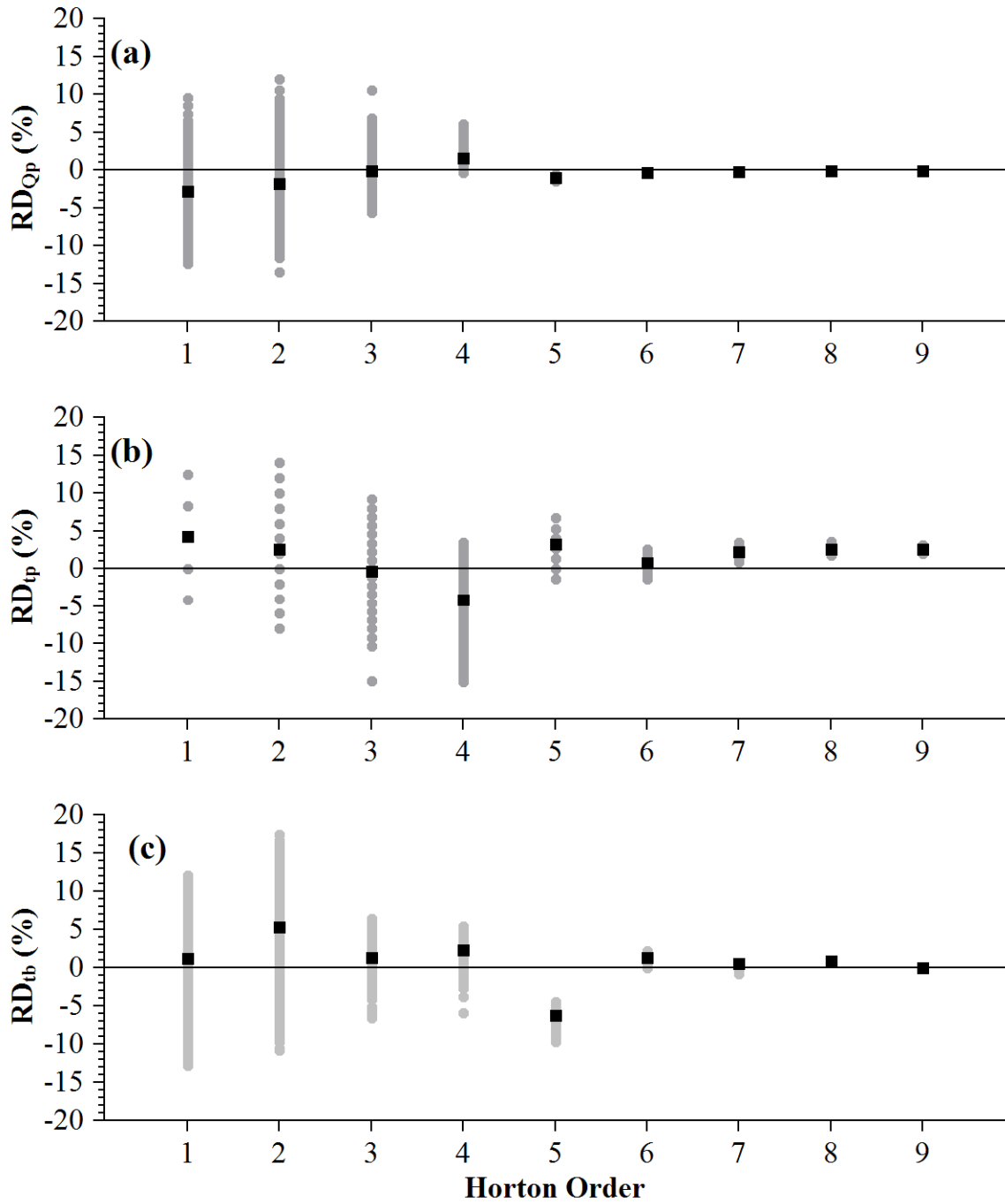


Figure 24 Relative differences vs. Horton order. (a) relative difference in peak discharge (b) relative difference in time to peak discharge (c) relative difference in time of duration

Figures 22-24 demonstrate a clear trend of reduction in variability of routed hydrographs with increasing Horton order. In addition to a reduction in variability, the hydrographs apparently converge toward the baseline simulation. This observation inspires the question, is the hydrograph produced by the baseline simulation equivalent to the expected value of the MC simulations? A rigorous approach to answering this question is to establish a confidence interval for the mean of the MC simulations and determine if the baseline simulation lies within the bounds.

The distributions for  $Q_p$ ,  $t_p$ , and  $t_b$  are not easily approximated by a normal distribution; therefore a non-parametric approach must be taken to establish confidence intervals for their means. One such way to derive confidence intervals is by the use of the bootstrap method (DeVore 2004; Efron and Tibshirani 1986). Using bootstrap sampling with replacement, 95% confidence intervals are established for the means of  $Q_p$ ,  $t_p$ , and  $t_b$  and summarized in Table 6.

Horton order	$Q_p$ (cms)	$t_p$ (hr)	$t_b$ (hr)
1	13.75 - 13.81	0.416 - 0.418	0.461 - 0.464
2	24.69 - 24.82	0.853 - 0.857	1.08 - 1.09
3	58.74 - 58.92	1.44 - 1.45	1.86 - 1.87
4	109.83 - 109.95	2.76 - 2.77	4.08 - 4.09
5	205.51 - 205.54	6.45 - 6.46	9.16 - 9.17
6	386.01 - 386.03	13.02 - 13.03	20.34 - 20.35
7	722.61 - 722.63	26.99 - 27.00	44.62 - 44.63
8	1350.49 - 1350.51	57.80 - 57.83	98.90 - 98.91
9	2522.20 - 2522.22	127.56 - 127.59	219.31 - 219.32

Table 6 95% bootstrap confidence intervals on simulated hydrograph characteristics

By comparing the values from the baseline simulations in Table 5 with the confidence intervals in Table 6, it is apparent that the prismatic baseline simulation is not a statistically equivalent substitution to the case where the model accounts for all inter-cross-section variability. Specifically, the expected value of the simulations is different from the baseline simulation with a statistical level of significance of 5%.

Strictly one cannot replace bathymetric cross-section data with a reach wise average cross-section as shown by the confidence intervals in Table 6. This seems to conflict with the results presented in Figures 23-24, which suggests that the error committed by such a substitution is small. This example illustrates an understated point; that statistical significance is a very restrictive condition, and may not be absolutely necessary in engineering applications.

A less restrictive condition that is appropriate for engineering application is the condition of practical significance. The condition of practical significance is that the maximum difference between measurements of interest falls below some acceptable tolerance level. While there are no objective criteria to specify what tolerance level is acceptable, consideration of the relative uncertainty in model input parameters provides one systematic approach to establish acceptable performance. Other, more subjective, methods to establish such tolerance levels would be to evaluate the relative change in impact between outputs, for example if a flood peak is 1,350 cms, the inundated area will not be much different from a flood wave of 1,355 cms, or societal perception, such as whether a two minute difference in flood peak arrival times is significant.

Using the approaches described above, it is argued that there is no practical significance in the difference between the MC simulations and the baseline simulation. To assess this statement, tolerance levels are placed upon the characteristics,  $Q_p$ ,  $t_p$ , and  $t_b$  based upon uncertainty in model inputs and societal perception.

First, a tolerance level for difference in the magnitude of peak discharge,  $Q_p$ , is established based upon the uncertainty in peak discharge for the inflow hydrograph. The

peak discharge of the inflow for this study is assumed using the USGS regression equations for Iowa (Eash 2001). The error in estimates from regression equations comes both from inability for the mathematical regression equation to fit observed data (model error) and error induced from limited amount of observations among other things. While the reported errors in USGS regression equations vary from one region to another, they range from 34% – 45% in the state of Iowa as reported by Eash (2001). Another common source of inflow hydrograph in practice is from a gauging station located on the stream of interest (i.e. USGS gauges). Gauge read discharge values also have significant error, mostly due to neglecting hysteresis in the rating curves. Research has shown that the error in gauge measured discharge varies between sites and events, but has a mean value typically around 25% (Di Baldassarre & Montanari, 2009). Given this level of uncertainty, a suitable tolerance level can be assumed to be  $< 25\%$ . Figure 24 shows that the maximum difference between baseline simulation and MC simulation with respect to  $Q_p$ , is  $< 15\%$ , and the maximum expected difference is even less at  $< 3\%$ . Given that the divergence from the MC simulations of the baseline simulation is well below the expected uncertainty in the inflow hydrograph peak, the variance between simulations is considered within acceptable tolerance levels and therefore not of practical significance.

Second, a tolerance level for difference in time characteristics needs to be established. The criteria used to establish this tolerance level is a time interval that will not be perceived as considerable by the general population. This is a very difficult and subjective criteria as the perception of time varies considerably based upon environmental and psychological conditions. Because of the subjectivity in this criteria and the lack of research data available, the author assumes that a 10% difference in time is not perceivable, for example it is not believed that a group of people will react to a difference between 25 minutes and 28 minutes. Given a tolerance level of 10% on the time characteristics of a flood hydrograph, and the simulation data presented in Figure 24, it can be said that there is no practical significance between the baseline simulation

and the MC simulations. While there are significant differences for some of the simulations of Horton orders 1-3, the expected value of the differences is well within tolerance levels for all orders.

As a conclusion to the results of the MC simulations, it is found, as expected, that there is a statistically significant difference between the baseline simulations and the MC simulations. This statistically significant difference may not be enough to restrict the replacement of a fully detailed bathymetric description in river flood routing models with a reach wise averaged cross-section. It was demonstrated that given a definition of acceptable tolerance, the difference between the baseline simulations and the MC simulations may be practically insignificant. The potential for this result as it applies to hydraulic flood routing in practice is demonstrated further in the case study presented in Chapter 5.

## CHAPTER IV: THE EFFECT OF SIDE TRIBUTARIES ON FLOOD ROUTING MODELS

In a flood routing model, one is typically concerned with the transport of water from the head of a watershed to its outlet through its largest or main river. Often times, depending upon the size of the watershed, there can be hundreds of incoming streams that feed the main river with water from all over the watershed between the head and the outlet. Because of the potential number of streams involved, it can become practically impossible to account for all inflows in a flood routing model. Because the complexity of real river networks, and the lack of input data available, modelers often simplify the working network by neglecting some or all tributary streams (Cantone and Schmidt 2009; Choudhury et. al. 2002; Choudhury 2007). Another simplification often made is to consider lateral inflow as uniformly distributed over a particular reach rather than coming from a particular point of entrance (Moramarco et. al. 1999). While these simplifications are common, and in some situations justified, they can lead to significant errors in both outflow hydrograph timing and magnitude (Cantone and Schmidt 2009).

Because of the potential risk involved with errors in flood routing, it is desired to understand how side tributaries influence flood routing. In an effort to understand what effect model simplifications have on the routed flood hydrograph, a numerical experiment was conducted on a Mandelbrot-Vicsek tree network to evaluate the sensitivity of hydraulic flood routing to various simplifications.

### 4.1 Model Framework

The simple experiment conducted is a simulation of river network flow using an unsteady HEC-RAS model (Brunner 2010b). For the network, several cases were simulated, each with varying simplifications to be described in detail in section 4.1.3.

#### 4.1.1 Stream and Network Model

The simulation routes a hydrograph through a single stream of Horton-Strahler order 9 with lateral inflow. The stream geometry is equivalent to the baseline geometry described for the Horton-Strahler order 9 stream in section 3.1.6. A prismatic stream was chosen for the simulation because it is easily defined, and it is assumed that the general result would not be affected by inter-cross-section variability, based upon the results of chapter 3. The incoming side tributaries were evenly distributed along the reach with 1 kilometer (km) of stream length between them.

The side tributary order and magnitude was determined based upon a theoretical Tokunaga tree referred to as the Mandelbrot-Vicsek tree, which is described in section 2.4.6. The tree Horton-Strahler order is order 9, which results in 127 incoming side tributaries of Horton-Strahler orders 1-7. If we define a link as the stream segment between two tributaries, and the incoming side tributary for a given link as the tributary which enters at the downstream node of the link, then Figure 25 gives the structure of how the 127 incoming tributaries are distributed.

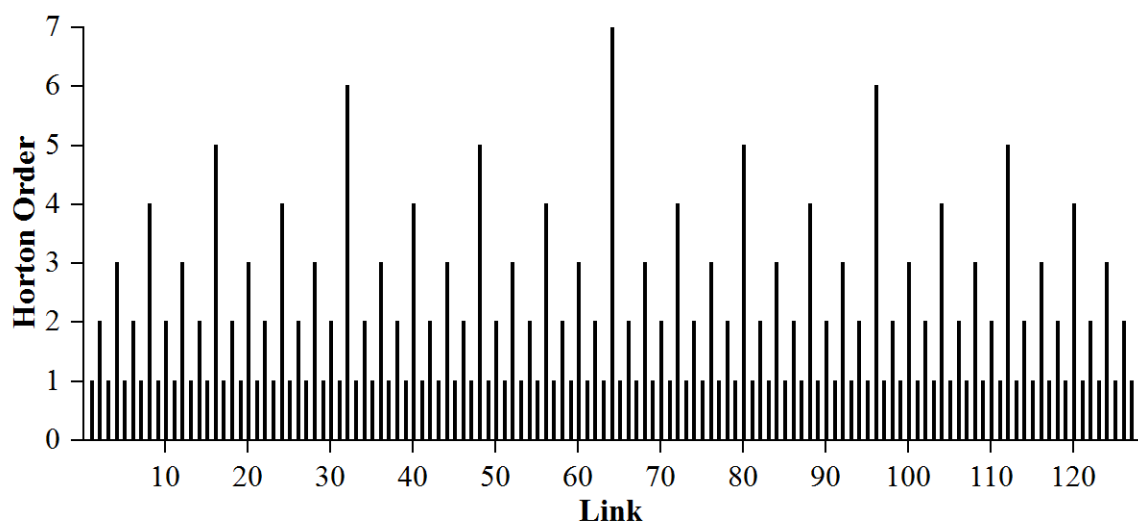


Figure 25 Side tributary structure for main stream of an order 9 Mandelbrot-Vicsek tree

As observed in Figure 25, the tributaries follow the following sequence:

$$Order = \begin{cases} 1 & \text{for link} = 1,3 \dots 127 \\ 2 & \text{for link} = 2k; \quad k = 1,3 \dots 63 \\ 3 & \text{for link} = 4k; \quad k = 1,3 \dots 31 \\ 4 & \text{for link} = 8k; \quad k = 1,3 \dots 15 \\ 5 & \text{for link} = 16k; \quad k = 1,3 \dots 7 \\ 6 & \text{for link} = 32k; \quad k = 1,3 \\ 7 & \text{for link} = 64 \end{cases} \quad (4.1)$$

#### 4.1.2 Inflow Hydrographs and Downstream Boundary

##### Condition

The model constructed has 128 points of inflow, one at the beginning of the modeled stream reach, and 127 inflow tributaries spaced at a uniform 1 km. The inflow hydrographs are calculated based upon the Horton-Strahler order of the tributary in the same manner as described in section 3.1.1. The inflow hydrograph at the beginning of the stream reach is calculated as the summation of two hydrographs for a Horton Strahler order 8 stream.

The downstream boundary condition is chosen to be the normal depth calculated using Manning's equation with a friction slope of 0.0009. The boundary condition is applied at the downstream node of the link 128.

#### 4.1.3 Simulations

For this experiment six simulations were performed with various simplifications of the model or modifications to the input hydrographs. Each case simulated was chosen to evaluate the effect from common practice.

The first simulation (S1) was considered the baseline simulation. The model was constructed with no simplifications to the inflow distribution or arrangement, and accounted for all inflows.

The second simulation (S2) accounts for all inflows, as does S1, but has the simplification of uniformly distributing the inflow from each side tributary over its respective link.

The third simulation (S3) maintains the uniform distribution of each side tributary over its link, as does S2. An additional simplification is made to the model by removing all Horton-Strahler order 1 streams. This simplification effectively removes half of the incoming tributaries.

The fourth simulation, (S4) is similar to S3, except instead of removing the order 1 streams, the order 2 streams are removed.

The fifth simulation (S5) has no incoming flow from the side tributaries. This is the maximum simplification possible for a model.

The sixth simulation (S6) is designed to show the potential effect from timing on a hydrograph. It is designed to demonstrate the worst case scenario. For each of the side tributaries, the time to peak for the hydrograph was modified so that it coincided with the arrival of the flood peak from upstream in the main channel, resulting in a summation of peak flows.

#### 4.2 Results and Analysis

The results of the simulations are summarized in Figure 26-Figure 27. In addition to Figure 27, the NSE for simulations S2, S3, and S4 was calculated according to equation 3.8, using simulation S1 as the baseline simulation. This provides a quantitative evaluation of performance, and way to assess the effect of simplifications as compared to S1. For simulations S5 and S6, the magnitude of peak discharge was chosen as the more relevant evaluation metric rather than the NSE.

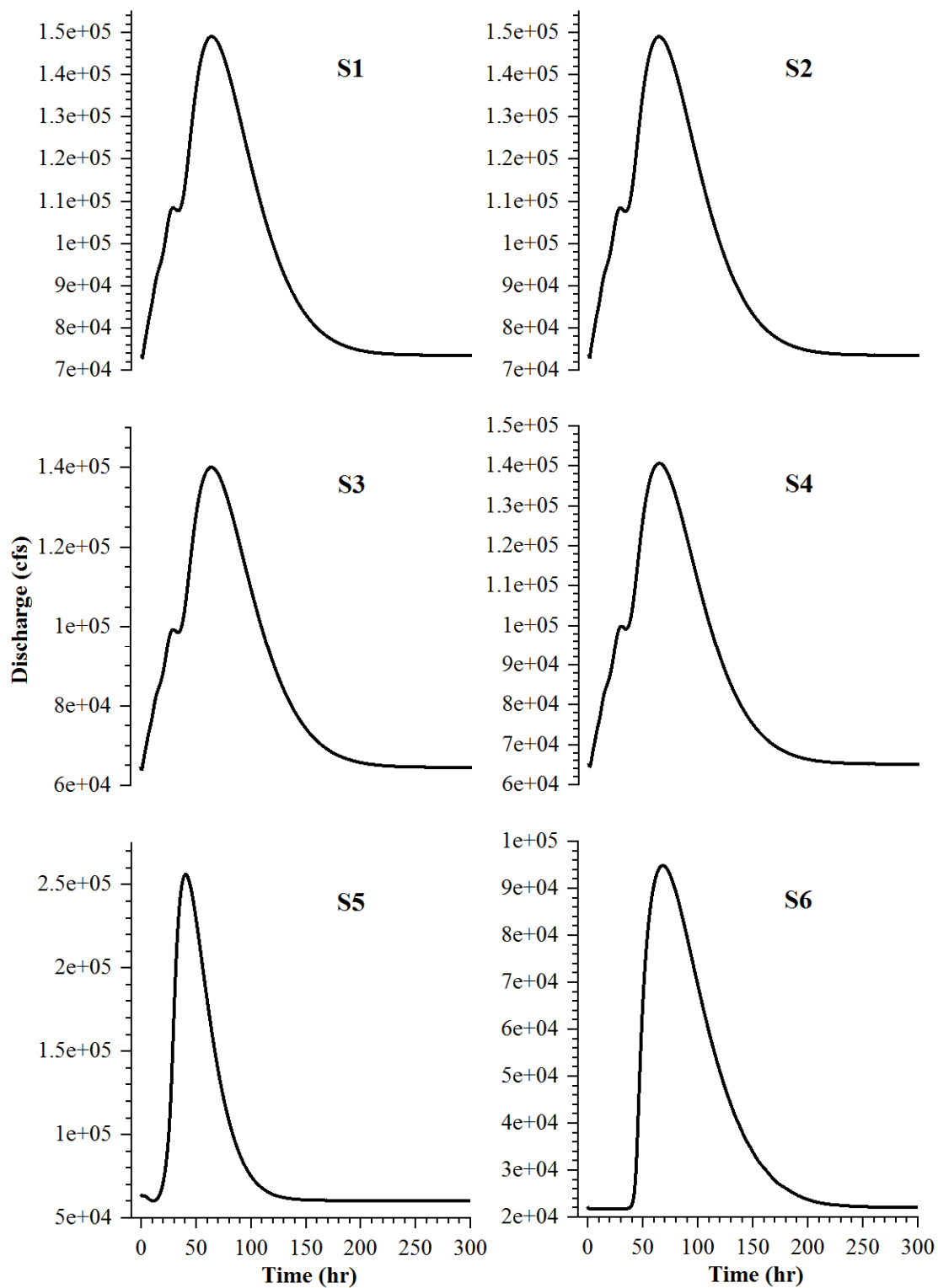


Figure 26 Hydrographs from simulations on Mandelbrot-Vicsek tree network.

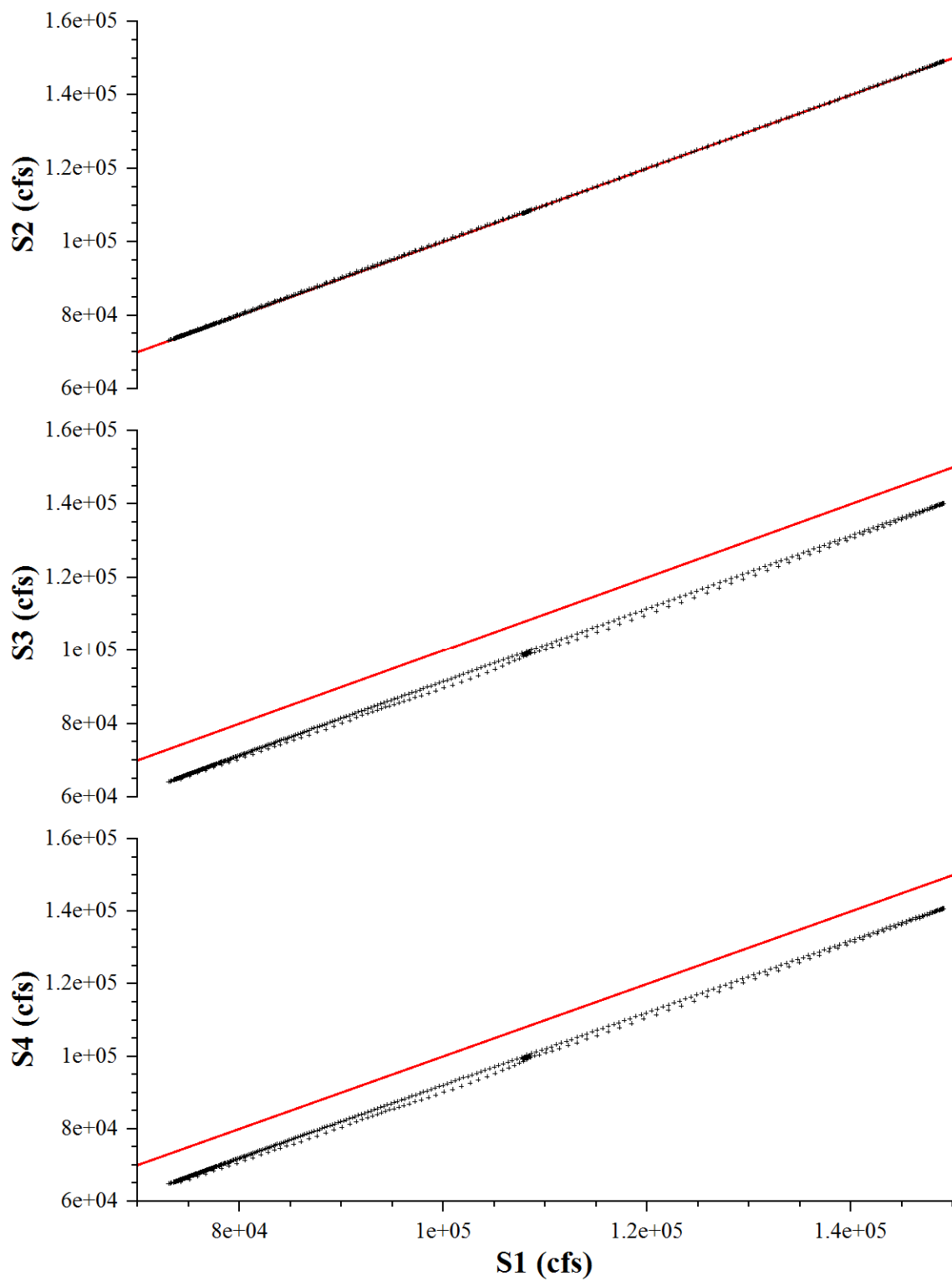


Figure 27 Plot of Simulations S2, S3, and S4 vs baseline simulation (S1). Red line is the 1:1 line

Simulation	NSE	Regression slope	Regression intercept	Q <sub>p</sub> (cfs)	t <sub>p</sub> (hr)
S1	1.0	1.0	0.0	149,097	63.5
S2	0.999	0.999	48.96	149,072	63.5
S3	0.828	0.998	-8835.32	140,111	63.67
S4	0.85	0.998	-8232.54	140,722	63.67
S5	N/A	N/A	N/A	94,912	67.75
S6	N/A	N/A	N/A	256,194	40.167

Table 7 Summary of comparison metrics for simulation on Mandelbrot-Vicsek tree

Table 7 provides a summary of calculated metrics to compare the simulations. The regression slope and intercept are calculated using the ordinary least squares method (DeVore 2004) with the ordinates of S1 as the independent variable, and the ordinates of S2, S3, and S4 as the dependent variables. The NSE and regression lines were not calculated for simulations S5 and S6 because they would have very poor fit.

Several interesting conclusions can be drawn from the results in Table 7. The first conclusion that can be made from simulation S2 is that uniformly distributing the incoming flow over a link has a negligible effect on hydraulic flood routing in terms of both timing and magnitude of the hydrograph. Simulations S3 and S4 suggest several things, first that the sum of incoming flows from order 1 streams is approximately equal in magnitude to the sum of inflow from order 2 streams. As far as effect on flow dynamics, it appears that there is limited effect from ignoring the lower order streams. This conclusion is from the fact that for both simulations the regression slope is approximately unity, and the line is only offset by a constant intercept. While both simulations S3 and S4 were close in comparison to each other, it can be concluded in this case that ignoring order 1 streams does have a greater effect than does ignoring order 2 streams. Simulation S5, as expected, greatly under predicts the magnitude of the flood,

but in spite of its great simplifications, it provides a reasonable estimate for time of arrival. Finally, simulation S6 demonstrates the potential for very large flows with a short arrival time in a network if the inflow tributaries are such that the peaks of hydrographs coincide with each other during a particular event.

### 4.3 Future Work

The work presented in this chapter is incomplete and the results given should be considered tentative. Two extreme cases have been presented, one where no tributary flow exists, and one where the maximum possible flow event occurs due to tributary flows timed such that there is direct interaction of the hydrograph peaks. More investigation however is necessary to provide a complete picture. Some potential future work to provide the missing detail is as following:

A more complete investigation of the effect from neglecting tributary flows is needed. In this simulation, first and second order streams were ignored and it was found that their individual effect was negligible. It is necessary to continue this systematic pruning of individual orders for streams of third through seventh order, while leaving all other orders intact. This analysis will provide insight on the individual influence of each order stream in the network.

The work here began to investigate the individual effect of each Horton order stream, but in practice a combination of several Horton order streams are neglected. To fully understand the impact of neglecting tributary streams, simulations need to be performed in which more than one stream order tributary is neglected. There are many combinations of this, but future research can consider that in practice a hierarchy will be assigned to streams and that an engineer would not choose to neglect a large order stream while including a lower order stream as a tributary. With this consideration, the simulation could be systematically pruning the network to reduce its order with the limit being the simulation S5 with no tributaries.

The simulation S6 demonstrates a potential maximum flow condition in the channel network due to interaction between peak flows. It is not obvious how this situation, should it arise, would be affected by the various simplifications discussed (uniform flow distribution and neglect of tributary flows). The connection can be made by performing the simulations already performed, and those discussed in this section, for the flow hydrographs that have a time to peak such that peak flows interact.

## CHAPTER V: CASE STUDY ON THE IOWA RIVER

The results of Chapter 3 gave considerable motivation to perform flood routing with very simplified cross-sectional geometry in a natural river. It was shown that the inter-cross-section variability did not play a significant role in influencing the routed hydrograph under the conditions simulated. The simulations performed in Chapter 3 were highly idealized however, and it was not clear if the result could be directly applied to a natural river. In Chapter 3, the only flows considered were extreme event in channels with no lateral inflows and no hydraulic structures, such as bridges. In an effort to resolve simplifications applied in Chapter 3, a simulation of the Iowa River between the USGS gauges at Iowa City, IA and at Lone Tree, IA was performed. The simulation period encompassed both extreme flows and frequent low flows. Also included in the model were several bridges and two lateral inflow hydrographs from the English River and Old Man's Creek. As will be shown, the results of Chapter 3 hold well.

### 5.1 Model Framework

The model constructed for evaluation is a HEC-RAS (Brunner 2010a, 2010b) model based upon measured cross-sections in the Iowa River. The river segment modeled begins at the USGS gauge in Iowa City, IA (USGS 05454500) and terminates at the USGS gauge in Lone Tree, IA (USGS 05455700) giving a river length of about 38 km. The model includes two lateral inflow hydrographs and 3 bridge crossings along its reach. The period of simulation is from May 1<sup>st</sup> 2008 to July 20<sup>th</sup> 2008.

#### 5.1.1 Inflow Hydrographs

There are three inflow hydrographs used to perform the simulation, an upstream hydrograph and two lateral inflow hydrographs. The upstream hydrograph used was observed directly from the USGS gauge at Iowa City, IA (USGS 05454500) and has a temporal resolution of 30 minutes. The lateral inflow hydrographs were routed from

USGS gauges on Old Man's Creek near Iowa City, IA (USGS 05455100) and on the English River near Kalona, IA (USGS 05455500) using the Muskingum routing method. The Muskingum parameters used in the routing were calibrated by Kyutae Lee of the Iowa Flood Center, Iowa City, IA and were used directly. Figure 28 gives a graphical representation of the inflow hydrographs used.

The Muskingum routing method is commonly used in practice; there are numerous examples of its use in the literature (e.g. Choudhury et. al. 2002; Dooge et. al. 1982; McCuen 1998). The parameters used in the Muskingum routing as provided by Kyutae Lee of the Iowa Flood Center are listed in Table 8.

River	K (hr)	X
Old Man's Creek	3.11	0.349
English River	9.35	0.417

Table 8 Muskingum routing parameters used in routing lateral inflows

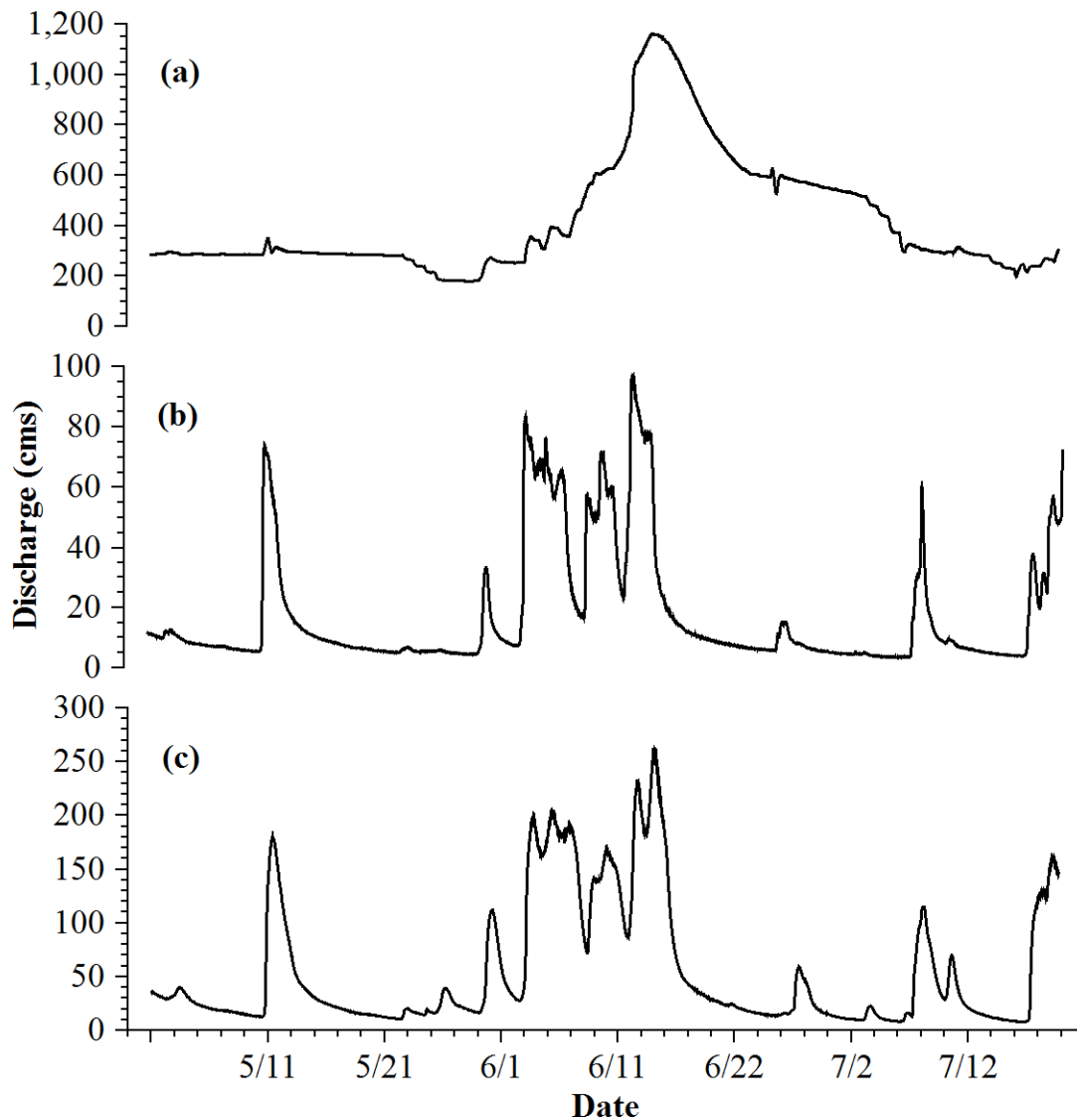


Figure 28 Inflow hydrographs observed in 2008. (a) Observed hydrograph at USGS gauge on the Iowa River near Iowa City, IA (b) Inflow hydrograph at the Iowa River from Old Man's Creek (c) Inflow hydrograph at the Iowa River from the English River

### 5.1.2 Downstream Boundary Condition

At the downstream boundary of the model (Lone Tree, IA), another USGS gauge was used to provide a stage hydrograph boundary condition, or the water surface elevation at the final cross-section vs. time. While the surface elevation does depend upon the hydraulic characteristics of the channel and its cross-sections, the same stage

hydrograph was used for both the river model with full, measured, bathymetric description of the channel cross-section, and the river model with a trapezoidal cross-section with reach averaged dimensions used (geometries are described in Section 5.1.3). Figure 29 gives a plot of the stage hydrograph used in the simulations.

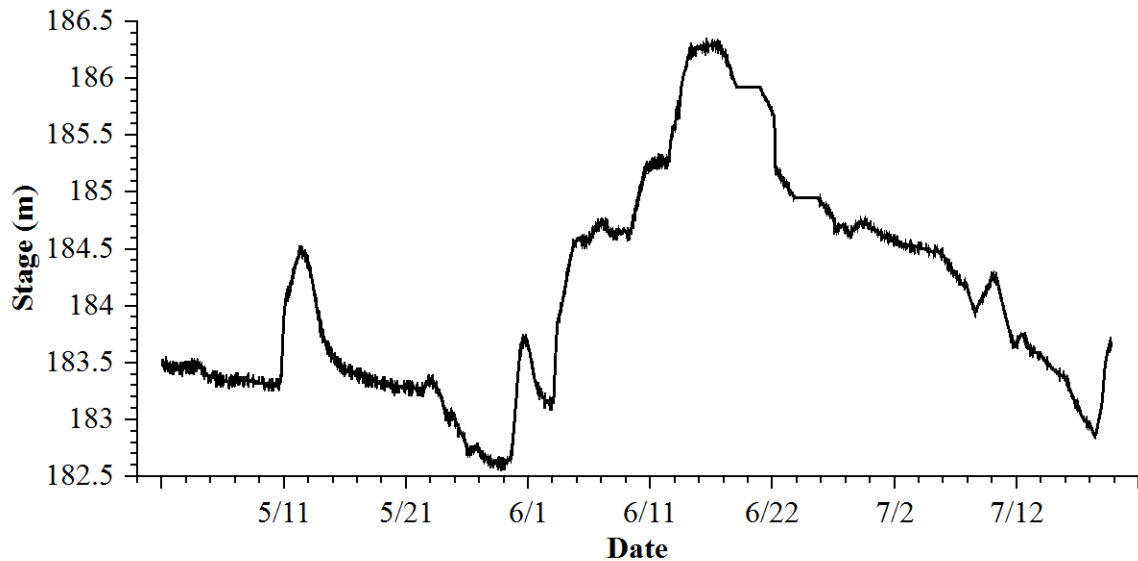


Figure 29 Stage hydrograph observed in 2008 at USGS gauge on Iowa River near Lone Tree, IA. Used as downstream boundary condition for river models

### 5.1.3 Channel and Floodplain Geometry

Two river models were constructed for numerical simulation, both equal in floodplain geometry, but with different channel geometries. The two channel geometry models used were one with geometric properties of the 67 cross-sections as observed in the Iowa River, and one with geometric properties of the 67 cross-sections approximated from a simple trapezoid with dimensions derived so that the cross-section has the reach wise averaged cross-sectional area. For both models, the floodplain geometry is extracted directly from an aerial LIDAR based digital elevation model (DEM) with a 1 m spatial resolution that was obtained through the Iowa Department of Natural Resources (IDNR).

The river lengths and stream centerline are from a digitized centerline prepared by visually tracing the stream from the DEM.

Both models contained three bridge crossings along the river reach. The cross-sections of the bridge were input using the original construction plans provided by the Johnson County Secondary Roads Department.

#### 5.1.4 Hydraulic Resistance and Model Calibration

Hydraulic resistance plays an important role in determining what water surface elevation is required to maintain a certain flow condition. The hydraulic resistance is also the parameter usually adjusted to achieve model calibration, or driving the model to agree with some measureable criteria (in this case other hydraulic parameters i.e. expansion and contraction coefficients are left at default values. See Brunner 2010b for more detail). The model with measured bathymetric description was calibrated to an observed water surface profile along the model reach during the June 2008 flood on the Iowa River with a Nash-Sutcliffe efficiency index of 98.4%. The river model with the approximated trapezoidal cross-section was run using two different sets of parameters: the same hydraulic resistance parameters as the detailed model, and hydraulic resistance parameters calibrated for the trapezoidal cross-section with a Nash-Sutcliffe efficiency index of 99%.

Initially the detailed model was assigned hydraulic resistance parameters from the National Land Cover Dataset (NLCD) to give a first order approximation and spatial distribution to the Manning's  $n$  parameters used in the cross-sections. After the model was constructed, each of the cross-sections had the Manning's  $n$  reduced to a single value for each overbank and a single value for the main channel, giving three degrees of freedom in adjusting the resistance at each cross-section. After several attempts, the Manning's  $n$  values at each cross-section were adjusted in a way to give both close agreement with observed water surface profiles and still be within a physically possible

range of values. This set of Manning's n values was also used for the uncalibrated approximate model.

The approximate model was calibrated to the same observed water surface profile as the detailed model. There were a couple motivations for this calibration: first to see if there was any influence on the routed hydrograph, second to see how much resistance is lost or gained by using approximate prismatic channels in a river model in terms of the average Manning's n, and finally to see if the approximate model could achieve a water surface profile comparable to the detailed model while remaining within a physically justifiable range of Manning's n values, therefore justifying its use in approximate flood inundation studies. Table 9 lists the average Manning's n values used in both calibrated models along with their coefficient of variation.

Statistic	Approximate			Detailed		
	Left Overbank	Channel	Right Overbank	Left Overbank	Channel	Right Overbank
Mean	0.089	0.052	0.089	0.071	0.037	0.073
CV	0.332	0.313	0.333	0.204	0.173	0.195

Table 9 Average Manning's n for calibrated models and its coefficient of variation (CV).

#### 5.1.5 CUENCAS Model

To provide an additional comparison with the hydraulics model, a simplified hydrologic routing model was also used to simulate the flood routing along the Iowa River reach between the USGS gauge in Iowa City, IA and at Lone Tree, IA. The routing method used by CUENCAS is that which is described in equation 2.35 with  $\lambda_1$  set to zero and  $V_c$  a constant 0.5 m/s providing a linear routing with velocity similar to that observed in various watersheds (personal communication with Ricardo Mantilla). The CUENCAS

model used had no rainfall input and was given the boundary conditions set by the USGS gauges.

### 5.1.6 Evaluation Criteria

There are several evaluation criteria available for comparing various flood routing models. Most are designed to give an overall “goodness of fit” for the model as it compares to observed data, and an extensive review of commonly used evaluation parameters is given by Moriasi et. al. (2007). For the case study there is an observed flow hydrograph at the Lone Tree, IA USGS gauge on the Iowa River which will be used as the comparison hydrograph for the models.

Three evaluation statistics were used to compare the four models used in the case study. They were all selected to evaluate how well routed flow hydrographs compared to the observed hydrograph. The three statistics used are percent bias (PBIAS), Nash-Sutcliffe efficiency (NSE), and the ratio of root mean square error to the observations standard deviation (RSR). A brief discussion of these statistics is provided here, and a further discussion is found in Moriasi et. al. (2007) and McCuen et. al. (2006) and included references.

PBIAS is a measure of the average tendency of the simulated data to be larger or smaller than the observed data (Moriasi et. al. 2007). Positive values indicate underestimation, and negative values indicate overestimation. The optimal value of PBIAS is 0.0 (Moriasi et. al. 2007). PBIAS is also an indicator of mass balance because it is calculated in a similar way as percent difference in volume, and in the case where both observed and simulated data have the same, constant time interval; the two are equivalent (Moriasi et. al. 2007). PBIAS is calculated as

$$PBIAS = \left[ \frac{\sum_{i=1}^n (Q_i^{obs} - Q_i^{sim})}{\sum_{i=1}^n (Q_i^{obs})} \right] (100\%) \quad (5.1)$$

NSE is calculated as shown in equation 3.8, with the parameter  $Q^{baseline}$  replaced with  $Q^{obs}$ . This was not chosen as the only measure of performance, because as noted by several researchers it is not the best suited to inter-model comparison (e.g. McCuen et. al. 2006; Moriasi et. al. 2007). One major reason stated for it not being well suited for comparing two different models is that there is no sampling distribution available for the NSE index and therefore it is difficult to interpret the values as being “good” or “bad” (McCuen et. al. 2006). Also, it has been shown that the NSE values are sensitive to outliers, magnitude bias, and time-offset bias (McCuen et. al. 2006). NSE is still a useful statistic, but because of certain limitations it was not solely used to compare the different models.

The ratio of root mean square error (RMSE) to observations standard deviation (RSR) is a statistic that has seen increasing use in hydrologic model evaluation (Moriasi et. al. 2007). RMSE has been a widely used error statistics in all fields of science and mathematics for many years, and while it is commonly accepted that the lower the RMSE, the better the prediction, no objective statement has been made about what is acceptably low (Moriasi et. al. 2007). Several researchers have suggested that RMSE less than half the standard deviation of observations may be considered low and have proposed (RSR) as a useful statistic for evaluation (Moriasi et. al. 2007). RSR can be calculated as

$$RSR = \frac{RMSE}{STDEV_{obs}} = \frac{\sqrt{\sum_{i=1}^n (Q_i^{obs} - Q_i^{sim})^2}}{\sqrt{\sum_{i=1}^n (Q_i^{obs} - \overline{Q^{obs}})^2}} \quad (5.2)$$

## 5.2 Results and Analysis

The simulations of the Iowa River utilized three hydraulic flood routing models and one hydrologic flood routing model. As a result of these models, four separate

hydrographs were obtained to compare with the observed flow hydrograph. Also, from the hydraulic flood routing models, various water surface profiles could be generated to compare how the water surface elevation is changed due to simplifications in cross-sectional geometry and what the potential is for calibration to overcome these limits.

Beginning with the hydrographs resulting from the simulation, it was found that all models performed well, confirming the results presented in Chapter 3 with respect to the hydraulic model and verifying the hydrologic model developed by Mantilla (2007). Graphical representations of the three evaluation statistics are presented in Figure 30

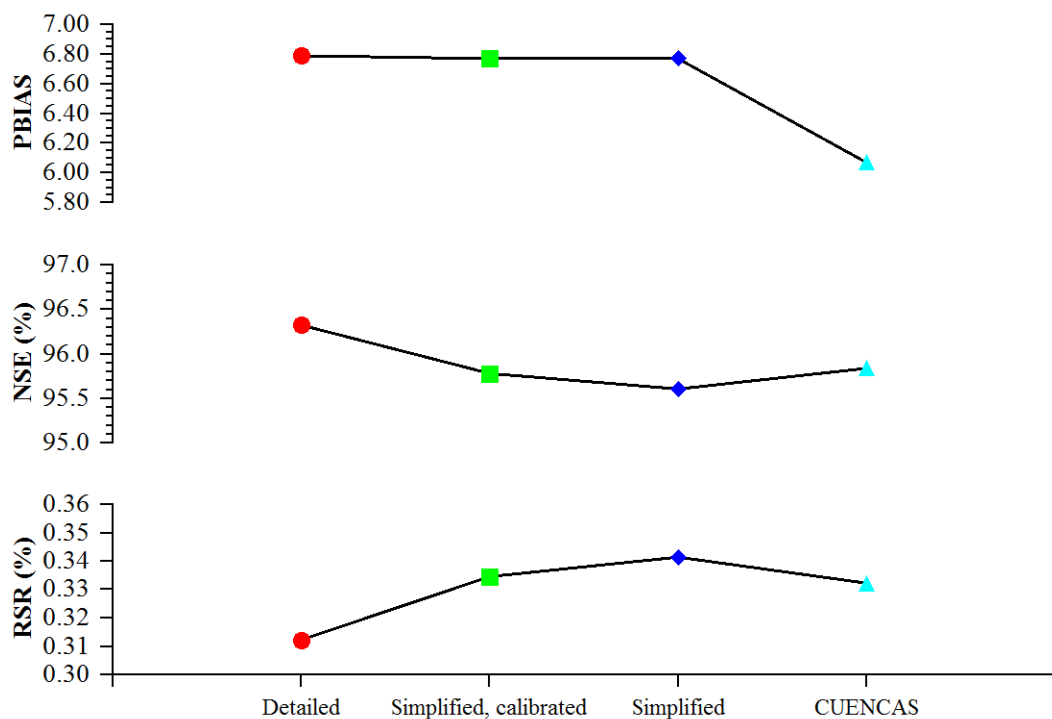


Figure 30 Summary of model performance. Ellipses represent detailed hydraulic routing model, squares represent calibrated approximate hydraulic model, diamonds represent approximate hydraulic model, triangles represent CUENCAS hydrologic model

It should be noted that the models were compared with the observed data beginning two days after the simulation began in an effort to eliminate any bias or error

coming from the initial conditions used in the models. This gave a simulation period of about 78 days and an observation sample size of about 3,750 points to compare with. For all models the output had the same temporal resolution as the observed data set.

As shown in Figure 30 the models all provided similar results. CUENCAS performed best with respect to PBIAS, but was comparable to the calibrated approximate hydraulic routing model for the other two statistics. These results once again confirm the potential for utilizing a simplified geometry in hydraulic river models in the absence of surveyed bathymetric data.

A more qualitative representation of how the models agree with observed flow values is a plot of the outflow hydrograph observed at the USGS gauge in Lone Tree, IA, and the outputs at the same location from the various models. This plot is given in Figure 31.

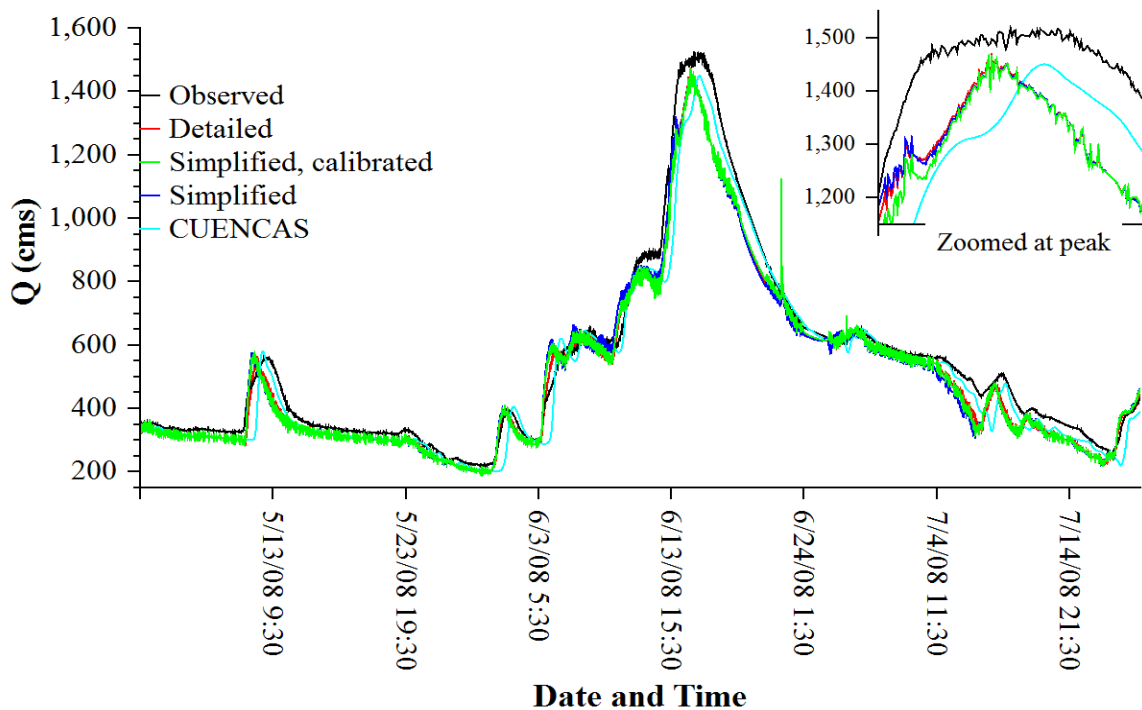


Figure 31 Outflow hydrographs at Lone Tree, IA

Figure 31 confirms the results of Figure 30 in a qualitative sense. As observed in Figure 31, the hydraulic models are very similar in estimated value, especially at their peak flow. The divergence is small between the calibrated models and the uncalibrated model. Also shown is that the hydrologic model, CUENCAS is able to satisfactorily approximate the observed hydrograph.

One greatly desired result from hydraulic routing models is an estimation of the water surface profile. A water surface profile allows estimation of inundated area and can be used as a risk monitoring tool during extreme flood events. Because this information is valuable it is important to assess whether or not a simplified geometry in the main channel can result in comparable estimation of the water surface to a detailed hydraulic routing model. Figure 32 is a graphical comparison of the maximum water surface elevation calculated for the three hydraulic models and a comparison of the minimum water surface elevation.

As is shown in Figure 32, there is a significant divergence in the water surface profile between the approximate models and the detailed model. The approximate model on average underestimates the water surface elevation along the river reach. While the results for the calibrated approximate model are significantly better, especially for the maximum water surface, they are not a suitable replacement for a detailed model in flood inundation mapping. They can be used as a first approximation, but any analysis depending upon reliable estimates of the water surface elevation would fail if using the approximate model.

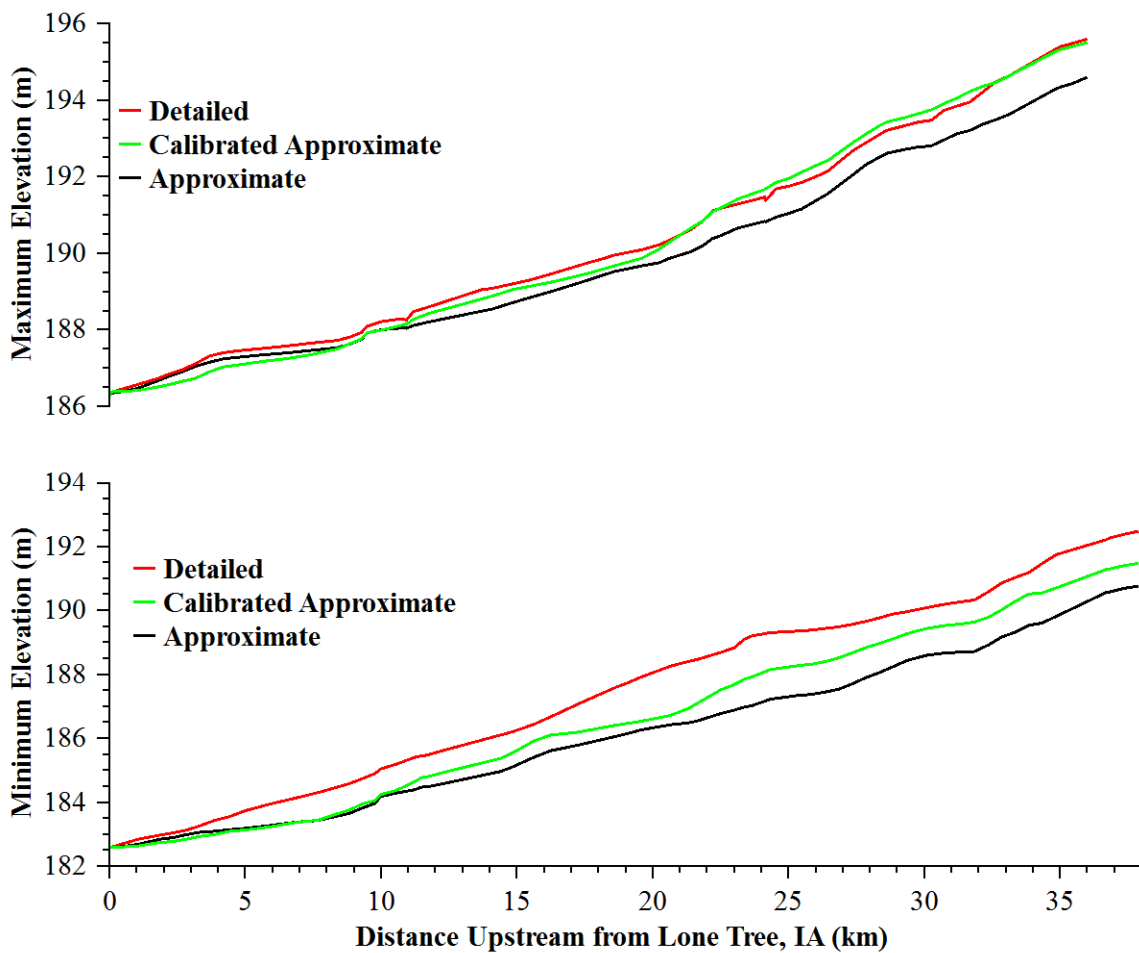


Figure 32 Plot of maximum and minimum water surface profiles computed by the three hydraulic routing models

## CHAPTER VI: SUMMARY, CONCLUSIONS, AND FUTURE WORK

Simple numerical experiments were conducted to estimate the sensitivity of hydraulic flood routing models to both variability in hydraulic geometry and to simplification in network flow and composition. The experiments were conducted within a multiscale framework, which led to further insight of how scale of a watershed influences results in flood routing models. The overall intent of the experiments was to address the question of how much detail in description of a river model is needed to provide reliable results for flood routing.

### 6.1 Variability in Hydraulic Geometry

Several important findings came from both the MC simulations and the case study found in Chapters 3 and 5 respectively. Most of the conclusions made are specific to the discharge hydrograph at the stream outlet, but the case study did provide an opportunity to examine how a water surface profile is influenced by the hydraulic geometry.

From the simulations, it was made apparent that the sensitivity of a given flood routing model to variability in hydraulic geometry is highly dependent on the scale of the modeled stream. In general it was found that a model becomes less sensitive to hydraulic geometry as the scale increases. In addition to being less sensitive to variability in hydraulic geometry, the average hydrograph characteristics (peak discharge, time to peak discharge, and time of duration) approached the baseline hydrograph characteristics as the scale increased.

It was found that the error committed in estimation of the peak discharge magnitude was insignificant when compared to the error in measurement or estimation using other standard practices (i.e. USGS observations or regional regression equations). This result held for all scales of streams simulated, and was also verified using data from a natural river in the case study conducted on the Iowa River.

The final important result addressed is the influence of variability in hydraulic geometry on the water surface profile. It was found that a river hydraulic model is highly sensitive to variations in hydraulic geometry with respect to the water surface profile and stage hydrograph. Even with calibration, a simplified river model does not perform comparatively to the detailed model.

In conclusion, the low sensitivity of a flood hydrograph to variation in hydraulic geometry suggests potential for deterministic flood routing methods in ungauged basins without the need for extensive field surveys, permitting greater confidence in the flow boundary conditions for more detailed hydraulic models. Also LIDAR derived data may provide a useful alternative to field surveys, in spite of low resolution, especially for strictly flow routing.

As far as the results extend to inundation mapping, the usefulness is limited due to poor performance. Even with calibration, the simplified geometry did not permit successful estimation of the water surface profile for conditions that departed from the calibration event. The use of simplified geometry for water surface estimation may be useful for planning purposes, but is unacceptable for risk assessment or detailed analysis.

### 6.2 Simplification to Tributaries and Lateral Inflows

The experiments performed on an idealized river network illuminated the effect from some common simplifications in river network hydraulic analysis. The primary analysis investigated how a uniform distribution of flows over a river reach modifies a flood hydrograph compared to a point insertion of the tributary flow, and what is the error committed by neglecting certain lower order streams as is common in engineering practice.

For the conditions tested, it was found that distributing the flood hydrograph uniformly over a stream reach had little effect on the calculated flood hydrograph. The

magnitude of the peak was attenuated more ( $<0.1\%$ ) with uniformly distributing the flow along a stream reach, but the time of arrival for the peak was unchanged.

Neglecting smaller tributaries does affect the magnitude of the flood hydrograph ( $<6\%$ ), but interestingly had a small effect on the time to peak and the overall flow dynamics. Also it was found that the 2<sup>nd</sup> order streams had almost the same contribution as the 1<sup>st</sup> order streams.

An attempt was also made to identify what the maximum flood would be if all the hydrograph peaks coincided with each other. It was found that the result is a peak magnitude about 67% greater than the conditions where the arrival time is based upon stream scale, and that the flood peak arrived about 27 hours earlier. This demonstrates that serious error can come from incorrectly estimating the timing of hydrographs.

In conclusion, it was found that many of the common practices in engineering analysis and design (i.e. neglecting low order streams and uniformly distributing lateral inflows) do cause error in flood routing, but the level of error is within acceptable tolerance levels. Also, the flow dynamics are not greatly affected by these simplifications, and the hydrographs demonstrate the same characteristics. Furthermore, a constant correction can be added to the case where lower order streams are neglected in order to preserve magnitude of flow and volume.

### 6.3 Future Work

The main future work suggested by the investigation described is further analysis of hydraulic geometry and its influence on the flood hydrograph. Several issues still need to be addressed to further the understanding of the role of hydraulic geometry in flood routing. The first issue to address is whether the results are an artifact from high magnitude, low frequency flows. All of the experiments conducted in this work were based upon an assumed 100 yr return period flood, which may significantly affect the outcome. It would be suggested to repeat the results for the return period floods with

intervals of 2 yr, 5 yr, 10 yr, 25 yr, 50 yr, and 500 yr to verify that the results hold true for other magnitudes flows.

Another point to address is that the hydrograph was of simple, smooth shape, whereas in nature multi-peak hydrographs are common. It is recommended that the simulations be repeated for at least one multi-peak hydrograph.

While it is necessary to conduct these experiments to verify the conclusions of this thesis, it is expected that the outcome will be positive based upon the case study described in Chapter 5 because the observed hydrograph used in that simulation had multiple peaks and a wide range of peak magnitudes for the simulation period.

## REFERENCES

- Abrahams, A. D. (1984). Channel networks: A geomorphological perspective. *Water Resources Research*, 20(2), 161-168.
- Aldama, A. A. (1990). Least-squares parameter estimation for Muskingum flood routing. *J. of Hydraulic Engineering*, 116(4), 580-586.
- Anderson, B. G., Rutherford, I. D., & Western, A. W. (2006). An analysis of the influence of riparian vegetation on the propagation of flood waves. *Environmental Modelling & Software*, 21, 1290-1296.
- Aral, M. M., Zhang, Y., & Jin, S. (1998). Application of relaxation scheme to wave-propagation simulation in open-channel networks. *J. of Hydraulic Engineering*, 124(11), 1125-1133.
- Beer, T., & Borgas, M. (1993). Horton's laws and the fractal nature of streams. *Water Resources Research*, 29(5), 1475-1487.
- Bhunya, P. K., Mishra, S. K., & Berndtsson, R. (2003). Simplified two-parameter gamma distribution for derivation of synthetic unit hydrograph. *J. of Hydrologic Engineering*, 8(4), 226-230.
- Bhunya, P. K., Berndtsson, R., Singh, P. K., & Hubert, P. (2008). Comparison between weibull and gamma distributions to derive synthetic unit hydrograph using Horton ratios. *Water Resources Research*, 44(W04421)
- Bhunya, P. K., Panda, S. N., & Goel, M. K. (2011). Synthetic unit hydrograph methods: A critical review. *The Open Hydrology Journal*, 5, 1-8.
- Blackburn, J., & Hicks, F. E. (2002). Combined flood routing and flood level forecasting. *Can. J. Civ. Eng.*, 29, 64-75.
- Blöschl, G., & Sivapalan, M. (1995). Scale issues in hydrological modelling: A review. *Hydrological Processes*, 9, 251-290.
- Bradie, B. (2006). *A friendly introduction to numerical analysis*. (1st ed., pp. 249-260). Upper Saddle River, NJ: Pearson Prentice Hall.
- Bridge, J. S. (2003). *Rivers and floodplains: Forms, processes, and sedimentary record*. (pp. ix-x). Oxford: Blackwell Science Ltd.
- Brunner, G.W., 2010a. HEC-RAS, River Analysis System Hydraulic Reference Manual. US Army Corps of Engineers. Hydrologic Engineering Center, Davis, 417pp.
- Brunner, G.W., 2010b. HEC-RAS, River Analysis System User's Manual. US Army Corps of Engineers. Hydrologic Engineering Center, Davis, 790pp
- Cappelaere, B. (1997). Accurate diffusive wave routing. *J. of Hydraulic Engineering*, 123(3), 174-181.
- Carlston, C. W. (1969). Downstream variations in the hydraulic geometry of streams: Special emphasis on mean velocity. *American Journal of Science*, 267, 499-509.

- Castellarin, A., Di Baldassarre, G., Bates, P. D., & Brath, A. (2009). Optimal cross-section spacing in Preissmann scheme 1D hydrodynamic models. *J. of Hydraulic Engineering*, 135(2), 96-105.
- Castro, J. M., & Jackson, P. L. (2001). Bankfull discharge recurrence intervals and regional hydraulic geometry relationships: Patterns in the Pacific Northwest, USA. *Journal of the American Water Resources Association*, 37(5), 1249-1262.
- Chang, C., Singer, E. D. M., & Koussis, A. D. (1983). On the mathematics of storage routing. *J. of Hydrology*, 61, 357-370.
- Chang, C. H., Tung, Y. K., & Yang, J. C. (1994). Monte Carlo simulation for correlated variables with marginal distributions. *J. of Hydraulic Engineering*, 120(3), 313-331.
- Chang, H. H. (2002). *Fluvial processes in river engineering*. (2 ed.). Malabar: Krieger Publishing Company.
- Choudhury, P., Shrivastava, R. K., & Narulkar, S. M. (2002). Flood routing in river networks using equivalent Muskingum inflow. *J. Hydrologic Engineering*, 7(6), 413-419.
- DeVore, J. L. (2004). *Probability and statistics for engineering and the sciences*. (6th ed.). Belmont, CA: Brooks/Cole—Thompson Learning.
- Di Baldassarre, G., & Montanari, A. (2009). Uncertainty in river discharge observations: A quantitative analysis. *Hydrology and Earth System Sciences*, 13, 913-921.
- Di Baldassarre, G., & Uhlenbrook, S. (2012). Is the current flood of data enough? A treatise on research needs for the improvement of flood modelling. *Hydrological Processes*, 26, 153-158.
- Dingman, S. L. (2007). Analytical derivation of at-a-station hydraulic-geometry relations. *J. of Hydrology*, 334, 17-27.
- Dodds, P. S., & Rothman, D. H. (1999). Unified view of scaling laws for river networks. *Physical Review E*, 59(5), 4865-4877.
- Dodov, B., and Foufoula-Georgiou E. (2004), Generalized hydraulic geometry Derivation based on a multiscaling formalism, *Water Resources. Research*, 40, W06302, doi:10.1029/2003WR002082.
- Dooge, J. C., Strupcowski W. G., & Napiórkowski, J. J. (1982). Hydrodynamic derivation of storage parameters of the Muskingum model. *J. of Hydrology*, 54, 371-387.
- Dooge, J. C., & Napiórkowski, J. J. (1987). Applicability of diffusion analogy in flood routing. *Acta Geophysica Polonica*, 35(1), 65-75.
- Eash, D. A. (2001). Techniques for estimating flood-frequency discharges for streams in Iowa. *U. S. Geological Survey Water-Resources Investigation Report*, 00-4233.

- Eaton, B. C., and Church M. (2007), Predicting downstream hydraulic geometry: A test of rational regime theory, *J. Geophys. Res.*, 112, F03025, doi:10.1029/2006JF000734.
- Efron, B., & Tibshirani, R. (1986). Bootstrap methods for standard errors, confidence intervals, and other measures of statistical accuracy. *Statistical Science*, 1(1), 54-77.
- Ferguson, R. I. (1986). Hydraulics and hydraulic geometry. *Progress in Physical Geography*, 10(1), 1-31.
- France, P. W. (1985). Hydrologic routing with a microcomputer. *Adv. Eng. Software*, 7(1), 8-12.
- Garcia, R., & Kahawita, R. (1986). Numerical solutions of the Saint Venant equations with the MacCormack finite difference scheme. *International Journal for Numerical Methods in Fluids*, 6, 259-274.
- Ghavasieh, A. R., Poulard, C., & Paquier, A. (2006). Effect of roughened strips on flood propagation: Assessment on representative virtual cases and validation. *J. of Hydrology*, 318, 121-137.
- Gupta, V. K., & Wavmire, E. (1998). Spatial variability and scale invariance in hydrologic regionalization. In G. Sposito (Ed.), *Scale dependence and scale invariance in hydrology* (pp. 88-135). Cambridge, UK: Cambridge University Press.
- Hager, W. H., Hager, K., Rappaz, J., & Caussignac, P. (1986). Non-linear diffusive flood routing. *Acta Mechanica*, 60, 181-198.
- Harman, C., Stewardson, M., & DeRose, R. (2008). Variability and uncertainty in reach bankfull hydraulic geometry. *J. of Hydrology*, 351, 13-25.
- Henderson, F. M. (1966). *Open channel flow*. New York: Macmillan Publishing Co., Inc.
- Hicks, F. E., & Steffler, P. M. (1994). Comparison of finite element methods for the St. Venant equations. *International Journal for Numerical Methods in Fluids*, 20, 99-113.
- Hicks, F. E. (1996). Hydraulic flood routing with minimum channel data: Peace River, Canada. *Can. J. Civ. Eng.*, 23, 524-535.
- Horton, R. E. (1945). Erosional development of streams and their drainage basins: hydrophysical approach to quantitative morphology. *Geological Society of America Bulletin*, 56(3), 275-283.
- Hsu, M. H., Fu, J. C., & Liu, W. C. (2003). Flood routing with real-time stage correction method for flash flood forecasting in the Tanshui River, Taiwan. *J. of Hydrology*, 283, 267-280.

- Huang, H. O., & Nanson, G. C. (2000). Hydraulic geometry and maximum flow efficiency as products of the principle of least action. *Earth Surface Processes and Landforms*, 25, 1-16.
- Jin, M., & Fread, D. L. (1997). Dynamic flood routing with explicit and implicit numerical solution schemes. *J. of Hydraulic Engineering*, 123(3), 166-173.
- Johnson, P. A. (1996). Uncertainty of hydraulic parameters. *J. of Hydraulic Engineering*, 122(2), 112-114.
- Johnson, P. A., & Heil, T. M. (1996). Uncertainty in estimating bankfull conditions. *Water Resources Bulletin*, 32(6), 1283-1291.
- Jothityangkoon, C., & Sivapalan, M. (2003). Towards estimation of extreme floods: examination of the roles of runoff process changes and flood plain flows. *J. of Hydrology*, 281, 206-229.
- Julien, P. Y. (2002). *River mechanics*. Cambridge, UK: Cambridge University Press.
- Karmegam, M., Rangapathy, V., & Haribabu, S. (1991). Development of conveyance routing. In L. C. Wrobel & C. A. Brebbia (Eds.), *Computational modeling of free and moving boundary problems: Fluid flow* (pp. 235-248). Berlin: Computational Mechanics Publications de Gruyter.
- Keskin, M. E., & Ađiraliođlu, N. (1997). A simplified dynamic model for routing in rectangular channels. *J. of Hydrology*, 202, 302-314.
- Kirchner, J. W. (1993). Statistical inevitability of Horton's laws and the apparent randomness of stream channel networks. *Geology*, 21, 591-594.
- Kim, J. H., Geem, Z. W., & Kim, E. S. (2001). Parameter estimation of the nonlinear Muskingum model using harmony search. *J. of the American Water Resources Association*, 37(5), 1131-1138.
- Knighton, A. D. (1975). Variations in at-a-station hydraulic geometry. *American Journal of Science*, 275, 186-218.
- Leopold, L. B. (1953). Downstream changes of velocity in rivers. *American Journal of Science*, 251, 606-624.
- Leopold, L.B., Maddock, T., 1953. The hydraulic geometry of stream channels and some physiographic implications. *United States Geological Survey*, 1-57.
- Liu, F., Feyen, J., & Berlamont, J. (1992). Computation method for regulating unsteady flow in open channels. *J. of Irrigation and Drainage Engineering*, 118(10), 674-689.
- Lyn, D. A., & Goodwin, P. (1987). Stability of a general Preissmann scheme. *J. of Hydraulic Engineering*, 113(1), 16-28.
- Mandelbrot, B. B., & Vicsek, T. (1989). Directed recursive models for fractal growth. *J. Phys. A: Math. Gen.* 22, L377-L383.

- Mantilla, R., & Gupta, V. K. (2005). A GIS numerical framework to study the process basis of scaling statistics in river networks. *IEEE Geoscience and Remote Sensing Letters*, 2(4), 404-408.
- Mantilla, R., Gupta, V. K., & Mesa, O. (2006). Role of coupled flow dynamics and real network structures on Hortonian scaling of peak flows. *J. of Hydrology*, 322, 155-167.
- Mantilla, R. (2007). *Physical basis of statistical scaling in peak flows and stream flow hydrographs for topologic and spatially embedded random self-similar channel networks*. (Doctoral dissertation, University of Colorado).
- Mantilla, R. (2009). *Cuencas user's guide*. Iowa City, Iowa: Retrieved from <http://old.iuhr.uiowa.edu/~ricardo/cuencas/CuencasUsers12182009.pdf>
- Maritan, A., Rinaldo, A., Rigon, R., Giacometti, A., & Rodriguez-Iturbe, R. (1996). Scaling laws for river networks. *Physical Review E*, 53(2), 1510-1515.
- McCuen, R. H., & Snyder, W. M. (1975). A proposed index for comparing hydrographs. *Water Resources Research*, 11(6), 1021-1024.
- McCuen, R. H. (1998). *Hydrologic analysis and design*. (2 ed.). Upper Saddle River, NJ: Prentice Hall.
- McCuen, R. H., Knight, Z., & Cutter, A. G. (2006). Evaluation of the Nash-Sutcliffe efficiency index. *J. of Hydrologic Engineering*, 11(6), 597-602.
- Mediero, L., Jimenez-Alvarez, A., & Garrote, L. (2010). Design flood hydrographs from the relationship between flood peak and volume. *Hydrology and Earth System Sciences*, 14, 2495-2505.
- Mejia, A. I., & Reed, S. M. (2011a). Evaluating the effects of parameterized cross section shapes and simplified routing with a coupled distributed hydrologic and hydraulic model. *J. of Hydrology*, 409, 512-524.
- Mejia, A. I., & Reed, S. M. (2011b). Role of channel and floodplain cross-section geometry in the basin response. *Water Resources Research*, 47(W09518), 1-15
- Melton, M. A. (1959). A derivation of Strahler's channel-ordering system. *The Journal of Geology*, 67(3), 345-346.
- Menabde, M., & Sivapalan, M. (2001). Linking space-time variability of river runoff and rainfall fields: a dynamic approach. *Advances in Water Resources*, 24, 1001-1014.
- Moriasi, D. N., et al., (2007). Model evaluation guidelines for systematic quantification of accuracy in watershed simulations. *Transactions of the ASABE*, 50(3), 885-900.
- Moussa, R., & Bocquillon, C. (1996). Criteria for the choice of flood-routing methods in natural channels. *J. of Hydrology*, 186, 1-30.
- Myers, W. R. C. (1991). Influence of geometry on discharge capacity of open channels. *J. of Hydraulic Engineering*, 117(5), 676-680.

- Nash, J. E., & Sutcliffe, J. V. (1970). River flow forecasting through conceptual models 1: a discussion of principles. *J. of Hydrology*, 10(3), 282-290.
- Orlandini, S., & Rosso, R. (1998). Parameterization of stream channel geometry in distributed modeling of catchment dynamics. *Water Resources Research*, 34(8), 1971-1985.
- Park, C. C. (1976). The relationship of slope and stream channel form in the river Dart, Devon. *J. of Hydrology*, 29, 139-147.
- Peckham, S. D. (1995). New results for self-similar trees with applications to river networks. *Water Resources Research*, 31(4), 1023-1029.
- Peckham, S. D., & Gupta, V. K. (1999). A reformulation of Horton's laws for large river networks in terms of statistical self-similarity. *Water Resources Research*, 35(9), 2763-2777.
- Phillips, P. J., & Harlin, J. M. (1984). Spatial dependency of hydraulic geometry exponents in a subalpine stream. *J. of Hydrology*, 71, 277-283.
- Phillips, J. D. (1990). The instability of hydraulic geometry. *Water Resources Research*, 26(4), 739-744.
- Pramanik, N., Panda, R. K., & Sen, D. (2010). Development of design flood hydrographs using probability density functions. *Hydrological Processes*, 24, 415-428.
- Reggiani, P., Sivapalan, M., Hassanizadeh, S. M., & Gray, W. G. (2001). Coupled equations for mass and momentum balance in a stream network: theoretical derivation and computational experiments. *Proc. R. Soc. Lond. A*, 457, 157-189.
- Reis, A. H. (2006). Constructal view of scaling laws of river basins. *Geomorphology*, 78(3-4), 201-206.
- Rigon, R., Rodriguez-Iturbe, I., Maritan, A., Giacometti, A., Tarboton, D. G., & Rinaldo, A. (1996). On Hack's law. *Water Resources Research*, 32(11), 3367-3374.
- Sabur, M. A., & Steffler, P. M. (1996). A conservative diffusion wave flood routing scheme for channel networks. *Can. J. Civ. Eng.*, 23, 566-570.
- Samuels, P. G., & Skeels, C. P. (1990). Stability limits for Preissmann scheme. *J. of Hydraulic Engineering*, 116(8), 997-1012.
- Scharffenberg, W. A., & Kavvas, M. L. (2011). Uncertainty in flood wave routing in a lateral-inflow-dominated stream. *J. of Hydrologic Engineering*, 16(2), 165-175.
- Scheidegger, A. E. (1968a). Horton's law of stream numbers. *Water Resources Research*, 4(3), 655-658.
- Scheidegger, A. E. (1968b). Horton's laws of stream lengths and drainage areas. *Water Resources Research*, 4(5), 1015-1021.
- Sholtes, J. S., & Doyle, M. W. (2011). Effect of channel restoration on flood wave attenuation. *J. of Hydraulic Engineering*, 137(2), 196-208.

- Shrestha, R. R., Theobald, S., & Nestmann, F. (2005). Simulation of flood flow in a river system using artificial neural networks. *Hydrology and Earth System Sciences*, 9(4), 313-321.
- Singh, V. P. (2003). On the theories of hydraulic geometry. *International Journal of Sediment Research*, 18(3), 196-218.
- Singh, V. P., Yang, C. T., & Deng, Z. O. (2003). Downstream hydraulic geometry relations: 1. theoretical development. *Water Resources Research*, 39(12), 1337, 1-15.
- Singh, V. P., & Zhang, L. (2008). At-a-station hydraulic geometry relations, 1: Theoretical development. *Hydrological Processes*, 22, 189-215.
- Singh, A. K., Kothvari, U. C., & Ranga Raju, K. G. (2004). Rapidly varying transient flows in alluvial rivers. *Journal of Hydraulic Research*, 42(5), 473-486.
- Singh, S. (2009). Time base as an invertible function of the parameters of gamma unit hydrograph. *J. of Irrigation and Drainage Engineering*, 135(6), 802-805.
- Sivapalan, M., Bates, B. C., & Larsen, J. E. (1997). A generalized, non-linear, diffusion wave equation: Theoretical development and application. *J. of Hydrology*, 192, 1-16.
- Sivapalan, M., et al. (2003). IAHS decade on predictions in ungauged basins (pub), 2003-2012: shaping an exciting future for the hydrological sciences. *Hydrological Sciences Journal-Journal Des Sciences Hydrologiques*, 48(6), 857-880.
- Sivapragasam, C., Maheswaran, R., & Venkatesh, V. (2008). Genetic programming approach for flood routing in natural channels. *Hydrological Processes*, 22, 623-628.
- Snell, J., & Sivapalan, M. (1995). Application of the meta-channel concept: Construction of the meta-channel hydraulic geometry for a natural catchment. *Hydrological Processes*, 9, 485-505.
- Stelling, G. S. & Verwey, A. (2006). *Numerical Flood Simulation, Encyclopedia of Hydrological Sciences*. John Wiley & Sons Ltd., UK
- Stewardson, M. (2005). Hydraulic geometry of stream reaches. *J. of Hydrology*, 306, 97-111.
- Strahler, A. N. (1957). Quantitative analysis of watershed geomorphology. *Transactions, American Geophysical Union*, 38(6), 913-920.
- Sturm, T. W. (2010). *Open channel hydraulics*. (2 ed.). Boston: McGraw Hill.
- Szymkiewicz, R. (1996). Numerical stability of implicit four-point scheme applied to inverse linear flow routing. *J. of Hydrology*, 176, 13-23.
- Szymkiewicz, R. (2010). Numerical modeling in open channel hydraulics. (pp. 301-365). Dordrecht: Springer.

- Tayefi, V., Lane, S. N., Hardy, R. J., & Yu, D. (2007). A comparison of one- and two-dimensional approaches to modelling flood inundation over complex upland floodplains. *Hydrological Processes*, 21, 3190-3202.
- Todini, E. (1988). *Hvdraulic and hvdrologic flood routing schemes*. In Bowles, D. S., and P. E. O'Connell (Eds.). *Recent advances in the modeling of hydrologic systems* (pp. 389-405). Dordrecht: Kluwer Academic Publishers.
- Tsai, C. (2005). Flood routing in mild-sloped rivers –wave characteristics and downstream backwater effects. *J. of Hydrology*, 308, 151-167.
- Venutelli, M. (2002). Stability and accuracy of weighted four-point implicit finite difference scheme for open channel flow. *J. of Hydraulic Engineering*, 128(3), 281-288.
- Venutelli, M. (2011). Analysis of dynamic wave model for unsteady flow in an open channel. *J. of Hydraulic Engineering*, 137(9), 1072-1078.
- Warwick, J. J., & Cale, W. G. (1986). Effects of parameter uncertainty in stream modeling. *J. of Environmental Engineering*, 112(3), 479-489.
- Wilkerson, G. V. (2008). Improved bankfull discharge prediction using 2-year recurrence-period discharge. *Journal of the American Water Resources Association*, 44(1), 243-258.
- Williams, G. P. (1978). Bank-full discharge of rivers. *Water Resources Research*, 14(6), 1141-1154.
- Wohl, E. E. (1998). Uncertainty in flood estimates associated with roughness coefficient. *J. of Hydraulic Engineering*, 124(2), 219-223.
- Wolff, C. G., & Burges, S. J. (1994). An analysis of the influence of river channel properties on flood frequency. *J. of Hydrology*, 153, 317-337.
- Woltemade, C. J., & Potter, K. W. (1994). A watershed modeling analysis of fluvial geomorphologic influences on flood peak attenuation. *Water Resources Research*, 30(6), 1933-1942.
- Wormleaton, P. R., & Karmegam, M. (1984). Parameter optimization in flood routing. *J. of Hydraulic Engineering*, 110(12), 1799-1814.
- Yang, C. T., Song, C. C. S., & Woldenberg, M. J. (1981). Hydraulic geometry and minimum rate of energy dissipation. *Water Resources Research*, 17(4), 1014-1018.
- Yen, B. C. (1992). Dimensionally homogeneous manning's formula. *J. of Hydraulic Engineering*, 118(9), 1326-1332.
- Yen, B. C., & Tsai, C. W. S. (2001). On noninertia wave versus diffusion wave in flood routing. *J. of Hydrology*, 244, 97-104.
- Yen, B. C. (2002). Open channel flow resistance. *J. of Hydraulic Engineering*, 128(1), 20-39.